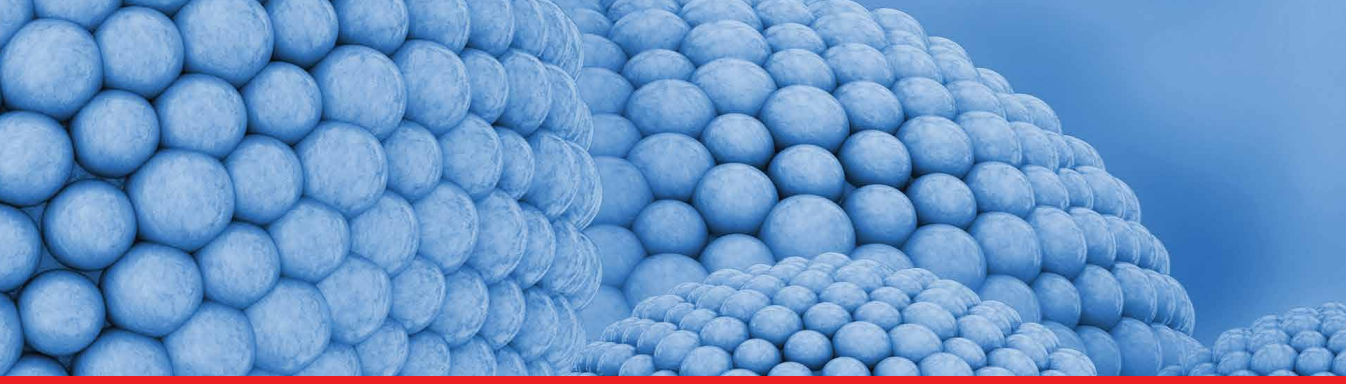

IntechOpen

IntechOpen Series
Nanotechnology and Nanomaterials,
Volume 14

Nanogenerators

Fundamentals, Technologies, and Emerging Applications

Edited by Shahab Ahmadi Seyedkhani, Azam Irajizad and Raheleh Mohammadpour

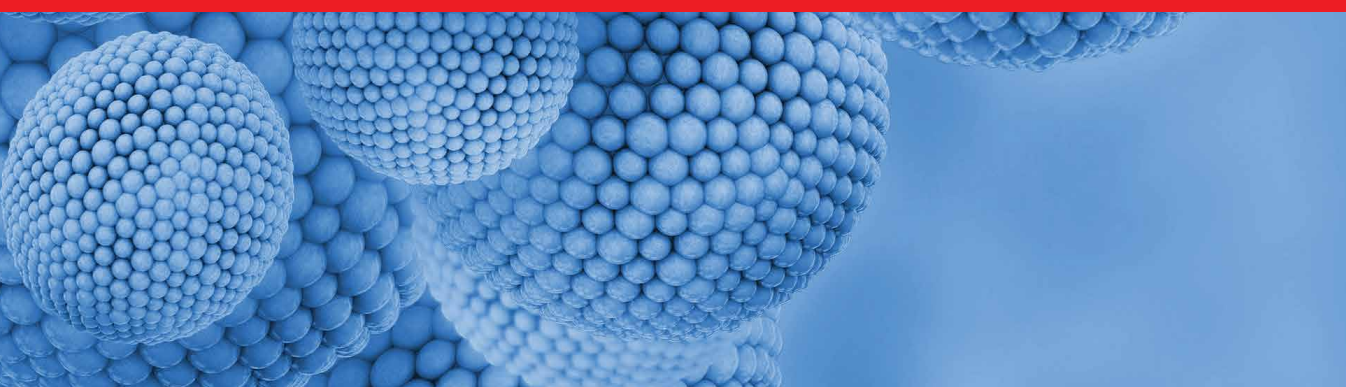

Nanogenerators - Fundamentals, Technologies, and Emerging Applications

Edited by Shahab Ahmadi Seyedkhani, Azam Irajizad and Raheleh Mohammadpour

Published in London, United Kingdom

Nanogenerators - Fundamentals, Technologies, and Emerging Applications
http://dx.doi.org/10.5772/intechopen.1008075
Edited by Shahab Ahmadi Seyedkhani, Azam Irajizad and Raheleh Mohammadpour

Contributors
Abdelkrim Khelif, Azam Irajizad, Bingang Xu, Fahimeh Zamanpour, Hong Fu, Kashif Riaz, Mahdi Zekavat, Muhammad Umaid Bukhari, Raheleh Mohammadpour, Shahab Ahmadi Seyedkhani, Yujue Yang, Zahra Razzaghi

First published in London, United Kingdom, 2026 by IntechOpen
IntechOpen is the global imprint of INTECHOPEN LIMITED, registered in England and Wales, registration number: 11086078, 167-169 Great Portland Street, London, W1W 5PF, United Kingdom

For EU product safety concerns: IN TECH d.o.o., Prolaz Marije Krucifikse Kozulić 3, 51000 Rijeka, Croatia, info@intechopen.com or visit our website at intechopen.com.

British Library Cataloguing-in-Publication Data
A catalogue record for this book is available from the British Library

Nanogenerators - Fundamentals, Technologies, and Emerging Applications
Edited by Shahab Ahmadi Seyedkhani, Azam Irajizad and Raheleh Mohammadpour
p. cm.

This title is part of the Nanotechnology and Nanomaterials Book Series, Volume 14
Topic: Nanotechnology and Nanodevices
Series Editor: Jung Huang
Topic Editors: Sadia Ameen, M. Shaheer Akhtar and Ing Kong

Print ISBN 978-1-83635-181-8
Online ISBN 978-1-83635-180-1
eBook (PDF) ISBN 978-1-83635-182-5
ISSN 3029-0538

IntechOpen Book Series

Nanotechnology and Nanomaterials

Volume 14

Aims and Scope of the Series

Humans face growing challenges in environmental sustainability. We need better materials, more effective devices, and higher computing power to conquer these challenges. Researchers have long explored the realm of science at the nanometer scale for developing novel problem-solving technologies. In the past decades, breakthroughs in multiscale computer simulation, novel hierarchical material and device structures, nanometrology, and new functionalities from interfacial and quantum size effects have enhanced our ability to utilize nanotechnology to solve real-world problems. This book series addresses important advancements in nanotechnology and nanomaterials. It showcases how nanotechnology is being continually developed and implemented in a variety of domains of science and technology. The two main topics this series covers are Nanotechnology and Nanodevices, and Nanomaterials and Nanostructures.

Meet the Series Editor

Jung Y. Huang, a university educator and researcher, has been working to unravel the structures and functional properties of materials and cellular events in living cells with varying optical methodologies. He has co-authored hundreds of journal papers and five book chapters. He also holds tens of patents in laser techniques and single-molecule/hyperspectral imaging and has developed architectural photonics based on hierarchically structured materials. Currently, his research focuses on the integration of artificial intelligence methodology with optics to automatically discover meaningful information from optical sensing/imaging data cubes. He has been an editorial board member and reviewer for several scientific journals. As a member of the global scientific community, he sincerely supports and endeavors to promote the spread of scientific knowledge.

Meet the Volume Editor

Shahab Ahmadi Seyedkhani is a researcher and Ph.D. candidate in nanoscience and nanotechnology at Sharif University of Technology. With over a decade of experience in designing and fabricating nanomaterials for advanced biotechnological applications, including tissue engineering, drug delivery, wound healing, and biosensing, his current research focuses on developing nanostructured human–machine interfaces (HMIs), particularly brain–computer interfaces (BCIs). A young Iranian scientist, he has authored numerous peer-reviewed publications and several academic books. His primary research interests center on exploring nanoscale interactions between living systems and biomaterials, with particular emphasis on enhancing tissue–electronic interfaces.

Associate Prof. Raheleh Mohammadpour is an experimental physicist and Head of the Center for Nanoscience & Nanotechnology, Sharif University of Technology. She received her Ph.D. in Nanotechnology from Sharif University and has conducted research at Uppsala University in Sweden and National Chiao Tung University in Taiwan. Her work focuses on wearable electronics, magnetoelastic and triboelectric nanogenerators, nanostructured solar cells, and nanosensors. With over 15 years of experience in physics, materials science, and device engineering, she has led multidisciplinary teams advancing perovskite and oxide-based solar technologies. Her research bridges materials innovation, advanced characterization, and scalable fabrication toward sustainable energy and self-powered sensing solutions.

Prof. Azam Irajizad is a physicist and a leading figure in nanoscience, currently serving as the Head of the Institute for Convergent Science and Technology at Sharif University of Technology. She earned her Ph.D. in Solid-State Physics, specializing in surface physics, from the University of Sussex, UK. Prof. Irajizad has made pioneering contributions to surface physics, thin films, and nanostructured materials. A member of the UNESCO World Commission on the Ethics of Scientific Knowledge and Technology (COMEST), she has authored over 250 scientific papers and also received numerous honors, including the title of Distinguished Professor in 2017. Her research spans the synthesis of nanomaterials, gas sensors, solar cells, supercapacitors, nanogenerators, and other emerging technologies, inspiring generations of scientists in Iran and beyond.

Contents

Preface

The ever-growing demand for sustainable, autonomous power sources for modern electronics, sensors, and biomedical systems has driven extensive research into nanoscale energy-harvesting technologies. Traditional batteries, though indispensable, are limited by finite lifespans, chemical instability, and environmental concerns. In this context, nanogenerators (NGs) have emerged as a revolutionary concept capable of converting ubiquitous mechanical and thermal energy into electrical signals at the nanoscale.

Since the introduction of nanogenerators in the early 21st century, the field has experienced remarkable progress in both theoretical understanding and practical implementation. These devices now represent one of the most promising solutions for powering self-sustained, miniaturized, and wearable electronics. The book *Nanogenerators – Fundamentals, Technologies, and Emerging Applications* aims to offer an integrated and comprehensive understanding of this emerging technology, from its fundamental mechanisms to materials, fabrication strategies, and future prospects in intelligent systems.

We have organized this volume into three major sections, each focusing on a distinct aspect of nanogenerator science and technology. The contributors to this book include researchers and scholars working at the intersection of materials science, nanotechnology, electronics, and energy systems, and their collective insights aim to guide readers through the diverse dimensions of this dynamic field.

Section 1. *Fundamentals and Evolution of Nanogenerators*

In this section, we provide an overview of the conceptual foundations, working mechanisms, and developmental trends of nanogenerators. We trace their scientific evolution and explain the key operational principles that govern their performance and functionality.

Chapter 1. *Introductory Chapter: Nanogenerators – New Insights in Small Energy Conversion Systems*

We begin by presenting the origin, evolution, and classification of nanogenerators, tracing their progression from initial experimental concepts to practical energy systems. We describe the various types of nanogenerators—piezoelectric (PENGs), triboelectric (TENGs), thermoelectric (ThNGs), pyroelectric (PyNGs), and hybrid (HNGs)—and compare their mechanisms and advantages. We further discuss how nanogenerators can serve as integral components of energy-autonomous electronic systems, and conclude the chapter by outlining a vision for future self-powered nanosystems in smart, wearable, and implantable technologies.

Chapter 2. *Principles and Working Mechanisms of Nanogenerators*

In this chapter, we present the scientific principles and underlying mechanisms of various nanogenerators in detail. We begin by explaining the piezoelectric effect and the role of nanoscale polarization in piezoelectric nanogenerators, followed by a description of pyroelectric and thermoelectric nanogenerators, which harness thermal fluctuations and gradients for energy generation. We then discuss the triboelectric effect and the charge-transfer mechanisms that drive triboelectric nanogenerators, emphasizing material selection, surface modification, and device geometry. Finally, we address hybrid nanogenerators, which combine multiple conversion principles to enhance performance, and conclude with future perspectives on multifunctional nanogenerator design and system-level integration.

Section 2. *Materials, Design, and Technologies*

In this section, we focus on materials engineering, eco-friendly approaches, and structural designs that underpin high-performance, sustainable nanogenerator systems. We emphasize the development of biocompatible, flexible, and recyclable materials that align with global goals of environmental responsibility and the circular economy.

Chapter 3. *Green and Eco-Friendly Triboelectric Nanogenerators*

Here, we provide a comprehensive discussion on the role of sustainable materials in the fabrication of triboelectric nanogenerators. We introduce the waste-to-energy concept and discuss the environmental and economic implications of non-recycled waste, highlighting how TENGs can contribute to global sustainability goals. We then review advances in recycled-material-based TENGs, including devices constructed from polymers, papers, and composite waste. Subsequently, we focus on biopolymer-based TENGs, categorizing them into synthetic and natural biopolymers. We describe polysaccharide-based systems such as cellulose, chitosan, starch, alginate, and pullulan, as well as protein-based systems, and analyze their triboelectric properties, processability, and energy conversion efficiency. Finally, we provide an outlook on the challenges and future opportunities for developing environmentally benign and high-performance triboelectric nanogenerators.

Chapter 4. *Textile-Based Nanogenerators as Wearable Electronics for Energy Harvesting*

We address the emerging field of textile-integrated nanogenerators that enable on-body and wearable energy harvesting. We describe textile-based triboelectric nanogenerators (T-TENGs) and their various configurations, including single-fiber, woven-fabric, multilayer, and 3D structures, emphasizing flexibility and durability. We also discuss textile-based piezoelectric nanogenerators (T-PENGs) and explain how fiber geometry and textile architecture influence device performance. Furthermore, we include textile-based thermoelectric generators (TEGs) that utilize body heat as a power source, with a particular focus on fiber- and fabric-based systems. We conclude this chapter by presenting applications of textile nanogenerators in self-powered wearable electronics, physiological monitoring, motion sensing, and smart garments, and by providing insights into scalability and material optimization for practical use.

Section 3. *Advanced Topics and Future Prospects in Nanogenerators*

In the final section, we expand the scope of nanogenerator technology toward intelligent and neuromorphic applications, where nanoscale energy systems can not only power but also emulate biological functions. We explore how nanogenerators can interface with neural architectures to enable energy-autonomous signal processing and adaptive learning.

Chapter 5. *Toward Energy-Autonomous Neuromorphic Systems: Piezoelectric and Triboelectric Nanogenerators for Synaptic Plasticity Emulation*

In this chapter, we explore the integration of nanogenerators into neuromorphic computing platforms, where mechanical and electrical stimuli can modulate electronic states to mimic the functioning of biological synapses. We begin by outlining the biological foundations of neural communication, including neuronal structure, synaptic transmission, and synaptic plasticity. We then discuss existing hardware approaches to emulate synaptic behavior and describe how piezoelectric and triboelectric nanogenerators can replicate synaptic learning rules via piezotronic and tribotronic effects. We demonstrate how these systems can function simultaneously as energy sources and neuromorphic elements, capable of sensing, learning, and adapting to external stimuli. Finally, we present a forward-looking perspective on energy-autonomous neuromorphic architectures, in which nanogenerators enable the realization of self-powered artificial intelligence systems.

Through its five chapters, *Nanogenerators – Fundamentals, Technologies, and Emerging Applications* provides a comprehensive exploration of nanoscale energy conversion systems, from the fundamental physics of piezoelectric, triboelectric, thermoelectric, and pyroelectric effects to applied research in eco-friendly materials, textile-based devices, and intelligent energy systems. We aim to deliver both scientific depth and technological foresight, offering readers a roadmap for innovation in self-powered, sustainable, and adaptive nanotechnologies.

We express our deepest appreciation to all contributing authors for their scholarly efforts and valuable insights, as well as to the reviewers and editors who have supported the development of this volume. We hope that this book serves as an essential reference for students, researchers, and professionals in nanotechnology, materials science, energy engineering, and bioelectronics, and that it inspires continued progress toward a future defined by autonomous and sustainable energy solutions.

Shahab Ahmadi Seyedkhani, Raheleh Mohammadpour and Azam Irajizad
Sharif University of Technology,
Tehran, Iran

Section 1

Fundamentals and Evolution of Nanogenerators

Chapter 1

Introductory Chapter: Nanogenerators – New Insights in Small Energy Conversion Systems

Shahab Ahmadi Seyedkhani

1. Concept and evolution of nanogenerators

Do more with less; this is the mantra of nanotech. As technology advances, smaller devices are expected to perform more tasks with more efficiency than their larger predecessors. Often, this requires taking advantage of special physical behaviors that arise only at nanoscales. On the other hand, in order to miniaturize devices while increasing the efficiency, essential approaches involve creating multifunctional systems and eliminating purely consumer components. Accordingly, there is a need to develop new technologies for small-scale but widespread distributed energy production. Nanogenerators (NGs) represent micro- or nanoscale devices that are designed to convert mechanical and thermal energies to operational electrical energy. These mechanical and thermal energies can be captured from ubiquitous and often irregular phenomena such as movements, vibrations, airflow, acoustic waves, biomechanical activities, and even small thermal fluctuations. Additionally, NGs can act not only as energy generators but also as sensors simultaneously. In fact, since their performance is highly sensitive to environmental stimuli such as pressure, strain, and temperature, the NGs' electrical response resulting from these changes can be analyzed as a sensory feedback. According to recent improvement in their electrical output and mechanical stability, NGs can be widely used in the field of self-power sensing systems and different continuous monitoring applications. Meanwhile, one of the main problems of conventional sensors is the need for an external power supply such as batteries, which makes sensor systems more complex and less handy for mobile applications. Hence, NGs can be applied for two main goals simultaneously: (1) *Sensing changes in environmental mechanical and thermal energies*, and (2) *providing electrical energy from these changes*. **Figure 1** shows the role of NGs as converters for production of electrical energy.

It is worth noting that the concept of harvesting energy from ambient sources is not new; however, the systematic development of NGs is a relatively recent achievement in nanoscience. The primary motivation for developing NGs was to overcome the inherent limitations of conventional batteries, including their limited lifespan, bulky structure, and requirement for periodic replacement or recharging. In addition, fabricating a self-powered device, which could provide the energy needed to operate itself and other parts of the system, was an important goal. The breakthrough came in 2006, when scientists proposed the idea of NGs (or self-powered device) in 2006 by

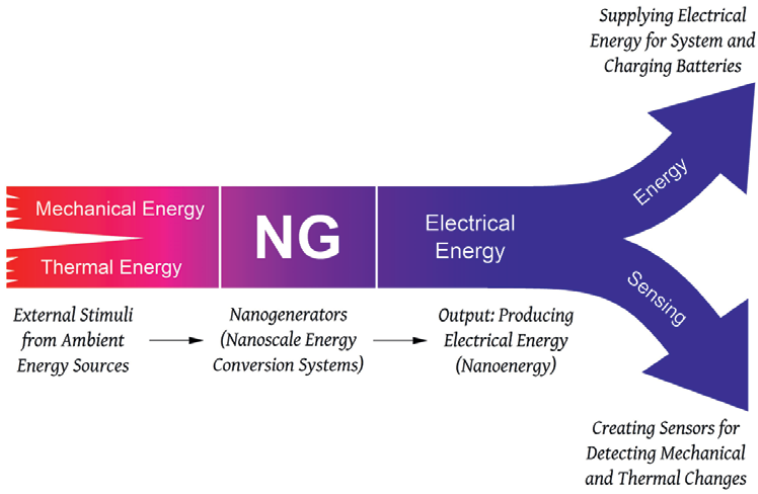

Figure 1.
Overall function of NGs for conversion of mechanical and thermal energies to operational electrical energy, which can be used as (1) the energy required for devices and/or (2) the signal for NG-based sensors. It should be noted that, although other nanoscale energy conversion systems such as photovoltaic solar cells can also be considered as subsets of NGs, what are generally known today as NGs are devices that convert mechanical and thermal changes into electrical energy.

employing the piezoelectric effect of crystalline materials for converting mechanical energy to electrical energy [1]. This finding significantly inspired the nanotech and created a new field called nanoenergy. After great research in this field, a triboelectric effect–based NG was first proposed in 2012 [2]. Since then, the continuous improvement in designing and fabricating NGs has led to an increase in their efficiency, so that the current NGs can provide in situ energy harvesting pathways at the point of use. Moreover, NGs can be promising devices for reducing reliance on conventional batteries and wired power sources. Moreover, unlike conventional large-scale renewable technologies such as photovoltaic solar panels and wind turbines, NGs can operate at small power levels, typically ranging from microwatts (μW) to milliwatts (mW). Such small energy levels can be proper for powering sensors, implantable medical devices, wearable electronics, and wireless nodes. Furthermore, the nanoscale configurations of NGs make them ideal for integrating into flexible, transparent, and biological systems, which can pave the way for the development of advanced technologies. Currently, the interest in NGs has expanded worldwide due to their extensive applications, which are not limited to small power sources but also include self-powered sensors and systems in the Internet of Things (IoT), environmental monitoring, security systems, infrastructure monitoring, healthcare, and human–machine interfaces (HMIs).

2. Different types of nanogenerators

Following the invention of the first NGs, rapid advances were made for developing different kinds of nanoscale energy conversion systems. Todays, the main types of NGs can be classified in four categories, including (1) *piezoelectric NGs* (PENGs), (2) *triboelectric NGs* (TENGs), (3) *thermoelectric NGs* (ThNGs), and (4) *pyroelectric*

NGs (PyNGs). Moreover, it is possible to integrate two or more types of NGs within a single platform, which are called *hybrid NGs* (HNGs). In the following sections, we briefly introduce each of these systems.

2.1 Piezoelectric nanogenerators (PENGs)

PENGs work based on the *piezoelectric effect*. The piezoelectricity is a fundamental electromechanical phenomenon in which non-centrosymmetric materials generate an electric potential when subjected to mechanical stress. This effect occurs because the applied deformation, such as compression, stretching, or bending, shifts the position of ions in the crystal lattice, thereby creating a dipole moment and separating charges on opposite faces of the material. Designing circuits that collect and use this potential difference is the operational principle of PENG-based devices. Accordingly, by harvesting biomechanical motions such as heartbeats, respiration, muscle contraction, blood flow, or even subtle skin vibrations, PENGs have demonstrated the feasibility of powering small-scale electronic devices [3–5].

2.2 Triboelectric nanogenerators (TENGs)

TENGs operate based on the *triboelectric effect*, a process introduced in 2012 in which electrical charges are generated when two dissimilar materials come into contact and then separate [6]. When materials contact, electrons are exchanged due to differences in the materials' electron affinity. Upon separation, one of the materials' surfaces becomes positively charged while the other one becomes negatively charged. Hence, a potential difference is created. When these surfaces are connected through an external circuit, this potential can drive electron flow, resulting in an electric current. It is worth noting that the process is further enhanced by electrostatic induction, which amplifies charge transfer during repeated contact–separation cycles. Hence, TENGs are capable of generating relatively high voltages and moderate current densities from simple mechanical actions such as tapping, sliding, pressing, or rotating. The simple fabrication, lightweight design, and compatibility of TENGs with flexible and transparent substrates make them highly attractive for wearable electronics, self-powered sensors, and energy-harvesting systems [7].

2.3 Thermoelectric nanogenerators (ThNGs)

The *thermoelectric phenomenon* was first observed in 1821 by Thomas Seebeck and was explored in more detail by Jean Peltier. In this phenomenon, a voltage is generated across a material when there is a temperature gradient along its length. At the microscopic level, the thermoelectric effect arises because charge carriers; namely electrons or holes, in the hotter region of a conductor or semiconductor gain more thermal energy and diffuse toward the colder region. This results in a charge separation, making an electric potential. Using an external circuit, this potential can drive current flow, converting thermal energy directly into electricity without any mechanical movement. The performance of thermoelectric materials is quantified by the dimensionless figure of merit ($ZT = S^2\sigma T/\kappa$), where S is the Seebeck coefficient, σ is electrical conductivity, T is absolute temperature, and κ is thermal conductivity. Achieving a high ZT requires maximizing the Seebeck coefficient and electrical conductivity while minimizing thermal conductivity, which is notoriously difficult in bulk materials due to their interdependent nature. Nevertheless, advances in

nanotechnology and low-dimensional materials such as nanowires, quantum dots, and superlattices have enabled phonon scattering to reduce thermal conductivity without significantly hindering the electrical transport. This great opportunity to exploit the highly efficient thermoelectric conversion, which has been created by the participation of nanotechnology, has led to the development of a new class of energy conversion technologies that we know today as ThNGs. Moreover, recent research focuses on flexible and printable ThNGs, enabling their integration into wearable electronics and implantable biomedical devices as well as expanding their applications. Having proper performance, ThNGs are particularly attractive for waste heat recovery, as they can recycle otherwise unused thermal energy from microelectronic devices, wearable electronics, automotive engines, and industrial processes into useful electrical power [8, 9].

2.4 Pyroelectric nanogenerators (PyNGs)

PyNGs convert time-dependent temperature fluctuations into electricity based on the *pyroelectric effect*. This effect is a property of some non-centrosymmetric polar crystalline materials in which spontaneous electric polarization changes with temperature. When the temperature of a pyroelectric material fluctuates, the polarization shift induces redistribution of charges on its surface, leading to a potential difference. It should be noted that unlike ThNGs, which rely on *spatial temperature gradients*, PyNGs harvest energy from *temporal temperature fluctuations*. Therefore, PyNGs are particularly well-suited for small-scale waste heat harvesting such as recovering energy from temperature oscillations in microelectronics and biological systems. They have also been investigated as self-powered sensors, capable of monitoring thermal signatures, infrared radiation, and environmental changes without the need for external batteries [10, 11].

2.5 Hybrid nanogenerators (HNGs)

To overcome the limitations of single-mechanism NGs and maximize energy harvesting efficiency, researchers have developed hybrid systems that integrate two or more types of NGs within a single platform. Through hybrid systems, such as piezoelectric–triboelectric, triboelectric–pyroelectric, thermoelectric–piezoelectric, or even photovoltaic–triboelectric, these NGs can simultaneously convert mechanical, thermal, and solar energies into electricity. The principle of HNGs lies in synergistic energy harvesting, where multiple transduction mechanisms operate either independently or cooperatively in one device. For instance, wearable triboelectric–piezoelectric HNGs can generate power using body movements through both lattice polarization and surface charge transfer, significantly boosting the final output. Similarly, thermoelectric–piezoelectric HNGs can harvest both waste heat and mechanical vibrations, ensuring continuous operation under varying environmental conditions. Furthermore, HNGs can address the challenges of intermittent or fluctuating energy sources through broadening of harvestable stimuli. This capability improves the stability and reliability of power supply for self-sustained electronics. Recent innovations in materials and fabrication processes, such as creating flexible composites, multilayer thin films, and micro/nanostructured surfaces, have enabled seamless integration of different mechanisms without compromising device performance or miniaturization. Therefore, applications of hybrid NGs are rapidly expanding, ranging from wearable and implantable biomedical devices to environmental

monitoring, IoT, robotics, and HMIs [12, 13]. These key milestones have transformed NGs from a conceptual novelty into a multifunctional technological platform. Today, NGs are being explored not only as appropriate energy harvesters but as integral components of next-generation electronics, particularly where self-sustainability, flexibility, and integration with biological systems are essential.

3. Vision for future energy-autonomous systems

Looking ahead, NGs are envisioned as important technologies for energy-autonomous systems. With continued advances, they are expected to play significant roles in the following technologies:

- *Smart homes*: Smart homes refer to residential houses that use security, network communication, automation and remote control systems, as well as entertainment technologies to integrate facilities related to home life. Building a well-organized management system for residential facilities and family schedule affairs can boost home safety, convenience, comfort, and artistry and attain an environmentally friendly living platform. In this regard, NGs can not only help identify the environmental changes and manage intelligent systems as sensors but can also be used as self-powered technologies to provide the energy required for applied technologies.

- *Integrated healthcare system*: Incorporated healthcare systems comprising data gathering, sharing, and analyzing can pave the way for solving modern health issues. Wearable NGs enable remote data collection from patients through IoT-based healthcare systems. Moreover, NGs have been demonstrated to be fruitful in sensing and harvesting energy from biomechanical movement, which can be used for health monitoring, rehabilitation, tissue repairing, drug delivery, and diagnosis applications.

- *Distributed micro-nano energy*: The modern information era relies on the miniaturization of electronic devices. Future energy systems will be complicated technologies consisting of collecting and intelligent distributing nodes simultaneously. Hence, numerous small mobile energy grids would be created to build a smart energy network, which is directly targeted to customers and supplied on demand. It has been proved that NGs can collect distributed energies, including mechanical energy from human stepping and car motion, thermal energy waste from manufacturing factories, wind energy produced by high-speed trains, or even hybrid energy sources such as solar + falling raindrop energies. It is feasible that we finally replace clean energy with fossil fuels and shift the current systems to achieve carbon neutrality by energy collection using NGs and other renewable technologies.

- *Eco-smart agriculture*: Smart agriculture, which is also known as smart farming, is the use of technologies like sensors, IoT, AI, and robotics to automate and enhance agriculture practices in order to increase efficiency, productivity, and profitability while reducing waste and environmental impacts. In this regard, advanced sensing platforms such as NGs can be beneficial for monitoring light intensity, humidity, temperature, soil nutrients, and plant growth, as well as

controlled release of pesticides and developing customized agriculture. Also, it is anticipated that eco-smart agriculture will be fully integrated into the future smart city ecosystem to attain a more automated, data-driven, and optimized agricultural production mode.

- *Blue energy*: About 70% of the Earth's surface is ocean, which is one of the biggest available energy reservoirs. Based on estimates, the annual generation of wave energy from the ocean can reach more than 80,000 TWh, far exceeding the current human annual demand of 16,000 TWh. If we can properly exploit and utilize this opportunity, it will be a new kind of sustainable green energy. Creating floating wave energy harvesters using NGs, such as mechanical-to-electrical energy-conversion systems of TENGs and PENGs, can be an appropriate design for large-scale energy production. Future organization of mature NG-based marine energy harvesting devices can basically change the global energy landscape, affecting all facets of the economy and society.

- *Sustainable green factory*: Green factory refers to low-carbon manufacturing through maximum energy efficiency. NGs can capture most of the ubiquitous and waste mechanical energy in factories, which reduces consumption and subsequent pollution. Also, they can realize the energy cycle chain, thus enhancing the benefits while reaching an environmentally friendly economy. As we discussed, the IoT based on NGs offers a new revolution for smart identification, control, and management during industrial processes, leading to more efficient factories. Moreover, NG-based robots and HMIs can be used for next-generation advanced factories.

- *Smart monitoring of environmental changes*: Intelligent ecological environment monitoring systems belong to the implementation of the IoT. These systems use ecological data captured from sensors and equipment for different environmental monitoring of air, water, and soil. To this end, NGs have been proved capable of monitoring meteorological data such as air purification and quality, ambient temperature and humidity, water pollutants, CO_2 concentration, wind speed and direction, soil pH, automobile exhaust, and so on. Having multisource self-powered sensing advantages, NGs can develop environmental monitoring systems at the technical level. Furthermore, they can enhance pollution monitoring based on dynamic monitoring networks and real-time treatment technologies.

- *Green intelligent transportation*: Green and intelligent transportation refers to self-driven energy supply, wireless signal transmission, better driving experience, and environmental protection of vehicle operation, which will ultimately lead to increased safety and improved quality of the transportation system. Real-time data collection and analysis of traffic information is essential for management of roads, drivers, and vehicles. NGs can be utilized to harvest energy from the movement of vehicles on roads, wind flow from high-speed trains, and exhaust gas flow of automobiles. Moreover, as sensing platforms, NGs can help detect traffic ways, monitor vehicle health, and manage street intersections. We hope that incorporation of NGs into transportation systems results in boosting the next autonomous, safe, and efficient transportation system, as well as the vision of carbon-neutral and zero-death transportation.

4. Conclusion

In this chapter, we discussed nanogenerators (NGs). We first described the concept of NGs and reviewed their historical evolution. We found that NGs can be used in two major areas: (1) electrical power production and (2) sensing. Having the ability to generate energy from environmental sources, NGs are self-powered devices that can provide energy for themselves and other components of the system, thereby reducing the system's dependence on batteries. Next, we introduced four main categories of NGs, including PENGs, TENGs, ThNGs, and PyNGs, and briefly described their principles, hybrid structures, and applications. By surpassing other renewable energy technologies, NGs are very promising for system miniaturization and integration, design and manufacture of self-powered devices, and biological applications. Finally, although challenges remain, the trajectory of research and innovation strongly indicates that NGs will play an important role in building the future of portable, wearable, and energy-autonomous technologies.

Conflict of interest

The author declares no conflict of interest.

Author details

Shahab Ahmadi Seyedkhani
Sharif University of Technology, Tehran, Iran

*Address all correspondence to: ahmadi.sh67@yahoo.com

References

[1] Wang ZL, Song J. Piezoelectric nanogenerators based on zinc oxide nanowire arrays. Science (80–). 2006;**312**:242-246. DOI: 10.1126/science.1124005

[2] Fan F-R, Tian Z-Q, Wang ZL. Flexible triboelectric generator. Nano Energy. 2012;**1**:328-334

[3] Jean F, Khan MU, Alazzam A, Mohammad B. Advancement in piezoelectric nanogenerators for acoustic energy harvesting. Microsystems & Nanoengineering. 2024;**10**:197. DOI: 10.1038/s41378-024-00811-4

[4] Chen B, Feng Z, Yao F-Z, Zhang M-H, Wang K, Wei Y, et al. Flexible piezoelectrics: Integration of sensing, actuating and energy harvesting. npj Flexible Electronics. 2025;**9**:58. DOI: 10.1038/s41528-025-00432-5

[5] Zhang T, Liang H, Wang Z, Qiu C, Peng YB, Zhu X, et al. Piezoelectric ultrasound energy-harvesting device for deep brain stimulation and analgesia applications. Science Advances. 2025;**8**:eabk 0159. DOI: 10.1126/sciadv.abk0159

[6] Wang S, Lin L, Wang ZL. Nanoscale triboelectric-effect-enabled energy conversion for sustainably powering portable electronics. Nano Letters. 2012;**12**:6339-6346. DOI: 10.1021/nl303573d

[7] Cheng T, Shao J, Wang ZL. Triboelectric nanogenerators. Nature Reviews Methods Primers. 2023;**3**:39. DOI: 10.1038/s43586-023-00220-3

[8] Jaziri N, Boughamoura A, Müller J, Mezghani B, Tounsi F, Ismail M. A comprehensive review of thermoelectric generators: Technologies and common applications. Energy Reports. 2020;**6**:264-287. DOI: 10.1016/j.egyr.2019.12.011

[9] Zhang Q, Deng K, Wilkens L, Reith H, Nielsch K. Micro-thermoelectric devices. Nature Electronics. 2022;**5**:333-347. DOI: 10.1038/s41928-022-00776-0

[10] Lheritier P, Torelló A, Usui T, Nouchokgwe Y, Aravindhan A, Li J, et al. Large harvested energy with non-linear pyroelectric modules. Nature. 2022;**609**:718-721. DOI: 10.1038/s41586-022-05069-2

[11] Pandya S, Velarde G, Zhang L, Wilbur JD, Smith A, Hanrahan B, et al. New approach to waste-heat energy harvesting: Pyroelectric energy conversion. NPG Asia Materials. 2019;**11**:26. DOI: 10.1038/s41427-019-0125-y

[12] Prasanna APS, Anithkumar M, Kim S-J. Hybrid triboelectric nanogenerators: Revolutionizing the energy harvesting through material diversity and device architecture for different applications. Nano Energy. 2024;**131**:110253. DOI: 10.1016/j.nanoen.2024.110253

[13] Hussain SZ, Singh VP, Bin Sadeque MS, Yavari S, Kalimuldina G, Ordu M. Piezoelectric-triboelectric hybrid nanogenerator for energy harvesting and self-powered sensing applications. Small. 2025:2504626. DOI: 10.1002/smll.202504626

Chapter 2

Principles and Working Mechanisms of Nanogenerators

Mahdi Zekavat, Fahimeh Zamanpour, Shahab Ahmadi Seyedkhani, Raheleh Mohammadpour and Azam Irajizad

Abstract

This chapter introduces the foundational principles, classifications, and emerging applications of nanogenerators—innovative energy harvesting systems that convert ambient mechanical, thermal, and environmental stimuli into electrical energy at the micro- and nanoscale. The discussion encompasses four primary types of nanogenerators: piezoelectric, pyroelectric, thermoelectric, and triboelectric, each based on distinct physical phenomena such as mechanical deformation, temperature fluctuation, thermal gradients, and contact electrification, respectively. The working mechanisms, material considerations, and operational characteristics of each category are systematically reviewed, providing a comprehensive overview of their functional diversity and technological significance. Furthermore, the chapter outlines the broad spectrum of nanogenerator applications in energy harvesting, biomedical systems, environmental monitoring, robotics, health care, and catalysis. Special emphasis is given to the role of hybrid nanogenerator architectures that integrate multiple energy transduction modes to enhance performance and multifunctionality. This introductory chapter sets the stage for subsequent in-depth discussions, positioning nanogenerators as a cornerstone in the development of self-powered electronic systems and sustainable energy solutions for next-generation technologies.

Keywords: piezoelectric, pyroelectric, thermoelectric, triboelectric, energy harvesting, hybrid nanogenerators

1. Introduction

The rapid advancement of micro- and nanotechnologies has necessitated the development of sustainable, miniaturized, and efficient energy sources capable of powering small-scale electronic devices. Among the most promising solutions to this challenge is the class of energy conversion devices known as nanogenerators. Nanogenerators are micro- to nanoscale systems designed to harvest ambient mechanical, thermal, and electromagnetic energy from the environment and convert it into usable electrical energy. Their compactness, scalability, and compatibility with flexible and wearable electronics have made them an essential component in the era of

self-powered nanosystems and the Internet of Things (IoT). Nanogenerators function by utilizing various physical effects to transduce energy, including piezoelectricity, pyroelectricity, thermoelectricity, and triboelectricity. These mechanisms stem from fundamental interactions between materials and their environment, often relying on deformation, temperature gradients, or surface charge transfer. Each nanogenerator type offers unique advantages and operating principles that cater to specific energy harvesting scenarios and application requirements.

2. Piezoelectric nanogenerators

2.1 Fundamentals of piezoelectric nanogenerators

Piezoelectric Nanogenerators (PENGs) operate based on the piezoelectric effect, which was first discovered by Pierre and Jacques Curie in 1880 [1]. The term piezoelectricity is derived from two words: piezo, meaning "pressure" or "stress", and electricity, referring to electric charge generated by electron movement [2]. The effect depends on the piezoelectric materials' non-centrosymmetric crystal structure, enabling them to create electric polarization in response to mechanical stress. When mechanical stress is applied, it displaces the internal charge centers from their equilibrium positions. This displacement causes charge separation and creates an internal electric field. As a result, electrons flow through an external circuit to restore equilibrium, effectively converting mechanical energy into electrical energy. Alternatively, when an electric field is applied to piezoelectric materials, they respond by physical deformation—a behavior referred to as the inverse piezoelectric effect [1]. For instance, zinc oxide (ZnO) exhibits piezoelectric properties due to its non-centrosymmetric tetrahedral crystal structure, specifically in the wurtzite phase. Its structure consists of alternating layers of Zn^{2+} and O^{2-} ions, each coordinated tetrahedrally with lattice parameters a = 0.3296 and c = 0.52065 nm. However, the four Zn–O bonds are not equal in length—the bond along the c-axis is longer than the other three. This structural asymmetry disturbs the charge distribution, resulting in a net dipole moment along the c-axis. When external pressure is applied—such as at the corner of the tetrahedron—the relative positions of the Zn^{2+} cations and O^{2-} anions shift further, enhancing the dipole moment. If all tetrahedra in the crystal are aligned in the same direction, this results in a macroscopic polarization, giving rise to the piezoelectric effect [3, 4]. **Figure 1** shows the working mechanism of the PENGs and the key factors of PENG output performance.

The piezoelectric effect is described by the following equations, which define the relationship between mechanical and electrical quantities:

$$\sigma_p = c_{pq}\ \varepsilon_q - e_{kp}E_k \tag{1}$$

$$D_i = e_{iq}\ \varepsilon_q - \kappa_{iK}E_k \tag{2}$$

Here, E_k represents the electric field, D_i is the electric displacement, σ_p denotes the stress tensor, and ε_q is the strain tensor. The term c_{pq} refers to the elastic modulus tensor, e_{kp} is the piezoelectric tensor, and κ_{iK} represents the dielectric tensor [5].

Naturally occurring materials—like quartz, Rochelle salt, topaz, and the tourmaline group—deliver intrinsic piezoelectric response; however, their brittleness, processing challenges, and limited supply hinder their large-scale utilization [6, 7].

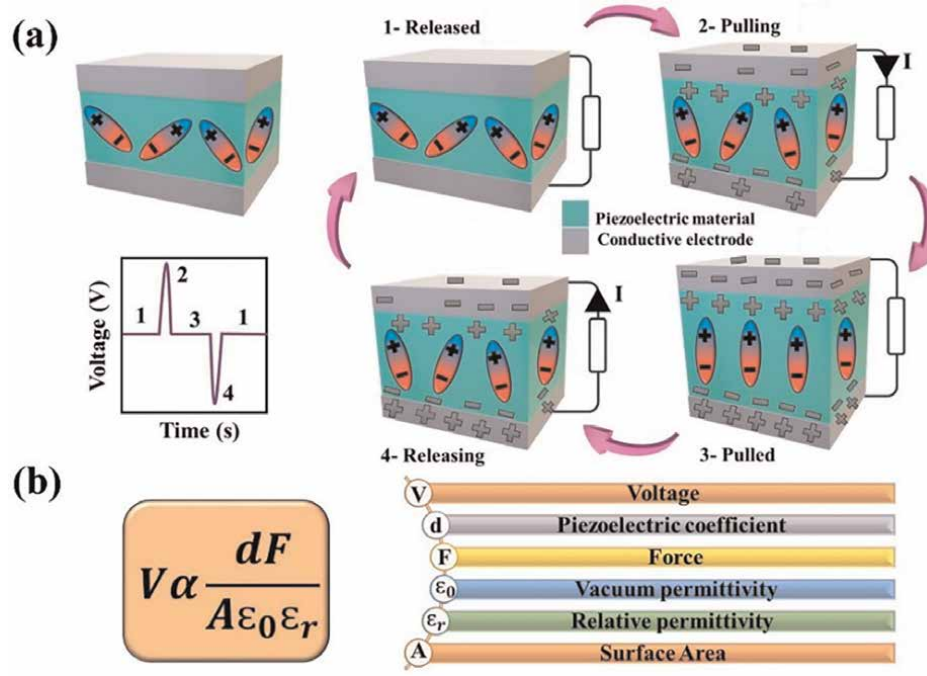

Figure 1.
(a) Working principle of piezoelectric nanogenerator (PENG). (b) Key factors of PENG output performance.

Piezoelectric properties are primarily associated with ceramics, as these materials offer the greatest versatility thanks to their high stability, excellent piezoelectric response, and cost-effectiveness. Among these, piezoelectric materials that crystallize in the perovskite structure generally demonstrate a more pronounced piezoelectric effect than those with other crystal structures. Perovskite-type piezoceramics such as lead zirconate titanate (PZT), barium titanate ($BaTiO_3$), and lead titanate ($PbTiO_3$) are the most well-known members of this family, possessing the highest piezoelectric coefficients among various materials [8].

In many applications, it is essential that the material exhibit sufficient flexibility to withstand bending or tensile stresses while maintaining its original shape. Due to their inherent brittleness, ceramics face significant limitations under such conditions. In contrast, piezoelectric polymers present a highly suitable alternative, owing to their excellent flexibility, low density, and ease of shaping and processing [9, 10]. Since the pioneering discovery of the piezoelectric effect in polyvinylidene fluoride (PVDF) by Kawai in 1969, considerable attention has been directed toward the development and application of piezoelectric polymers. The piezoelectric coefficient observed in PVDF was found to be nearly ten times greater than that were reported for other polymers up to that time**.** PVDF is a semi-crystalline polymer that can exist in five major crystalline polymorphs, including α, β, γ, δ, and ε phases. Among them, the β-phase is primarily responsible for its piezoelectric behavior due to its zigzag all-trans (TTTT …) planar zigzag conformation. This configuration aligns the dipole moments of the C–F bonds in the same direction, resulting in a net polarization under mechanical stress [11, 12]. **Table 1** summarizes different piezoelectric materials and their characteristics.

Family/ Class	Examples	Advantages	Limitations	References
Natural Polymers	Quartz, Rochelle salt, Topaz, Tourmaline group;	Environmentally benign, lead-free, and intrinsically biocompatible	low piezoelectric modulus, brittleness, processing challenges, and limited supply	[6, 7, 13]
Wurtzite-structure ceramics	ZnO, aluminum nitride (AlN),	Non-toxicity, earth abundant	Temperature-dependent performance, fabrication and scalability limits, and polarization fatigue issues	[14]
Lead-based perovskite	PZT ($Pb[Zr,Ti]O_3$), $BaTiO_3$, $PbTiO_3$	• High stability • Strong piezoelectric response • Cost-effective	Brittle (poor flexibility under bending/tension), environmental and health issues due to Pb	[8–10, 15]
Lead-free perovskites	BaTiO3, Potassium Sodium Niobate (KNN)-based material ($K_{0.5}Na_{0.5}NbO_3$), Bismuth Sodium Titanate (BNT-BKT);	• High stability • Strong piezoelectric response	processing complexity	[8–10, 15]
Piezoelectric polymers	PVDF and P(VDF-TrFE)	• Flexible • Low density • Easy shaping/ processing	Lower piezoelectric coefficient compared to ceramics	[9–12]

Table 1.
Different piezoelectric materials and their properties.

2.2 Piezoelectric nanogenerators applications

Due to the advantages of PENGs, including simple structure, low cost, environmental compatibility, scalability, safety, portability, and suitable power density, much attention has been drawn to these systems for attractive and unique applications [16]. These applications are categorized into the fields of energy supply [17] (harvesting of motion, vibration, wind, wave etc.), health care [18] (measuring heart rate and blood pressure etc.), human-machine interaction [19], and various types of sensors [20] (chemical, position sensing etc.) for daily life, factories, space, and transportation [21]. Many examples of applications are detailed below. **Figure 2** illustrates different applications of PENGs.

Sensing: Researchers fabricated a piezoelectric device with a sandwich structure based on Nafion, polyvinylidene fluoride (PVDF), silver, and carbon tape that can generate electrical energy and detect mechanical vibrations. In addition to lighting up many LEDs, the nanogenerator is capable of recognizing words when attached to the throat, as well as detecting rest and overwork states when placed on the wrist (**Figure 2**) [22].

Health care: Dagdeviren et al. developed a piezoelectric-based device capable of measuring and monitoring arterial pressure, including materials such as lead zirconate titanate (PZT), polyimide, platinum, silicone, gold, and metal oxides. Measuring the radial artery and examining it will be very helpful in the areas of health monitoring and prevention of cardiovascular diseases with the help of this research [18].

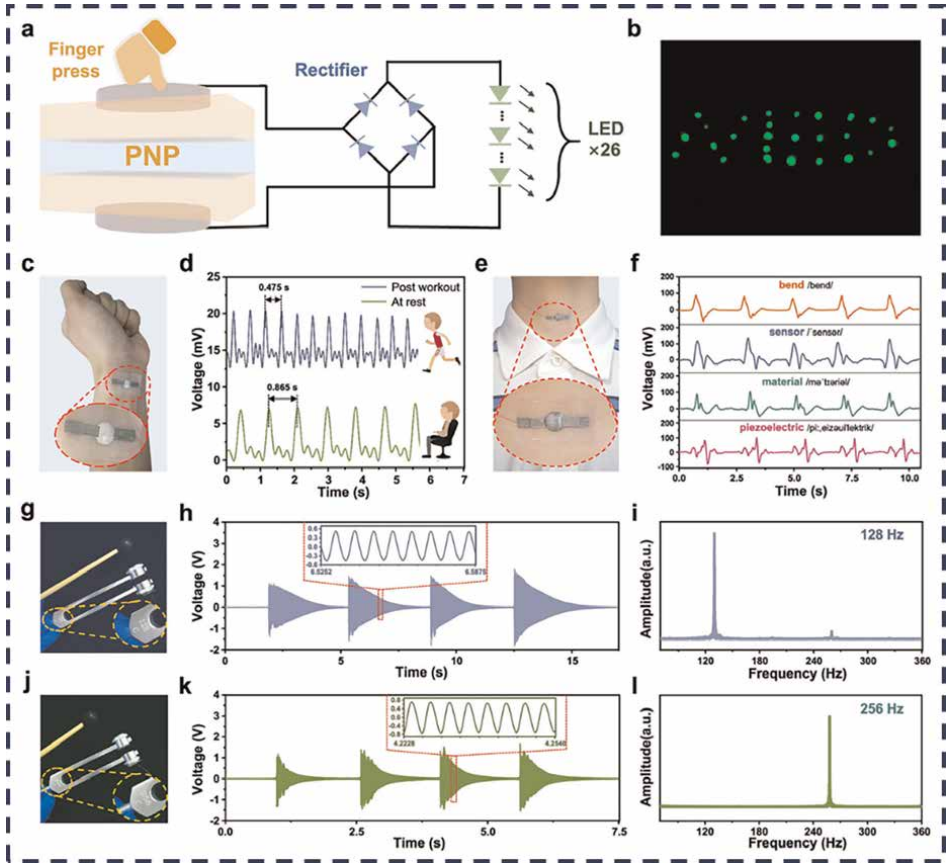

Figure 2.
Piezoelectric nanogenerators applications. (a) Schematic image of the designed circuit connected to the device to light the LEDs. (b) Displaying and writing the word "NED" using LEDs. (c) Wrist-attached piezoelectric nanogenerator. (d) Different electrical signals produced at rest and during high-intensity exercise. (e) Connecting the device to the throat. (f) Differences in the shape of voltage signals produced by pronouncing different words. (g) Piezoelectric coupling to the diapason at a frequency of 128 Hz. (h) Voltage-time plot. (i) The plot of the frequency-domain (with Fast Fourier Transform). (j) Piezoelectric coupling to the diapason at a frequency of 256 Hz. (k) Voltage-time plot. (l) The plot of frequency-domain (with Fast Fourier Transform) [22]. Reproduced by permission from Nature, licensed under a Creative Commons Attribution 4.0 International License, http://creativecommons.org/licenses/by/4.0/.

Energy harvesting: Ren's group made a flexible piezoelectric generator composed of polydimethylsiloxane (PDMS), PZT, and interdigital electrodes (IDEs) that can produce high-power electrical energy. This system shows an excellent power density of 63.5 mW/cm^3 that can turn on many LEDs and power portable electronics [17].

3. Pyroelectric nanogenerators

3.1 Principles and concepts of pyroelectric nanogenerators

Temperature fluctuations in certain polar materials lead to changes in their spontaneous polarization, a phenomenon known as the pyroelectric effect. In this context, the fluctuations refer to temporal variations in temperature [23, 24]. As long as the

temperature remains constant, the random fluctuation of each electric dipole does not contribute to a net change in the spontaneous polarization. With increasing temperature, the amplitude of thermal vibrations of the dipoles increases, leading to a disruption in their alignment. Therefore, the net spontaneous polarization of the material decreases. This reduction in net polarization results in a decreased number of free charges bound to the surface of the material. Under short-circuit conditions, an electric current flows between the material's two polar surfaces to counteract the change in population of bound charge. Similarly, if the material is cooled rather than heated, a pyroelectric current will still be generated, but it will flow in the opposite direction [25, 26]. **Figure 3** shows the working principle of pyroelectric nanogenerators.

The relationship between pyroelectric current (i_p) and rate of temperature change (dT/dt) can be expressed as:

$$i_p = pA\frac{dT}{dt} \tag{3}$$

where p is the pyroelectric coefficient and A is the surface area. According to Eq. (3), the pyroelectric current is independent of the material's thickness [24]. The pyroelectric coefficient, p, is defined by:

$$p = E\frac{\partial \varepsilon}{\partial T} + \frac{\partial P_s}{\partial T} \tag{4}$$

Wherein, ε stands for the permittivity, E is the external electrical field, and P_s represents spontaneous polarization [23]. Under a constant stress and electric field, Eq. (4) can be written as:

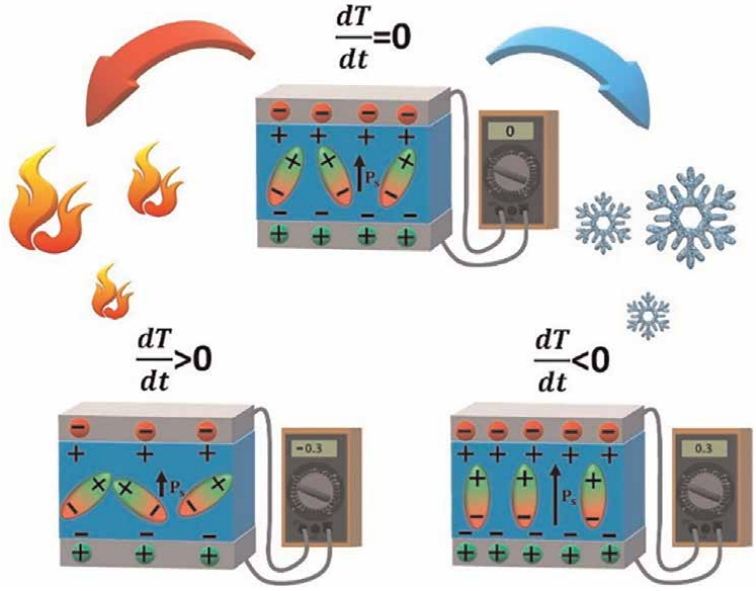

Figure 3.
Working mechanism of pyroelectric nanogenerators.

$$p = \left(\frac{\partial P_s}{\partial T}\right)_{\sigma,E} \tag{5}$$

Eq. (5) reveals that all pyroelectric materials are inherently piezoelectric because they must exhibit a level of polarization [27, 28].

The wide range of applications for pyroelectric materials and the varying performance requirements associated with them have led to the development of multiple figures-of-merit (FOMs). When detecting temperature changes through pyroelectric current, the maximum current response per unit of thermal energy input is achieved under closed-circuit conditions [28, 29]. The relevant FOMs can be expressed as:

$$F_i = \frac{p}{\rho c_p} \tag{6}$$

where c_p and ρ are the specific heat capacity (J.kg^{-1}. K^{-1}) and the density (kg. m^{-3}) of the pyroelectric material, respectively.

The pyroelectric response to thermal fluctuations can also be quantified by measuring the open-circuit voltage as a function of temperature change. In this scenario, the objective is to maximize the voltage generated per unit of heat input under open-circuit conditions [30]. Accordingly, the relevant FOMs can be represented as:

$$F_V = \frac{p}{\rho c_p \varepsilon^{\sigma}_{\ni\ni}} \tag{7}$$

Where $\varepsilon^{\sigma}_{\ni\ni}$ refers to the permittivity evaluated under conditions of constant stress [30].

However, in energy harvesting applications, the key performance metrics include the amount of converted energy, output power, and conversion efficiency from thermal to electrical energy. Accordingly, the electrothermal coupling factor (k) has been introduced to evaluate the efficiency of thermal energy harvesting under temperature cycling conditions between two distinct temperature levels, as expressed by Eq. (8):

$$k^2 = \frac{p^2 T_{hot}}{\rho c_p \varepsilon^{\sigma}_{\ni\ni}} \tag{8}$$

where T_{hot} stands for the maximum operating temperature during the thermal cycling process [28, 29]. Another FOM for pyroelectric energy harvesting (PyEH) has also been proposed and is defined as follows:

$$F_E = \frac{p^2}{\varepsilon^{\sigma}_{\ni\ni}} \tag{9}$$

It is important to note that F_E does not take into account the heat capacity [28, 29]. To consider the effect of heat capacity, a modified version of Eq. (9) can be proposed as Eq. (10):

$$\frac{p^2}{\varepsilon^{\sigma}_{\ni\ni} p^2 c_p^2} \tag{10}$$

The triglycine sulfate ($(NH_2CH_2COOH)_3H_2SO_4$) family of isomorphous compounds is one of the most well-known pyroelectric materials. It has been utilized in

Family/Class	Key examples	Main advantages	Main limitations/ Concerns	References
Triglycine sulfate (TGS) family	$(NH_2CH_2COOH)_3H_2SO_4$ and isomorphs	Excellent pyroelectric figures-of-merit for IR detectors	Low TC; poor mechanical strength; not suited for high-temperature energy harvesting	[31]
Lead-based perovskite ceramics (PZT family)	$Pb(Zr,Ti)O_3$ (soft and hard PZT grades)	Mature processing, large pyroelectric coefficients, robust	Contains toxic Pb → environmental/ health issues	[32]
Lead-free perovskite ceramics	KNN ($K_{0.5}Na_{0.5}NbO_3$), $BaTiO_3$, $Bi_{0.5}Na_{0.5}TiO_3$ (BNT), $LiTaO_3$	Lead-free, tunable compositions, comparable performance to PZT	Still lower FOM than optimized PZT; processing complexity	[25]
Polymeric pyroelectrics	PVDF and P(VDF-TrFE) copolymers	Outstanding mechanical flexibility, lightweight, ease of fabrication	Lower pyroelectric coefficient vs. ceramics; limited temperature range	[33]

Table 2.
Different pyroelectric materials and their properties.

the production of pyroelectric detectors since 1996. Despite its excellent FOMs, the triglycine sulfate has not been widely adopted for energy harvesting applications, potentially due to its low Curie temperature of 49°C and poor mechanical properties [31]. Another important and widely utilized class of pyroelectric materials is the lead zirconate titanate (PZT) family of ceramics [32]. These classes of materials are valued for their straightforward fabrication process and superior pyroelectric performance, which has drawn considerable interest [24]. Nevertheless, the inclusion of lead in their structure raises environmental and health concerns, prompting extensive research into the development of lead-free perovskite ceramic materials as viable alternatives. Potassium sodium niobate (KNN), lithium tantalite ($LiTaO_3$), barium titanate ($BaTiO_3$), and bismuth sodium titanate (NBT or BNT) based structures are among these materials [25]. Moreover, the outstanding mechanical properties of polymeric materials have spurred significant interest in polymeric pyroelectrics such as PVDF [33]. **Table 2** shows different pyroelectric materials and their properties.

3.2 Pyroelectric nanogenerators applications

Theophrastus found the pyroelectric effect, electricity production in temperature gradients, in the fourth century BC [34, 35]. Many unique properties are considered for pyroelectrics, such as operation at room temperature, cost-effectiveness, compactness, do not need a cooling system, and are pollutant-free [36, 37]. Electrical energy generation [38], sensing [39] (thermal, motion, light, etc.), and pyro-catalysis [40] (hydrogen production, sterilization, etc.) are the most overriding applications of pyroelectric, which are explained by providing examples.

Energy harvesting: A flexible pyroelectric nanogenerator including lead zirconate titanate (PZT) nanoparticles/liquid crystalline elastomer (LCE) composite was developed by Li and colleagues. The electrical output was increased by secondary pyroelectricity that was produced from thermal stress applied to the elastomer. The

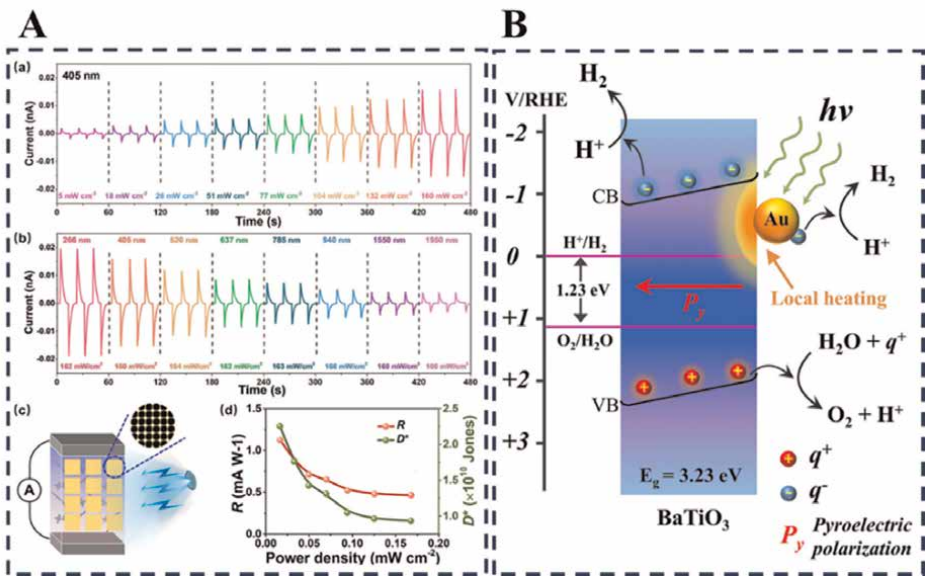

Figure 4.
Pyroelectric nanogenerators applications. Panel A: Changes in current-time curves as a result of (a) different power density at 405 nm. (b) different wavelength (266–1950 nm) of the laser. (c) Fabrication of the crystal device by gold sputtering. (d) Photodetection under low light power density (at 405 nm) [39]. Panel B: Pyro-catalytic hydrogen production by $BaTiO_3$/Au nanoparticles activated through heating of surface plasmon [40]. Reproduced by permission from Nature, licensed under a Creative Commons Attribution 4.0 International License, http://creativecommons.org/licenses/by/4.0/.

generator with a voltage of 6.23 V and current of 2.81 nA (at a heat rate of 0.20 K/s) can power electronic systems and turn on LEDs [38].

Sensing: Zeng et al. introduced a molecular pyroelectric with great polarization and a high pyroelectric coefficient, as illustrated in **Figure 4A**. This simple organic material, N-isopropylbenzylaminium trifluoroacetate (N-IBATFA), with its wide photo-pyroelectric property, can detect photocurrents from ultraviolet to near-infrared. So, it overcomes the limitation of absorption of different lights and enables self-powered wide detection of the light spectrum [39].

Pyro-catalysis: You and coworkers coupled thermal plasmonic metal: gold nanoparticle with pyro-catalytic: coral-like barium titanate ($BaTiO_3$) nanoparticles for effective hydrogen production. In fact, through the use of localized plasmonic heat sources, the material with pyro-catalytic property is heated efficiently without losing much energy to the environment. This increases the reaction rate for productive hydrogen generation. This research illuminates a bright future for applications such as clean energy generation, sterilization, and water/air purification [40]. **Figure 4B** shows the hydrogen production mechanism based on the pyro-catalytic process.

4. Thermoelectric nanogenerators

Humans rely on various sources to meet their daily energy needs, but a substantial amount is inevitably dissipated as waste heat, which is a common aspect of both industrial operations and everyday activities. Fortunately, thermoelectric materials offer a promising alternative by enabling the recovery of some of the wasted heat and converting it into electrical energy [41, 42].

4.1 Working mechanism and fundamentals of thermoelectric nanogenerators

Thermoelectric technology harnesses three fundamental phenomena—the Seebeck, Peltier, and Thomson effects—to enable direct conversion between thermal and electrical energy [43]. **Figure 5** shows these different thermoelectric effects.

The most well-known of these, the Seebeck effect, was discovered in 1821 by Thomas Johann Seebeck and occurs when two dissimilar conductors or semiconductors are joined in a closed circuit with their junctions maintained at different temperatures. As charge carriers (electrons or holes) diffuse from the hot to the cold region due to the temperature gradient, the difference in electron mobility between materials creates an asymmetric charge distribution, which results in a potential difference across the two open ends. The correlation between the temperature difference and the potential difference could be described as:

$$S_{ab} = \frac{\Delta V}{\Delta T} \tag{11}$$

where, S is the relative Seebeck coefficient between materials a and b, V is the thermoelectric voltage, and T is temperature [45].

The most crucial performance metric for thermoelectric devices is their conversion efficiency, which quantifies their effectiveness in both power generation and cooling operations. This parameter serves as a comprehensive indicator of a device's ability to convert thermal energy into electrical energy (or vice versa) while minimizing energy losses. The practical thermoelectric (TE) conversion efficiency of a thermoelectric generator (TEG) is expressed by the following equation:

$$\eta = \frac{\mathrm{P}}{\mathrm{Q}_h} \tag{12}$$

where P denotes the useful power output (electrical energy delivered to the load), and Q_h signifies the thermal energy input (heat absorbed at the hot junction) [46].

Theoretically, the maximum energy conversion efficiency could be described as:

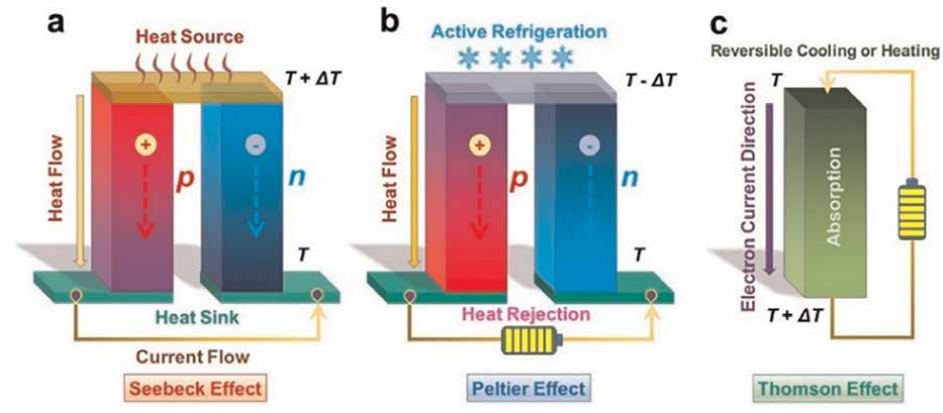

Figure 5.
Thermoelectric effects. Schematic diagrams of (a) the Seebeck effect for power generation, (b) the Peltier effect for refrigeration, and (c) the Thomson effect for reversible cooling or heating [44]. Reproduced by permission from American Chemical Society.

$$\eta_{max} = \frac{(T_H - T_C)}{T_H} \frac{\sqrt{1 + ZT_{avg}} - 1}{\sqrt{1 + ZT_{avg}} + \frac{T_H}{T_C}} \tag{13}$$

$$T_{avg} = \frac{T_H + T_C}{2} \tag{14}$$

where T_H represents the temperature at the hot side, while T_C denotes the corresponding cold-side temperature. Eq. (13) illustrates that the maximum energy conversion efficiency depends only on the temperature gradient between the two sides of the device and thermoelectric figure of merit ZT [45, 46].

The ZT is a dimensionless parameter that quantifies the efficiency of a material in converting heat into electrical energy (or vice versa) through the thermoelectric effect. It is represented by the following equation:

$$ZT = \frac{\sigma \times S^2}{\kappa} \tag{15}$$

where, σ stands for electrical conductivity, while κ represents thermal conductivity [45, 46].

To develop thermoelectric materials with enhanced performance, it is essential to increase both the electrical conductivity and the Seebeck coefficient, while at the same time reducing the thermal conductivity. Metals are limited in thermoelectric applications because electrons act as the carriers for both electrical and thermal conductivity; consequently, as electrical conductivity increases, thermal conductivity also rises. Insulating materials are likewise unsuitable for such applications owing to their inherently poor electrical conductivity. Since electrical conductivity in semiconductors is carried by electrons and holes, and thermal conductivity occurs mainly through phonons, it is possible in some semiconductors to achieve an optimal balance between these two processes by engineering the band structure and controlling phonon scattering [47].

Quantum confinement emerges when the physical dimensions of a material approach the electron's de Broglie wavelength in one or more directions. This spatial restriction imposes boundary conditions on the electron wavefunctions, leading to quantization and discretization of the energy states. As a result, the distribution of electrons within the energy bands becomes more localized, which intensifies the difference in electron density caused by the temperature gradient. Therefore, low-dimensional materials tend to have a higher Seebeck coefficient compared to the bulk material [48].

4.2 Materials for thermoelectric nanogenerators

Since thermoelectric properties exist to some extent in many materials, a wide range of substances have been developed for such applications. These include traditional chalcogenides [41] as well as more complex systems like skutterudites [49], half-Heusler alloys [50], Zintl phases [15, 51], and even oxide-based materials [52]. For example, Chalcogenide compounds like Bi_2Te_3 and PbTe have long been known to possess the highest ZT values near room temperature. Nonetheless, the potential toxicity of tellurium and lead remains a major obstacle to the widespread use of these materials [41]. Despite their high electrical conductivity, many binary skutterudites suffer from relatively high thermal conductivity at room temperature, which

significantly hinders their thermoelectric efficiency [49]. Half-Heusler (HH) alloys are recognized for their applicability in mid to high temperature thermal to electric energy conversion. These compounds demonstrate a combination of desirable properties, including a pronounced Seebeck coefficient, moderate levels of electrical resistivity, scalability, and exceptional thermal stability [50]. Zintl phase thermoelectrics, as another class of lead-free materials, include compounds such as Mg_3Sb_2 and $Yb_{10}MgSb_9$, which attain peak *ZT* values comparable to those of the highest-performing skutterudites and half-Heuslers. However, many Zintl antimonides are brittle, restricting them to small, planar pellets and increasing fracture risk during module fabrication [15, 51]. **Table 3** categorizes different thermoelectric materials.

4.3 Thermoelectric nanogenerators applications

Thermal energy is wasted abundantly in spaces such as homes, outdoors, factories, etc. It can be converted into usable electrical energy by the thermoelectric effect [53]. By creating a temperature difference between two conductive or semi-conductive components, a potential difference will be created because of the Seebeck effect [54]. Many applications for thermoelectric generators have been envisioned due to their advantages, including low cost, ability to produce energy continuously, simplicity, long life, no need for moving parts, portability, and environmental friendliness [55–57]. Applications including sensing [58] (temperature, radiation etc.) and electrical energy supply [59] by harvesting thermal energy from the human body, sun, factories, cars, spacecraft, space probes, etc. were proposed [54]. Some TEG applications have been presented in **Figure 6**.

Energy harvesting: Shen et al. designed a thermoelectric generator to convert thermal energy into electricity. The materials used in this research were: hydrogel ion thermoelectric cells of P-type and N-type, graphite paper electrode, and a heating plate. From this structure, a power of 85 μW and a voltage of 1.8 V have been obtained by connecting 10 pairs (N and P types). This thermoelectric generator (TEG) offers a

Family/Class	Examples	Principal Pros	Principal Cons/ Concerns	References
Traditional chalcogenides	Bi_2Te_3, PbTe, SnSe, Bi_2Se_3	Highest *ZT* near room temperature; mature processing	Toxicity of Te & Pb; scarcity of Te	[41]
Skutterudites	$CoSb_3$, $FeSb_3$, filled skutterudites (e.g., $Yb_{0.3}Co_4Sb_{12}$)	Good electrical conductivity	Intrinsically high lattice κ at room *T*; complex synthesis	[49]
Half-Heusler (HH) alloys	TiNiSn, ZrCoSb, HfFeSb	High Seebeck, excellent thermal stability, scalable casting, oxidation-resistant	Still modest *ZT* (≈ 1); needs nano-structuring to suppress κ	[50]
Zintl phases	$Yb_{0.4}MnSb_{11}$, $Ca_5Al_2Sb_6$, Mg_3Sb_2	Low κ *via* complex crystal structure; earth-abundant elements	Brittleness, reproducibility issues	[15, 51]
Oxide-based materials	$Ca_3Co_4O_9$, $SrTiO_3$, ZnO, In_2O_3	Chemically stable in air, non-toxic, high-temperature operation	Lower *ZT* (0.2–0.5) due to high κ and/or low mobility	[52]

Table 3.
Different thermoelectric materials and their characteristics.

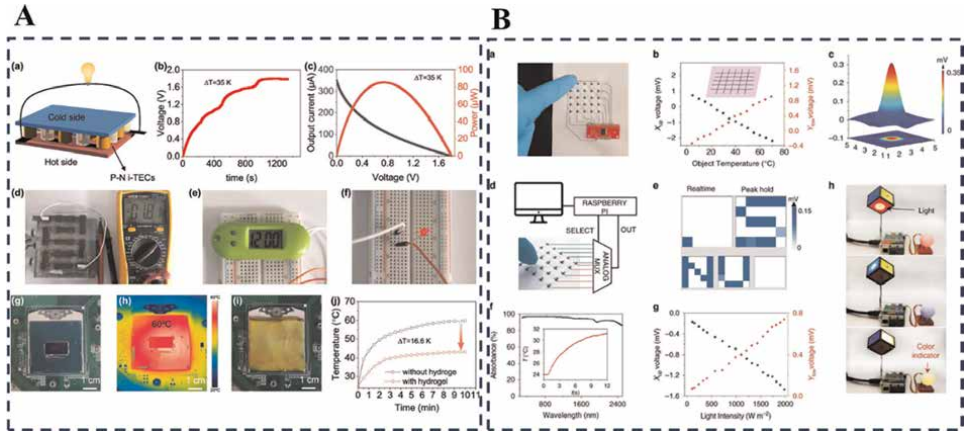

Figure 6.
Thermoelectric nanogenerators applications. Panel A: (a) Final structure layout. (b) and (c) Output Voltage, current, and power of 10 pairs of N/P types. (d) Flexible TEG working with temperatures of 25°C and 60°C. (e) and (f) powering the electronic watch and the LED. (g) and (h) Normal and thermal images of the central processing unit (CPU). (i) Device connected to the CPU for cooling and energy generation. (j) CPU temperature changes with/without using the hydrogel-based system [60]. Panel B: (a) Touch panel consists of thermoelectric fibers. (b) Signals of the fibers by contacting objects with different temperatures. (c) Measured signal as the result of touching by a finger (node (3,3)). (d) Designed circuit of the panel. (e) Written "NUS" on the panel. (f) The absorbance curve of a (SWCNT/PVA) fiber. (g) Measured signal as the result of irradiating with light at different intensities. (h) Sensing light direction [58]. Reproduced by permission from Nature, licensed under a Creative Commons Attribution 4.0 International License, http://creativecommons.org/licenses/by/4.0/.

great potential in energy harvesting of low-level heat and powering electrical systems (**Figure 6A**) [60].

Sensing: Ding and colleagues built resistant and flexible thermoelectric fibers for harvesting thermal energy and performing sensing. Thermoelectric fibers were produced under an alternating extrusion process from materials such as polyvinyl alcohol (PVA) hydrocolloids and single-walled carbon nanotubes (SWCNTs). By weaving N/P-type thermoelectric fibers into fabrics, this system, in addition to harvesting thermal energy and converting it into electricity, is capable of sensing light and recognizing the touched arrays on the panel (**Figure 6B**) [58].

5. Triboelectric nanogenerators

5.1 Fundamentals of triboelectric effect

Although the phenomenon of triboelectricity has been recognized for over 2600 years, the underlying mechanism—whether contact electrification results from ionic transfer, electronic transfer, or the movement of specific material species—remains a subject of ongoing debate and controversy. Contact electrification is a ubiquitous physical phenomenon occurring across all phase interfaces, including solid-solid, solid-liquid, liquid-liquid, liquid-gas, gas-gas, and gas-solid interactions. Understanding the mechanism of contact electrification is critically important for advancing knowledge in physics, chemistry, and biology [61–63].

It has been demonstrated that electron transfer is the dominant mechanism in contact electrification between solids. The interaction between a dielectric and a metal can be effectively described using the surface states model for dielectrics and the Fermi

level model for metals. When the distance between two materials exceeds the typical bond length, the atoms tend to attract one another. Experimentally, it has been shown that contact electrification occurs when the interatomic distance becomes shorter than the bond length and lies within the repulsive region of the interatomic potential [61–63].

To explain this electron transferring mechanism, the electron cloud overlap model has been proposed. According to this model, upon contacting electron clouds of two materials, a strong overlap of their electron clouds occurs, effectively reducing (or even eliminating) the potential barrier between the atoms, thereby facilitating electron transfer. Mechanical pressure is essential to decrease the interatomic spacing and maximize the overlap of the electron clouds. This model is considered a universal framework for understanding contact electrification between two materials and may be generalized to other types of contact electrification phenomena [61–63].

When two different materials come into contact through an external force, triboelectric charges are generated on their surfaces due to contact electrification. When the applied force is reduced, the materials separate, and the triboelectric charges induce a potential difference between the top and bottom electrodes. A physical model representing the working principle of TENGs is shown in **Figure 7**. As seen, in this state, the open-circuit voltage is denoted as V_{OC}. When a physical connection or a short-circuit condition is established, the induced potential difference leads to electron flow through the external circuit, resulting in an electric current. The short-circuit current in this can be indicated as I_{SC} [64, 65].

In TENGs, the strength of the electric field, based on Gauss's theory, in each region is described by Eqs. (16) and (17) for the air gap and a dielectric layer, respectively:

$$E = \frac{\sigma_0 - \frac{Q}{S}}{\varepsilon_0} \tag{16}$$

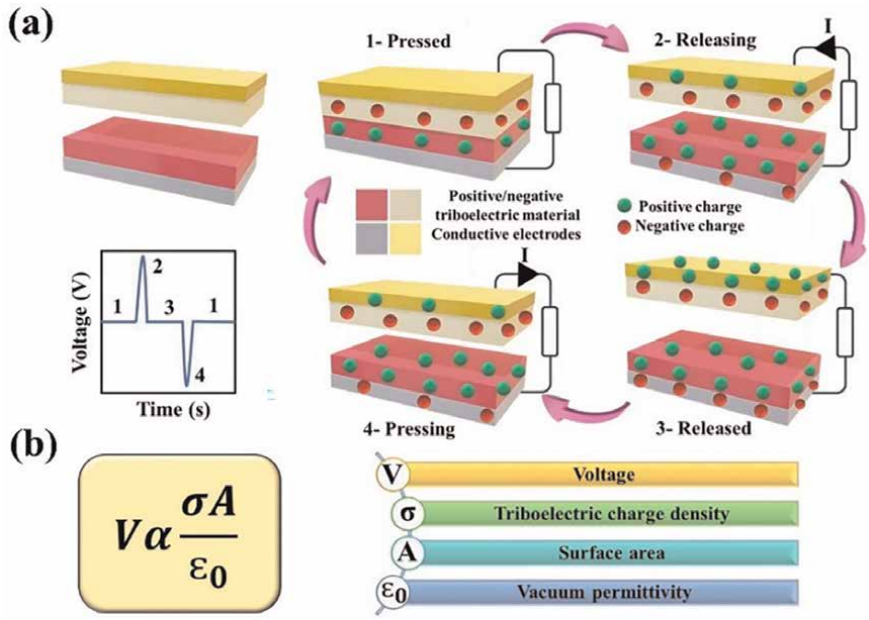

Figure 7.
(a) Working principle of triboelectric nanogenerator (TENG). (b) Key factors of TENG output performance.

$$E = \frac{Q}{\varepsilon\varepsilon_0 S} \tag{17}$$

where σ_0 is the charge density, ε_0 is the vacuum permittivity, Q is the amount of transferred charge, and ε is the relative dielectric constant of the dielectric layer.

The voltage between the two electrodes can be obtained using Eq. (18):

$$E = E_1 d_1 + E d_t \tag{18}$$

where d_1 and d_t represent the thickness of the dielectric layer and the thickness of the air gap, respectively [64, 65].

By substituting Eqs. (16) and (17) into Eq. (18), we obtain:

$$V = -\frac{Q}{\varepsilon_0 . S}\left(\frac{d_1}{\varepsilon_1} + d_t\right) + \frac{\sigma d_t}{\varepsilon_0} \tag{19}$$

Here, d_1 and d_t denote the thickness of the dielectric layer and the air gap, respectively. In the open-circuit condition, no current is transferred, indicating that Q is zero. In this case, V_{OC} is calculated using the following equation [64, 65]:

$$V_{OC} = \frac{\sigma d_t}{\varepsilon_0} \tag{20}$$

In the short-circuit condition, V equals zero. In this case, the transferred charge Q is given by:

$$Q = \frac{\sigma S d_t}{\frac{d_1}{\varepsilon_1} + d_t} \tag{21}$$

5.2 Working mechanism of TENGs

Figure 8 illustrates different TENG modes, including (i) contact-separation, (ii) sliding, and (iii) freestanding modes.

The contact-separation mode consists of two contact layers with different electronegativities in the middle of the device, each backed by an electrode. Initially, no charges are generated or induced. When the two surfaces come into physical contact, equal amounts of opposite charges are generated at the contact surface due to the triboelectric effect. The sign of the charge on each surface depends on its relative electronegativity. When the two surfaces are separated, a potential difference is generated, leading to a momentary flow of electrons from the bottom electrode to the top one, ultimately reaching equilibrium after full separation. When the surfaces come into contact again, the induced charges return through the external circuit to neutralize the electric potential difference created in the first state, eventually reducing the induced potential between the electrodes to zero [67–71].

On the other side, in sliding mode TENGs, when the triboelectric layers slide relative to each other, opposite charges are induced in the electrodes to maintain electrostatic balance, generating a potential difference. When the layers are in contact, electrons migrate between the electrodes. When the layers are no longer in contact, the induced charge in the electrode and the triboelectric layer reach electrostatic equilibrium, and no further electron transfer occurs. After sliding, the two layers

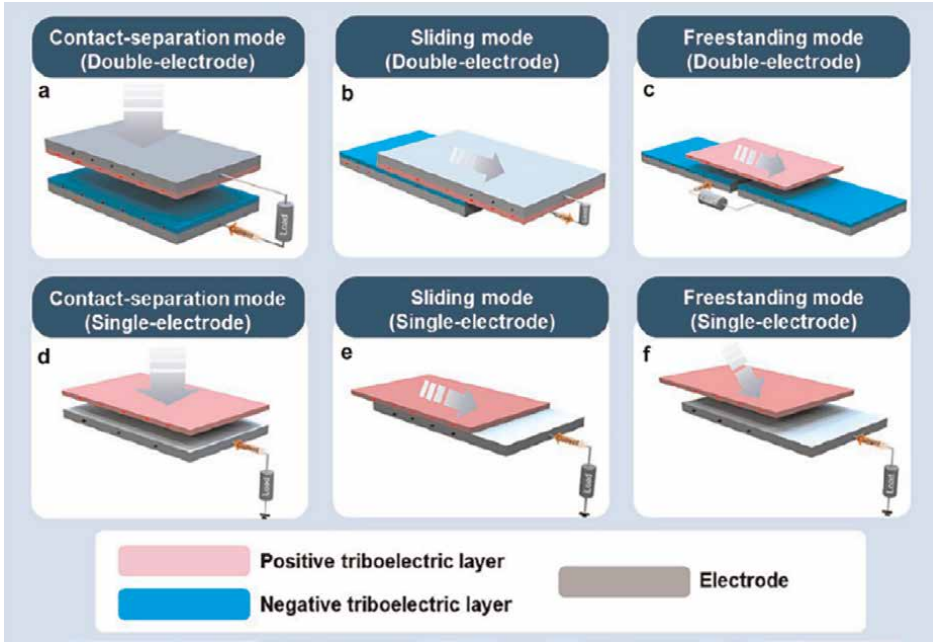

Figure 8.
Different TENG modes. (a) Contact-separation, (b) sliding, and (c) freestanding modes by double-electrode configuration. (d)–(f) represent the same modes of (a)–(c), respectively, in single-electrode configuration [66]. Reproduced by permission from American Chemical Society.

slowly reestablish contact, and electrons gradually flow until full contact is achieved and the electrode charges return to zero. This cycle repeats, generating an alternating current-like electrical output. The lateral sliding configuration is suitable not only for planar sliding but also for cylindrical, rotary, and other sliding types [67–71].

When substrates with different electronegativities come into contact, they become electrically charged. For certain materials, once surface charge saturation is reached upon contact, the static charge remains on the surface for a while. Through free-standing mode TENGs, the reciprocating motion of charged objects between two separate electrodes through friction leads to a varying potential difference, which causes a continuous electron flow between the electrodes [67–71].

The previously described operating modes involve two electrodes in contact. However, the single-electrode TENG mode (shown in **Figure 8(d-f)**) has only one electrode, which is grounded or connected to a reference electrode. Contact with the charged triboelectric layer and its approach or separation from the bottom electrode leads to changes in charge distribution on the electrode via the electrostatic induction principle. Thus, the potential difference between the electrode and the reference electrode varies continuously, driving the flow of free electrons and generating an electric current [67–71].

5.3 Triboelectric materials

Triboelectric materials encompass a wide range of substances, including polymers, inorganic compounds, metals, and semiconductors. The triboelectric series is an empirical ranking of materials based on their tendency to gain or lose electrons during

contact and separation [72]. Materials at the positive end of the series—such as glass, human hair, or polymers containing amino groups (e.g., PET, PA, PU)—readily lose electrons and become positively charged, while materials at the negative end, including fluoropolymers such as PTFE, FEP, and PVDF, strongly attract electrons and acquire negative charges due to the high electronegativity of fluorine [73, 74]. A material's position in the series is primarily governed by its surface chemistry and functional groups, which determine electron affinity and charge transfer. As shown in **Table 4**, this ranking provides valuable guidance for selecting effective triboelectric pairs, since combining materials from opposite ends maximizes charge density and enhances the output of triboelectric nanogenerators (TENGs) and other energy-harvesting systems [73, 74]. Nevertheless, triboelectric performance is also influenced by additional factors such as surface roughness, environmental conditions, and the intrinsic work function of materials, highlighting the importance of chemical

Materials	**Average TECD ($\mu C\ m^{-2}$)**	**STDEV**	**α**
Mica	61.80	1.63	0.547
Float glass	40.20	0.85	0.356
Borosilicate glass	38.63	1.18	0.342
BeO	9.06	0.21	0.080
PZT-5	8.82	0.16	0.078
Food-grade oil-resistant Buna-N/vinyl rubber	2.95	0.13	0.03
$MgSiO_3$	2.72	0.07	0.024
Oil-resistant Buna-N rubber	2.49	0.23	0.02
$CaSiO_3$	2.38	0.15	0.021
$Bi_4Ti_3O_{12}$	2.02	0.21	0.018
$Bi_{0.5}Na_{0.5}TiO_3$	1.76	0.05	0.016
$NiFe_2O_4$	1.75	0.07	0.0155
$Ba_{0.65}Sr_{0.35}TiO_3$	1.28	0.11	0.011
$BaTiO_3$	1.27	0.08	0.0112
PZT-4	1.24	0.12	0.011
ZnO	0.86	0.04	0.008
NiO	0.53	0.05	0.005
SnO_2	0.46	0.02	0.004
SiC	0.31	0.07	0.003
$CaTiO_3$	0.24	0.02	0.002
ZrO_2	0.09	0.07	0.001
Cr_2O_3	0.02	0.01	0.00013
Fe_2O_3	0.00	0.02	0.000
Al_2O_3	−1.58	0.14	−0.014
TiO_2	−6.41	0.18	-o.o57
Super-stretchable and abrasion-resistant natural rubber	−10.61	0.50	−0.09

Materials	Average TECD ($\mu C\ m^{-2}$)	STDEV	α
Wear-resistant slippery garolite	−11.47	0.50	−0.10
AlN	−13.24	1.35	−0.117
Wood (marine-grade plywood)	−14.05	0.99	−0.12
Delrin® Acetal Resin	−14.91	0.50	−0.13
BN	−16.90	0.97	−0.149
Chemical-resistant and low-temperature fluorosilicone rubber	−18.06	0.86	−0.16
Copy paper	−18.35	0.50	−0.16
Cast nylon 6	−18.35	0.99	−0.16
Polysulfone	−18.92	0.86	−0.17
Chemical- and steam-resistant Aflas rubber	−22.65	1.31	−0.20
Weather- and chemical-resistant Santoprene rubber	−25.23	0.50	−0.22
Slippery nylon 66	−26.09	0.50	−0.23
Polypropylene	−27.23	1.31	−0.24
Pigskin (smooth)	−30.10	0.86	−0.27
Poly(phenylene sulfide)	−31.82	0.86	−0.28
Noryl polyphenyl ether	−31.82	0.86	−0.28
Flexible leather strip (smooth)	−34.40	0.86	−0.30
High-temperature glass ceramic	−39.95	2.04	−0.353
Abrasion-resistant SBR rubber	−40.13	1.31	−0.35
Silicon	−47.30	1.49	−0.42
Clear cast acrylic	−48.73	1.31	−0.43
Oil-filled cast nylon 6	−49.59	0.99	−0.44
Leather strip (smooth)	−52.75	1.31	−0.47
Weather-resistant EPDM rubber	−53.61	0.99	−0.47
High-density polyethylene	−59.91	1.79	−0.53
Ultra-high-temperature quartz glass	−62.66	0.47	−0.554
High-impact polystyrene	−67.37	1.79	−0.60
Low-density polyethylene	−67.94	1.49	−0.60
Wear-resistant garolite	−68.51	1.99	−0.61
High-temperature silicone rubber	−69.95	0.50	−0.62
Polyethylene	−71.20	1.71	−0.63
Polyetheretherketone	−76.25	1.99	−0.67
PVDF	−87.35	2.06	−0.77
Duralar (PET)	−89.44	0.86	−0.79
Polyimide film (Kapton)	−92.88	2.58	−0.82
Food-grade high-temperature silicone rubber	−94.03	0.99	−0.83
Easy-to-machine electrical-insulating garolite	−100.33	1.79	−0.89

Materials	Average TECD ($\mu C\ m^{-2}$)	STDEV	α
Polyester fabric (Plain)	−101.48	1.49	−0.90
Polydimethylsiloxane (PDMS)	−102.05	2.16	−0.90
Ultem polyetherimide (PEI)	−102.91	2.16	−0.91
Polystyrene (PS)	−103.48	2.48	−0.92
Clear polycarbonate (Glossy) (PC)	−104.63	1.79	−0.93
Acrylonitrile butadiene styrene (ABS)	−108.07	0.50	−0.96
Abrasion-resistant polyurethane rubber	−109.22	0.86	−0.97
Polytetrafluoroethylene (PTFE)	−113.06	1.14	−1.00
Clear polyvinyl chloride (PVC)	−117.53	1.31	−1.04
Clear cellulose	−133.30	2.28	−1.18
Garolite G-10	−139.89	1.31	−1.24
Flame-retardant garolite	−142.76	1.49	−1.26
Acetal	−143.33	2.48	−1.27
Chemical-Resistant Viton® Fluoroelastomer Rubber	−148.20	2.63	−1.31

Note: STDEV refers to the standard deviation. The α refers to the measured triboelectric charge density of tested materials over the absolute value of the measured triboelectric charge density of the reference material.

Table 4.
Triboelectric series of materials and their triboelectric charge density (TECD) [75, 76].

modification and surface engineering as strategies to optimize polarity and improve device performance [72, 74].

5.4 Triboelectric nanogenerators applications

A new revolution in the field of nanogenerators occurred in 2012 with the discovery of TENGs, a combination of producing electricity and induction, by the Wang's Group [77]. Because the TENGs have high electrical output, low cost, simple structure, and no restrictions on the choice of materials, they can be productive for countless applications [78]. These devices can harvest energy from motions, vibrations, wind, rain, oceans, and sound to generate electrical energy for powering electrical systems [79]. Robotics (human-machine interface, smart toys etc.) [80], biomedical applications (wound healing, drug delivery etc.) [81], environmental applications (smart mask, air purification) [82], and sensing such as tactile, chemical, position and proximity sensing [83, 84] (in smart life, factory, and transportation) are other fields in which these triboelectric nanogenerators play a key role [85]. **Figure 9** shows different applications of TENGs. Subsequently, case studies are reviewed in the field of triboelectric nanogenerator applications.

Energy harvesting: Long and coworkers built a floating triboelectric nanogenerator (based on polytetrafluoroethylene (PTFE), polyamide, aluminum, copper, and acrylic) that is suitable for harvesting small and random energies due to their high efficiency. However, the low output of these types of nanogenerators limits their application because of the rapid decay in electric charge. This noncontact nanogenerator significantly increases the charge by self-reinforcing between the

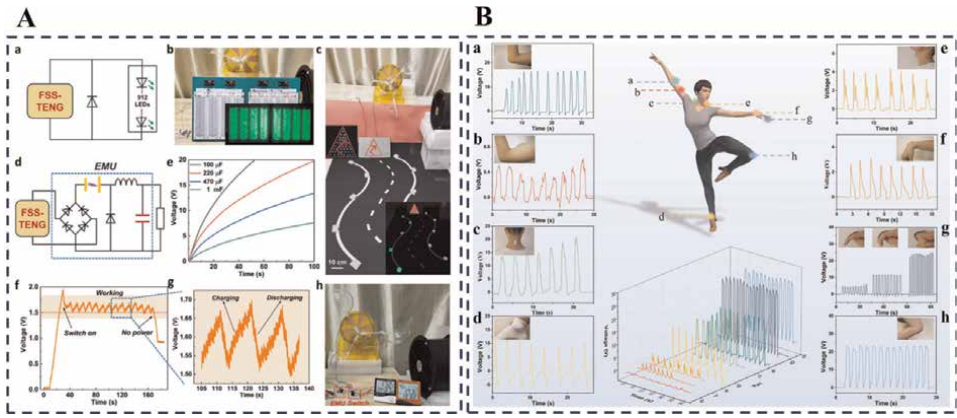

Figure 9.
Triboelectric nanogenerators applications. Panel A: (a) Designed circuit for lighting LEDs. (b) 912 LEDs in on mode. (c) Simulation of turning on roadside warning lights at a 5 m/s wind speed. (d) Designed circuit to power electronic systems. (e) Capacitors voltage under charging by the wind (at a speed of 5 m/s). (f) Two parallel hygrometers voltage at a wind speed of 3 m/s. (g) magnified the hygrometer's voltage. (h) photograph of powering hygrometers with TENG [79]. Panel B: human motions monitoring. Generated voltage as the result of movements by placing the nanogenerator at (a) elbow, (b) arm, (c) neck, (d) ankle, (e) throat, (f) wrist, (g) finger, and (h) knee [86]. Reproduced by permission from Nature, licensed under a Creative Commons Attribution 4.0 International License, http://creativecommons.org/licenses/by/4.0/.

rotating and stationary parts. By collecting wind energy and converting it into electricity, this system is able to light 912 LEDs that can be used in road warning lights. It also powers two temperature hygrometers in a parallel state at 3 m/s wind speed (**Figure 9A**) [79].

Robotics and sensing: Liu et al. developed a flexible and eco-friendly sensor based on triboelectric nanogenerators that can monitor the movements of humans. This structure includes polydimethylsiloxane (PDMS), alginate fiber and vermiculite nanosheets, polyethylene terephthalate (PET), and aluminum. By placing the flexible triboelectric nanogenerator at different points and joints of the body, electrical voltages with distinct signal shapes are generated, which makes it possible to monitor and predict human motions with the help of a machine learning method. This research has taken an effective step in the field of robotics and human health monitoring, and this path still has many steps to develop (**Figure 9B**) [86].

Biomedical application: Peng and friends have created an eco-friendly electric skin with antibacterial and breathable activity based on materials such as silver nanowires (AgNWs), polyvinyl alcohol (PVA), and polylactic-co-glycolic acid (PLGA). By varying the concentration of silver nanowires (AgNWs) and the appropriate selection of PLGA and PVA materials, it is possible to control the antibacterial and biodegradability properties of electronic skins, respectively. This electronic skin is capable of automatic monitoring of joint motions and physiological signals of the body [81].

Environmental application: A self-generating air filter that utilizes the triboelectric effect was developed by Peng's group. This structure, including electrospun poly (vinylidene fluoride) (PVDF), nylon, copper mesh, and conductive fabric, achieved efficient and long-lasting removal of airborne particles. The electrostatic adsorption plays an effective role in mechanical air filtration, but the charge decreases over time, especially in high humidity. Consequently, a self-charging air filter was introduced that continuously generates electrostatic charge by breathing, without the need for external

energy, and long-term absorbs airborne particles. This filter protects the valuable efficiency of 95.8% with 0.3 μm particles after 60 hours (30 hours of use) [82].

6. Hybrid nanogenerators: Design and applications

By hybridizing energy conversion systems, including piezoelectric, triboelectric, thermoelectric, and pyroelectric, an integrated system capable of generating electrical energy with high efficiency can be achieved. Using two energy systems simultaneously improves electrical outputs, but there are still challenges, such as the existence of different impedances in these devices. These problems can be solved by applying power management methods, including the use of rectifiers and storage units [54]. Hybrid systems will often be dual or triple (2 in 1) or (3 in 1), and applications are generally in the fields of energy supply [87], biomedical/health [88], environment, and sensing [87] in the smart world (daily life, factories, transportation, etc.). Examples of hybrid nanogenerators are detailed in terms of the number of components.

3 in 1: Sukumaran and colleagues constructed a triple hybrid nanogenerator consisting of triboelectric, piezoelectric, and pyroelectric to harvest mechanical and thermal energy and convert them into electrical energy. This structure contains materials such as PVDF, reduced graphene oxide (rGO), polyamide, aluminum, and gold. The electrical energy produced in this nanogenerator can be used to power microelectronic devices and small systems [89].

2 in 1: Jung et al. created a triboelectric/piezoelectric device that can be applied in an energy harvesting application. The hybrid structure consists of polyvinylidene difluoride (PVDF), polytetrafluoroethylene (PTFE), polyimide (PI) film, gold, and aluminum. This system, with a power density of 4.44 mW/cm^2, is capable of lighting up to 600 LEDs, charging a 10 μF capacitor in 25 seconds to a voltage of 10 V, and powering small electronics. This research demonstrates the high potential of hybrid nanogenerators for future innovative applications (**Figure 10**) [90].

7. Conclusions and future perspective

The advent of nanogenerators marks a transformative shift in the field of energy harvesting, enabling the development of self-powered microsystems and sustainable technologies suited for an increasingly connected and miniaturized world. This chapter has introduced the fundamental mechanisms behind piezoelectric, pyroelectric, thermoelectric, and triboelectric nanogenerators, emphasizing their underlying physics, materials, and distinct energy conversion pathways. Each nanogenerator type offers unique advantages tailored to specific application scenarios, ranging from biomechanical energy harvesting to environmental sensing, autonomous robotics, and biomedical implants.

Collectively, nanogenerators overcome the limitations of conventional batteries by scavenging energy from ubiquitous sources such as motion, heat, and vibration—converting ambient "waste" energy into a usable electrical form. Their compatibility with flexible substrates, lightweight nature, and miniaturized form factors make them especially suitable for integration into wearable electronics, implantable medical devices, and distributed sensor networks.

Looking ahead, several key directions will define the future landscape of nanogenerator research and development:

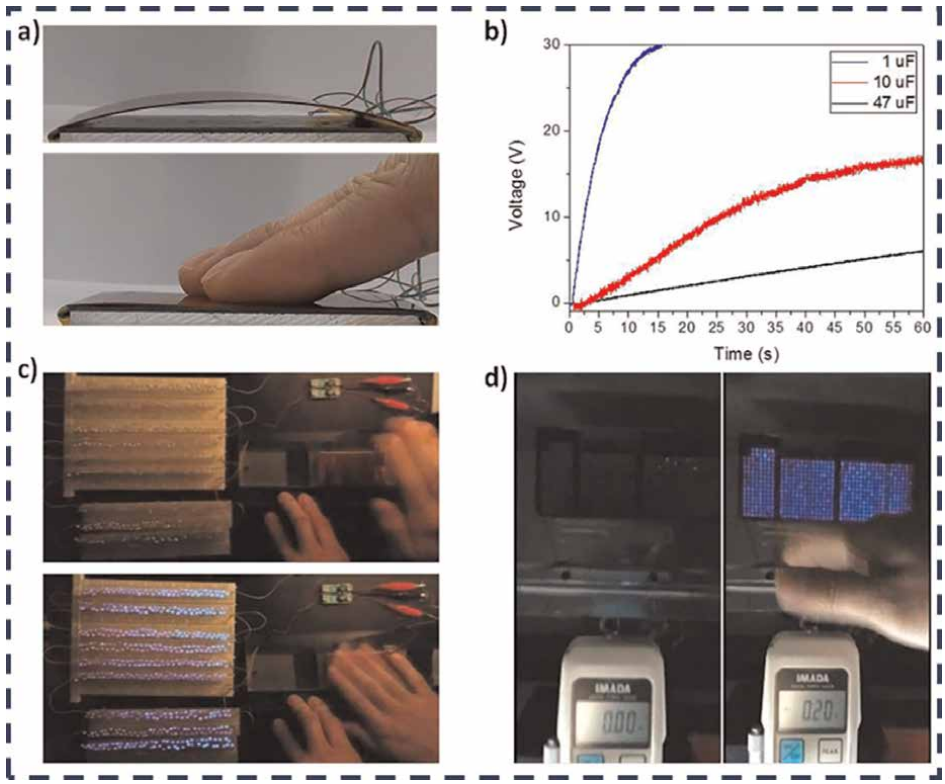

Figure 10.
Hybrid nanogenerators applications. (a) Contact-separation mode of the produced hybrid generator. (b) Charging curves of different capacitors. (c) Turning on 600 LEDs. (d) Applying a 0.2 N force to light 600 LEDs [90]. Reproduced by permission from Nature, licensed under a Creative Commons Attribution 4.0 International License, http://creativecommons.org/licenses/by/4.0/.

Material innovation: There remains a significant need for novel materials with enhanced electrical output, long-term stability, biocompatibility, and environmental sustainability. Low-dimensional materials (e.g., MXenes, 2D perovskites, organic-inorganic hybrids) and eco-friendly polymers offer exciting possibilities.

Hybrid nanogenerators: Combining multiple energy harvesting mechanisms (e.g., piezo-triboelectric or thermo-pyroelectric) within a single architecture can significantly improve energy conversion efficiency and expand functionality under varying environmental conditions.

Integration and miniaturization: Progress in nanofabrication and system-level integration will enable the seamless incorporation of nanogenerators into multifunctional devices and circuits, fostering the development of fully autonomous electronic platforms.

Smart and adaptive systems: Future nanogenerators will be embedded within intelligent systems capable of adaptive energy management, wireless communication, and real-time data processing, advancing their role in AI-powered IoT frameworks.

Biomedical and environmental frontiers: As materials and fabrication strategies mature, nanogenerators will increasingly penetrate biomedical domains—powering biosensors, pacemakers, drug delivery systems—as well as environmental sectors for pollution sensing, remediation, and pyro-catalytic applications.

Scalability and commercialization: For widespread adoption, scalable fabrication techniques, cost reduction, and standardization of performance metrics are critical. Bridging the gap between laboratory prototypes and industrial products remains a pressing challenge.

In conclusion, nanogenerators hold immense promise as key enablers of the self-powered era, transforming how we harvest, store, and utilize energy at the nanoscale. With interdisciplinary collaboration across materials science, electronics, bioengineering, and energy systems, the next decade is poised to witness the convergence of nanogenerators with future technologies that are smarter, more sustainable, and more integrated into the human environment.

Conflict of interest

The authors declare no conflict of interest.

Author details

Mahdi Zekavat, Fahimeh Zamanpour, Shahab Ahmadi Seyedkhani*,
Raheleh Mohammadpour and Azam Irajizad
Center for Nanoscience and Nanotechnology (INST), Institute for Convergence Science and Technology (ICST), Sharif University of Technology, Tehran, Iran

*Address all correspondence to: ahmadiseyedkhani@gmail.com;
sh.ahmadi@sharif.edu

References

[1] Deng W, Zhou Y, Libanori A, Chen G, Yang W, Chen J. Piezoelectric nanogenerators for personalized healthcare. Chemical Society Reviews. 2022;**51**:3380-3435

[2] Kumar N, Manikpuri N, Giri A, Shrivastava R. Role of polyphosphazene in piezoelectric applications: A review. Discover Chemistry. 2024;**1**:19

[3] Bhadwal N, Ben Mrad R, Behdinan K. Review of zinc oxide piezoelectric nanogenerators: Piezoelectric properties, composite structures and power output. Sensors. 2023;**23**:3859

[4] Pandey RK, Dutta J, Brahma S, Rao B, Liu C-P. Review on ZnO-based piezotronics and piezoelectric nanogenerators: Aspects of piezopotential and screening effect. Journal of Physics: Materials. 2021;**4**: 44011

[5] Xu Q, Wen J, Qin Y. Development and outlook of high output piezoelectric nanogenerators. Nano Energy. 2021;**86**: 106080

[6] Covaci C, Gontean A. Piezoelectric energy harvesting solutions: A review. Sensors. 2020;**20**:3512

[7] Bairagi S, Shahadat M, Mulvihill DM, Ali W. Mechanical energy harvesting and self-powered electronic applications of textile-based piezoelectric nanogenerators: A systematic review. Nano Energy. 2023;**111**:108414

[8] Habib M, Lantgios I, Hornbostel K. A review of ceramic, polymer and composite piezoelectric materials. Journal of Physics D: Applied Physics. 2022;**55**:423002

[9] Ali F, Koc M. 3D printed polymer piezoelectric materials: Transforming healthcare through biomedical applications. Polymers (Basel). 2023;**15**: 4470

[10] Mirjalali S, Mahdavi Varposhti A, Abrishami S, Bagherzadeh R, Asadnia M, Huang S, et al. A review on wearable electrospun polymeric piezoelectric sensors and energy harvesters. Macromolecular Materials and Engineering. 2023;**308**:2200442

[11] Kalimuldina G, Turdakyn N, Abay I, Medeubayev A, Nurpeissova A, Adair D, et al. A review of piezoelectric PVDF film by electrospinning and its applications. Sensors. 2020;**20**:5214

[12] Zhang M, Liu C, Li B, Shen Y, Wang H, Ji K, et al. Electrospun PVDF-based piezoelectric nanofibers: Materials, structures, and applications. Nanoscale Advances. 2023;**5**:1043-1059

[13] Wang R, Sui J, Wang X. Natural piezoelectric biomaterials: A biocompatible and sustainable building block for biomedical devices. ACS Nano. 2022;**16**:17708-17728

[14] Cheng X, Singh PK, Mishra A, Tiwari A, Ren W. Wurtzite nanostructured piezoelectric devices. Materials Today Sustainability. 2023;**23**: 100474

[15] Zheng T, Wu J, Xiao D, Zhu J. Recent development in lead-free perovskite piezoelectric bulk materials. Progress in Materials Science. 2018;**98**:552-624

[16] Ghazanfarian J, Mohammadi MM, Uchino K. Piezoelectric energy harvesting: A systematic review of reviews. Actuators (Basel, Switzerland). 2021;**10**:312. DOI: 10.3390/act10120312

[17] Ren Z, Deng S, Shao J, Si Y, Zhou C, Luo J, et al. Ultrahigh-power-density

flexible piezoelectric energy harvester based on freestanding ferroelectric oxide thin films. Nature Communications. 2025;**16**:3192

[18] Dagdeviren C, Su Y, Joe P, Yona R, Liu Y, Kim Y-S, et al. Conformable amplified lead zirconate titanate sensors with enhanced piezoelectric response for cutaneous pressure monitoring. Nature Communications. 2014;**5**:4496

[19] Han L, Liu Y, Qi Z, Zhao Y, Zhang N, Dong Y, et al. Highly polarized piezoelectret embedded versatile haptic devices for immersive human-robot interactions. Nano Energy. 2025;**136**: 110775

[20] Luo J-Q, Lu H-F, Nie Y-J, Zhou Y-H, Wang C-F, Zhang Z-X, et al. Porous flexible molecular-based piezoelectric composite achieves milliwatt output power density. Nature Communications. 2024;**15**:8636

[21] Mohamed Mustakim NS, Kamaruzaman D, Abdullah MH, Malek MF, Parimon N, Ahmad MK, et al. Review of recent advances in piezoelectric material for nanogenerator application: Preparation methods, material selection, performance, applications, and future outlook. Journal of Materials Science. 2024;**59**: 19380-19423

[22] Xu T, Jin L, Ao Y, Zhang J, Sun Y, Wang S, et al. All-polymer piezo-ionic-electric electronics. Nature Communications. 2024;**15**:10876

[23] Lingam D, Parikh AR, Huang J, Jain A, Minary-Jolandan M. Nano/microscale pyroelectric energy harvesting: Challenges and opportunities. International Journal of Smart and Nano Materials. 2013;**4**: 229-245

[24] Bowen CR, Taylor J, LeBoulbar E, Zabek D, Chauhan A, Vaish R. Pyroelectric materials and devices for energy harvesting applications. Energy & Environmental Science. 2014;**7**: 3836-3856

[25] He H, Lu X, Hanc E, Chen C, Zhang H, Lu L. Advances in lead-free pyroelectric materials: A comprehensive review. Journal of Materials Chemistry C. 2020;**8**:1494-1516

[26] Mondal R, Hasan MAM, Baik JM, Yang Y. Advanced pyroelectric materials for energy harvesting and sensing applications. Materials Today. 2023;**66**: 273-301

[27] Thakre A, Kumar A, Song H-C, Jeong D-Y, Ryu J. Pyroelectric energy conversion and its applications—Flexible energy harvesters and sensors. Sensors. 2019;**19**:2170

[28] Li S, Zhao Z, Zhao J, Zhang Z, Li X, Zhang J. Recent advances of ferro-, piezo-, and pyroelectric nanomaterials for catalytic applications. ACS Applied Nano Materials. 2020;**3**: 1063-1079

[29] Narayan B, Wang Q, Roscow J, Wan C, Bowen C. New pyroelectric figures of merit for harvesting dynamic temperature fluctuations. Journal of Materials Chemistry A. 2025;**13**:12977-12987. DOI: 10.1039/D5TA00704F

[30] Sebald G, Lefeuvre E, Guyomar D. Pyroelectric energy conversion: Optimization principles. IEEE Transactions on Ultrasonics, Ferroelectrics, and Frequency Control. 2008;**55**:538-551

[31] Ghane-Motlagh R, Woias P. A pyroelectric thin film of oriented triglycine sulfate nano-crystals for thermal energy harvesting. Smart

Materials and Structures. 2019;**28**: 104002

[32] Yang Y, Zhou Y, Wu JM, Wang ZL. Single micro/nanowire pyroelectric nanogenerators as self-powered temperature sensors. ACS Nano. 2012;**6**: 8456-8461

[33] Zabek D, Taylor J, Le Boulbar E, Bowen CR. Micropatterning of flexible and free standing polyvinylidene difluoride (PVDF) films for enhanced pyroelectric energy transformation. Advanced Energy Materials. 2015;**5**: 1401891

[34] Caley ER, Richards JFC. Theophrastus on Stones: Introduction, Greek Text, English Translation, and Commentary. USA: The Ohio State University; 1956

[35] Lang SB. A 2400 year history of pyroelectricity: From ancient Greece to exploration of the solar system. British Ceramic Transactions. 2004;**103**: 65-70

[36] Capper P, Elliott CT. Infrared Detectors and Emitters: Materials and Devices. New York, USA: Springer Science & Business Media; 2013

[37] Uthra B, Sinha R, Agarwal PB. CMOS compatible pyroelectric materials for infrared detectors. Materials Science in Semiconductor Processing. 2022;**140**: 106375

[38] Li S, Wang Y, Liu Z, Chen B, Liu M, He X, et al. Flexible pyroelectric energy harvesters from nanocomposites of liquid crystal elastomers/lead zirconate titanate nanoparticles. Science Advances. 2025;**11**:eadt6136

[39] Zeng X, Liu Y, Weng W, Hua L, Tang L, Guo W, et al. A molecular pyroelectric enabling broadband photo-pyroelectric effect towards self-driven wide spectral photodetection. Nature Communications. 2023;**14**:5821

[40] You H, Li S, Fan Y, Guo X, Lin Z, Ding R, et al. Accelerated pyro-catalytic hydrogen production enabled by plasmonic local heating of Au on pyroelectric BaTiO3 nanoparticles. Nature Communications. 2022;**13**:6144

[41] Wolf M, Hinterding R, Feldhoff A. High power factor vs. high zT—A review of thermoelectric materials for high-temperature application. Entropy. 2019; **21**:1058

[42] Tabaie Z, Omidvar A. Human body heat-driven thermoelectric generators as a sustainable power supply for wearable electronic devices: Recent advances, challenges, and future perspectives. Heliyon. 2023;**9**:1-23

[43] Hasan MN, Nafea M, Nayan N, Mohamed Ali MS. Thermoelectric generator: Materials and applications in wearable health monitoring sensors and internet of things devices. Advanced Materials Technologies. 2022;**7**:2101203

[44] Shi X-L, Zou J, Chen Z-G. Advanced thermoelectric design: From materials and structures to devices. Chemical Reviews. 2020;**120**:7399-7515

[45] Zhu S, Fan Z, Feng B, Shi R, Jiang Z, Peng Y, et al. Review on wearable thermoelectric generators: From devices to applications. Energies. 2022;**15**:3375

[46] Jiang J, Zhu H, Niu Y, Zhu Q, Song S, Zhou T, et al. Achieving high room-temperature thermoelectric performance in cubic AgCuTe. Journal of Materials Chemistry A. 2020;**8**: 4790-4799

[47] Zheng J. Recent advances on thermoelectric materials. Frontiers of Physics in China. 2008;**3**:269-279

[48] Han H, Zhao L, Wu X, Zuo B, Bian S, Li T, et al. Advancements in thermoelectric materials: Optimization strategies for enhancing energy conversion. Journal of Materials Chemistry A. 2024;**12**:24041-24083

[49] Hasan MN, Wahid H, Nayan N, Mohamed Ali MS. Inorganic thermoelectric materials: A review. International Journal of Energy Research. 2020;**44**:6170-6222

[50] Poon SJ. Recent advances in thermoelectric performance of half-Heusler compounds. Metals (Basel). 2018;**8**:989

[51] González-Barrios M, Tabuyo-Martínez M, Ávila-Brande D, Prado-Gonjal J. Perspective on crystal structures, synthetic methods, and new directions in thermoelectric materials. Small Structures. 2024;**5**:2400136

[52] Liu Y, Zhi J, Li W, Yang Q, Zhang L, Zhang Y. Oxide materials for thermoelectric conversion. Molecules. 2023;**28**:5894

[53] Seebeck TJ. Magnetische polarisation der metalle und erze durch temperatur-differenz. Germany: Engelmann; 1895

[54] Liu H, Fu H, Sun L, Lee C, Yeatman EM. Hybrid energy harvesting technology: From materials, structural design, system integration to applications. Renewable and Sustainable Energy Reviews. 2021;**137**:110473

[55] Jouhara H, Żabnieńska-Góra A, Khordehgah N, Doraghi Q, Ahmad L, Norman L, et al. Thermoelectric generator (TEG) technologies and applications. International Journal of Thermofluids. 2021;**9**:100063

[56] Castañeda M, Amell AA, Correa MA, Aguilar CE, Colorado HA. Thermoelectric generator using low-cost thermoelectric modules for low-temperature waste heat recovery. Sustainability. 2023;**15**:3681

[57] Wei J, Zhou Y, Wang Y, Miao Z, Guo Y, Gao D, et al. Recent advances in thermoelectric technology to harvest energy from the pavement. International Journal of Energy Research. 2022;**46**: 10453-10474

[58] Ding T, Chan KH, Zhou Y, Wang X-Q, Cheng Y, Li T, et al. Scalable thermoelectric fibers for multifunctional textile-electronics. Nature Communications. 2020;**11**:6006

[59] Miao L, Zhu S, Liu C, Gao J, Zhang Z, Peng Y, et al. Comfortable wearable thermoelectric generator with high output power. Nature Communications. 2024;**15**:8516

[60] Shen J, Huang X, Dai Y, Zhang X, Xia F. N-type and P-type series integrated hydrogel thermoelectric cells for low-grade heat harvesting. Nature Communications. 2024;**15**:9305

[61] Wang ZL. Triboelectric nanogenerator (TENG)—Sparking an energy and sensor revolution. Advanced Energy Materials. 2020;**10**: 2000137

[62] Wang ZL, Wang AC. On the origin of contact-electrification. Materials Today. 2019;**30**:34-51

[63] Zhou L, Liu D, Wang J, Wang ZL. Triboelectric nanogenerators: Fundamental physics and potential applications. Friction. 2020;**8**:481-506

[64] Lei H, Chen Y, Gao Z, Wen Z, Sun X. Advances in self-powered triboelectric pressure sensors. Journal of Materials Chemistry A. 2021;**9**: 20100-20130

[65] Zhou J, Lu C, Lan D, Zhang Y, Lin Y, Wan L, et al. Enhancing the output performance of a triboelectric nanogenerator based on modified polyimide and sandwich-structured nanocomposite film. Nanomaterials. 2023;**13**:1056

[66] Kim W-G, Kim D-W, Tcho I-W, Kim J-K, Kim M-S, Choi Y-K. Triboelectric nanogenerator: Structure, mechanism, and applications. ACS Nano. 2021;**15**:258-287

[67] Chen J, Wang ZL. Reviving vibration energy harvesting and self-powered sensing by a triboelectric nanogenerator. Joule. 2017;**1**:480-521

[68] Lin S, Xu L, Chi Wang A, Wang ZL. Quantifying electron-transfer in liquid-solid contact electrification and the formation of electric double-layer. Nature Communications. 2020;**11**:399

[69] Wu J, Zheng Y, Li X. Recent progress in self-powered sensors based on triboelectric nanogenerators. Sensors. 2021;**21**:7129

[70] Wang S, Lin L, Wang ZL. Triboelectric nanogenerators as self-powered active sensors. Nano Energy. 2015;**11**:436-462

[71] Niu S, Wang S, Lin L, Liu Y, Zhou YS, Hu Y, et al. Theoretical study of contact-mode triboelectric nanogenerators as an effective power source. Energy & Environmental Science. 2013;**6**:3576-3583

[72] Trinh V-L, Chung C-K. Advances in triboelectric nanogenerators for sustainable and renewable energy: Working mechanism, tribo-surface structure, energy storage-collection system, and applications. PRO. 2023;**11**: 2796

[73] Tofel P, Částková K, Říha D, Sobola D, Papež N, Kaštyl J, et al. Triboelectric response of electrospun stratified PVDF and PA structures. Nanomaterials. 2022;**12**:349

[74] Liu Y, Mo J, Fu Q, Lu Y, Zhang N, Wang S, et al. Enhancement of triboelectric charge density by chemical functionalization. Advanced Functional Materials. 2020;**30**:2004714

[75] Zou H, Zhang Y, Guo L, Wang P, He X, Dai G, et al. Quantifying the triboelectric series. Nature Communications. 2019;**10**:1427. DOI: 10.1038/s41467-019-09461-x

[76] Zou H, Guo L, Xue H, Zhang Y, Shen X, Liu X, et al. Quantifying and understanding the triboelectric series of inorganic non-metallic materials. Nature Communications. 2020;**11**:2093. DOI: 10.1038/s41467-020-15926-1

[77] Fan F-R, Tian Z-Q, Wang ZL. Flexible triboelectric generator. Nano Energy. 2012;**1**:328-334

[78] Wang Y, Yang Y, Wang ZL. Triboelectric nanogenerators as flexible power sources. npj Flexible Electronics. 2017;**1**:10

[79] Long L, Liu W, Wang Z, He W, Li G, Tang Q, et al. High performance floating self-excited sliding triboelectric nanogenerator for micro mechanical energy harvesting. Nature Communications. 2021;**12**:4689

[80] Liu Y, Wang J, Liu T, Wei Z, Luo B, Chi M, et al. Triboelectric tactile sensor for pressure and temperature sensing in high-temperature applications. Nature Communications. 2025;**16**:383

[81] Peng X, Dong K, Ye C, Jiang Y, Zhai S, Cheng R, et al. A breathable, biodegradable, antibacterial, and self-

powered electronic skin based on all-nanofiber triboelectric nanogenerators. Science Advances. 2020;**6**:eaba9624

[82] Peng Z, Shi J, Xiao X, Hong Y, Li X, Zhang W, et al. Self-charging electrostatic face masks leveraging triboelectrification for prolonged air filtration. Nature Communications. 2022;**13**:7835

[83] Razaghi Z, Zamanpour F, Vafaiee M, Letafati M, Gholami M, Taghavinia N, et al. Versatile hybrid transparent triboelectric nanogenerator-solar cell device enables efficient energy harvesting and personal handwriting recognition. Composites. Part B, Engineering. 2024;**283**:111615

[84] Zamanpour F, Shooshtari L, Mohammadpour R, Sasanpour P. Empowering smart toys and devices with stretchable and vivid triboelectric layers for enhanced interaction and monitoring. Nano Energy. 2024;**128**:109887

[85] Choi D, Lee Y, Lin Z-H, Cho S, Kim M, Ao CK, et al. Recent advances in triboelectric nanogenerators: From technological progress to commercial applications. ACS Nano. 2023;**17**: 11087-11219

[86] Liu Y, Shen Y, Ding W, Zhang X, Tian W, Yang S, et al. All-natural phyllosilicate-polysaccharide triboelectric sensor for machine learning-assisted human motion prediction. npj Flexible Electronics. 2023;**7**:21

[87] Dong W, Li M, Chen C, Xie K, Hong J, Yang L. Flexible hybrid self-powered piezo-triboelectric nanogenerator based on BTO-PVDF/PDMS nanocomposites for human machine interaction. Scientific Reports. 2025;**15**:15991

[88] Chahari M, Salman E, Stanacevic M, Willing R, Towfighian S. Performance of piezoelectric and triboelectric transducers under gait loading for energy harvesting and load monitoring in Total knee replacements. Nano Energy. 2025;**141**:111117. DOI: 10.1016/j.nanoen.2025.111117

[89] Sukumaran S, Szewczyk PK, Bajda T, Stachewicz U. Hybrid piezo-, pyro-, and triboelectric nanogenerator based on PVDF and rGO composite fibers for a multifunctional approach to energy harvesting applications. Materials and Design. 2025;**254**:114105. DOI: 10.1016/j.matdes.2025.114105

[90] Jung W-S, Kang M-G, Moon HG, Baek S-H, Yoon S-J, Wang Z-L, et al. High output piezo/triboelectric hybrid generator. Scientific Reports. 2015;**5**: 9309

Section 2

Materials, Design and Technologies

Chapter 3

Green and Eco-Friendly Triboelectric Nanogenerators

Kashif Riaz, Abdelkrim Khelif and Muhammad Umaid Bukhari

Abstract

The chapter will explore the burgeoning field of sustainable energy harvesting through triboelectric nanogenerators (TENGs) constructed from environmentally conscious and renewable resources. Recognizing the ecological challenges posed by conventional non-biodegradable and synthetic materials, this chapter will delve into the design, fabrication, and performance characteristics of TENGs that prioritize the utilization of waste byproducts and naturally occurring substances. The scope will encompass the environmental concerns associated with traditional TENG materials and the compelling motivation for developing greener alternatives, including addressing electronic waste and plastic pollution. It will further explore the innovative application of novel, eco-friendly materials, including naturally derived substances such as food-based materials. The chapter will also highlight facile, low-cost, and environmentally benign fabrication methodologies, emphasizing solvent-free and cleanroom-free processes. Furthermore, it will present the performance characterization of these sustainable TENGs, detailing key electrical parameters and offering comparisons with existing technologies, alongside demonstrations of their practical applications in powering portable electronics and self-powered systems. Ultimately, this chapter aims to provide a comprehensive understanding of the progress in creating environmentally responsible green TENGs, showcasing their potential as a sustainable energy solution by effectively harnessing waste and natural resources.

Keywords: triboelectric nanogenerators, green, eco-friendly, sustainable, electronic and plastic waste

1. Introduction

The escalating global energy demand, coupled with the environmental hazards of conventional batteries and the need to power a rapidly growing portable electronic market ($810 billion by 2030 [1]), necessitates urgent development of green and sustainable energy. This aligns with the global target of 90% renewable electrical energy by 2050 for a net-zero emissions scenario [2]. By 2030, the projected global battery demand for consumer electronics is set to reach 130 gigawatt-hours (GWh) [3], concurrently generating an estimated 2 million metric tons of Li-ion battery waste annually [4], with recycling rates in the United States and European Union remaining below 5% [4]. With such a low recycling rate, the vast majority of these batteries and their associated metal and chemical wastes pose a significant threat to life and

environment [5, 6]. The escalating demand for electronics and batteries, coupled with frequent device replacement, is significantly driving e-waste generation. Internet-connected devices and e-waste are increasingly significant contributors to greenhouse gas emissions [7], with their carbon dioxide equivalent (CO_2e) emissions projected to surge from 580 million metric tons (MMT) in 2020 to approximately 852 MMT by 2030 [8]. Addressing these challenges necessitates a growing global adoption of green and sustainable solutions—a market projected to reach USD 102.2 billion by 2033 growing at a CAGR of 20% between 2024 and 2033 [9].

Triboelectric nanogenerators (TENGs), first introduced by Wang's group in 2012, are emerging as a leading green and sustainable energy technology, marking a significant milestone in micro-nano energy harvesting [10]. They effectively convert ambient mechanical energy from various sources, such as waves, wind, and human motion, into usable electricity especially for portable electronic and sensing devices [10–12]. TENGs are highly valued for their straightforward design, excellent low-frequency performance, material versatility, affordability, and extensive applications in emerging fields of bioengineering, healthcare, human-machine interfaces, and more [10–16]. Their advantages include low-cost fabrication, lightweight nature, inherent flexibility and wearability, and high-energy conversion efficiency, particularly when harvesting low-frequency (below 10 Hz), irregular mechanical energy from sources, such as human movements, wind, ocean waves, and even raindrops [16–18]. This unique capability signifies a fundamental shift towards decentralized, ubiquitous, and low-power energy scavenging, offering a sustainable solution for autonomous energy systems and self-powered sensing capabilities crucial for IoT devices and next-generation smart electronics for smart cities [19, 20]. TENGs are evolving beyond micro-power sources to potentially pivotal contributors to large-scale sustainable energy infrastructure, due to their versatility in harvesting diverse mechanical energy forms (e.g., wind, human motion), making them crucial for achieving national and international climate goals [17, 19–21]. Since their initial report in 2012, TENGs have demonstrated remarkable advancements, with reported instantaneous output power densities exceeding 10 MW/m^2 [22] and instantaneous energy conversion efficiencies reaching approximately 70.6% [23]. By providing continuous energy and reducing reliance on traditional batteries, TENGs enhance device longevity, improve user convenience, and significantly lower the global electronic waste footprint, perfectly aligning with green technology principles [17, 24–26].

TENGs convert ambient mechanical energy into electricity by synergistically combining contact electrification and electrostatic induction. Contact electrification, a phenomenon understood for millennia, involves the spontaneous charge generation when two distinct materials frictionally contact. Although the exact mechanism of triboelectrification remains debated and under study, it is generally believed that upon contact, two distinct materials form a chemical bond (adhesion), facilitating charge transfer between them to equalize their electrochemical potential. When separated, some atoms retain charges while others release them, creating triboelectric charges on surfaces. The presence of these charges on dielectric surfaces drives electrons in an external conducting path to flow, balancing the resulting electric potential drop [11, 12, 16, 17]. During TENG operation, initially, no charge is generated or induced when materials are not in contact (**Figure 1I**). Upon physical contact, electrons transfer from a tribopositive (electron donor) to a tribonegative (electron acceptor) material, causing opposite charges to accumulate on their surfaces (**Figure 1II**). Subsequently, the separation of these oppositely charged materials induces an electrical potential difference, leading to an instantaneous electron flow

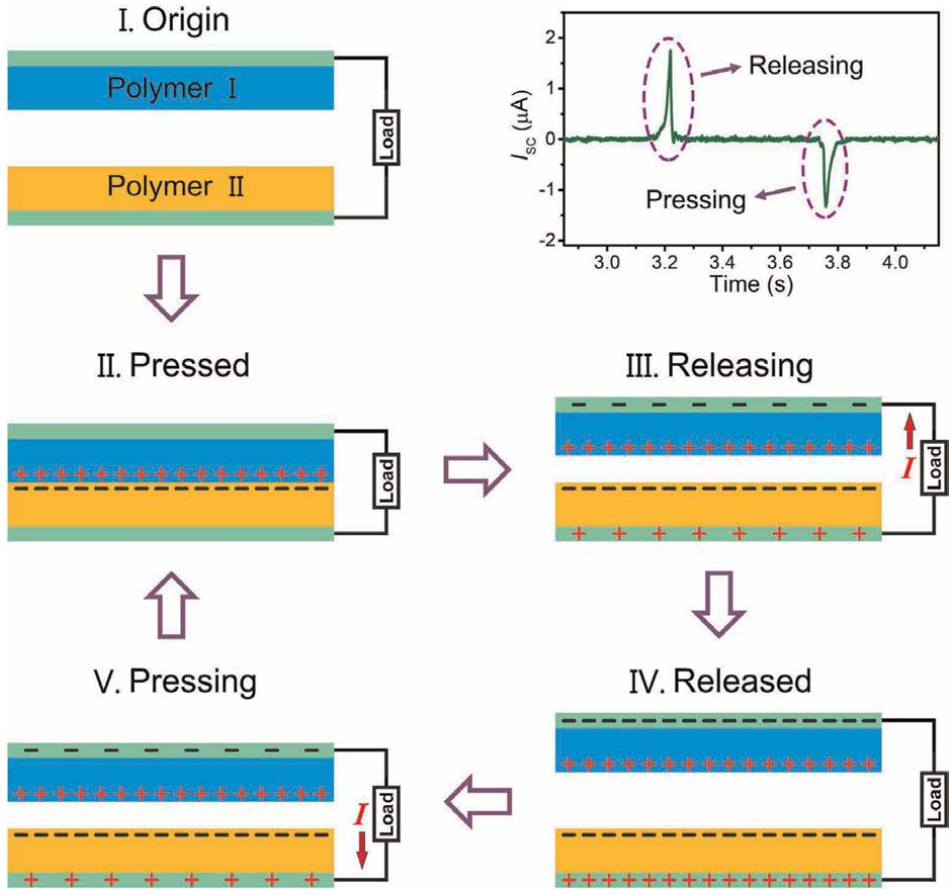

Figure 1.
Schematic illustration of the TENG working principle in contact-separation mode: (I) initial non-contact state, (II) physical contact, (III) current flow during separation, (IV) separated or released stated, and (V) re-contact; resulting AC signal shown in the top right. Reproduced from [16], under the Creative Commons Attribution 4.0 International (CC BY 4.0) license (https://creativecommons.org/licenses/by/4.0/).

from the bottom electrode to the top electrode (**Figure 1III**), which then drives an electrical current in an external circuit to power electronics. This process continues until the two surfaces are fully separated and equilibrium is reached (**Figure 1IV**). When the two surfaces are pressed together again, the electrostatically induced charges flow back through the external load to compensate for the electric potential difference (**Figure 1V**). The continuous cycle of contact and separation leads to ongoing charge reorganization and the generation of alternating current (AC) signal, as shown in the top right corner of **Figure 1**. The triboelectric series, an ordered list of materials indicating their relative tendency to gain or lose electrons upon contact, is vital for TENG design as it primarily predicts the direction and relative magnitude of charge transfer between materials [27].

The operation of TENGs can be categorized into four fundamental working modes, determined by their polarization change direction and electrode configuration: vertical contact-separation (cs), in-plane or lateral sliding (LS), single-electrode (SE), and free-standing triboelectric-layer (FT) modes as illustrated in **Figure 2** [11, 12, 16]. The vertical cs mode (**Figure 2A**), representing the most basic configuration, relies on

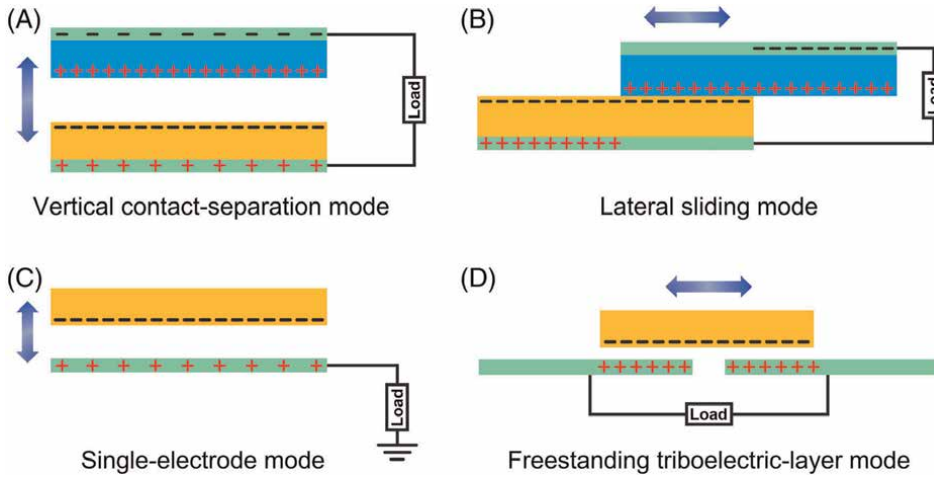

Figure 2.
Schematic illustration of TENGs' operational modes: (A) vertical contact-separation (cs) mode, (B) in-plane or lateral sliding (LS) mode, (C) single-electrode (SE) mode, and (D) free-standing triboelectric-layer (FT) mode. Reproduced from [16], under the Creative Commons Attribution 4.0 International (CC BY 4.0) license (https://creativecommons.org/licenses/by/4.0/).

perpendicular relative movement between two material surfaces. During its contact and separation cycle, a fluctuating potential difference is established between the two electrodes, driving an external current to equalize this potential. The LS mode (**Figure 2B**), conversely, utilizes relative parallel displacement along the contact interface, generating electrical output through an external circuit due to changes in potential between the electrodes; this mode can also be achieved via rotation-induced sliding. For harvesting mechanical energy from moving objects without requiring a direct conductive line, the SE mode was developed (**Figure 2C**), utilizing the ground as a reference electrode. Building upon the SE mode, the FT mode employs two sets of symmetric electrodes (**Figure 2D**); electrical output is generated by asymmetric charge distribution as a freely moving object's position changes.

However, most of the traditional TENGs commonly incorporate synthetic polymers, such as polytetrafluoroethylene (PTFE), polydimethylsiloxane (PDMS), polyvinylidene fluoride (PVDF), polyimide (Kapton), polymethyl methacrylate (PMMA), fluorinated ethylene propylene (FEP), and nylon, in conjunction with metal electrodes [28]. A significant drawback of these synthetic materials is their non-biodegradable nature or their extremely slow decomposition, often spanning decades to millennia [29].This dependence on non-biodegradable materials intensifies a pressing environmental concern that is global plastic/polymer waste. This highlights the critical need for developing sustainable, biodegradable, and eco-friendly triboelectric materials for TENG fabrication. In the context of TENG, the terms "green" and "eco-friendly" fundamentally describe a deliberate shift in material selection. This involves moving away from conventional synthetic polymers, often known for their non-degradable nature and non-eco-friendly fabrication, and instead focusing on the utilization of green, biodegradable, and waste-derived resources in sustainable manner. This pronounced emphasis on biopolymers, green, and waste-driven materials signifies a pivotal evolution in TENG research [24–26]. It marks a transition from solely prioritizing performance metrics to embracing a holistic approach that integrates environmental impact across the entire lifecycle, from material sourcing to end-of-life

degradation. This strategic pivot highlights the field's increasing maturity, where sustainability is no longer a secondary consideration but has become a core design principle [24–26, 30–32].

2. Waste to energy: Recycled waste-driven TENGs

The escalating global waste crisis and urgent demand for sustainable energy sources underscore a critical need for innovative solutions that integrate waste management with energy generation. This section will establish the profound environmental and economic consequences of inadequate waste disposal, highlighting how the development of sustainable TENGs from recycled waste aligns with international green and sustainable development agendas.

2.1 Environmental and economic ramifications of non-recycled waste

The linear "take-make-use-dispose" economic model has led to an unsustainable accumulation of waste, with far-reaching environmental and economic impacts across various material streams. The proliferation of polymer and plastic waste presents a formidable challenge. Projections show worldwide polymer and plastic waste production, roughly 350 MMT in 2019, could exceed 1 billion metric tons annually by 2060 [33]. Despite recycling efforts, only 9% of plastic waste is recycled, while 19% is incinerated and 50% is landfilled [33]. The remaining 22% is mismanaged, severely polluting land and marine ecosystems, increasing landfill waste, occupying valuable space, and emitting potent greenhouse gases (GHG) such as methane, which significantly contribute to climate change [33]. Failing to recycle polymers and plastics exacerbates the global waste crisis, contributing to resource depletion and increased energy consumption, as manufacturing from raw materials is more energy-intensive than using recycled ones, boosts carbon emissions and pollution, and causes widespread habitat destruction, deforestation, and ecosystem degradation [34]. Ultimately, non-recycled plastics unleash a cascade of interconnected problems: amplified GHG emissions, accelerated resource depletion, pervasive air, water, and soil pollution, reduced biodiversity, and exacerbated climate change [34]. Plastic debris degrading into microplastics and nanoplastics harms marine life, infiltrates food chains, and disrupts ecological balances across all ecosystems [35]. Alarmingly, individuals may consume up to 5 g of plastic weekly, potentially leading to serious health issues and health risks, such as cancers, asthma, infertility, diabetes and other diseases [36]. Plastic environmental damage incurs significant economic costs; marine plastic pollution alone leads to estimated annual losses of $500 billion to $2.5 trillion in marine ecosystem services, representing a 1–5% loss and directly impacting vital sectors, such as fisheries, aquaculture, and tourism [37]. This financial burden, roughly $33,000 per metric ton of plastic pollution, underscores that environmental degradation is a direct economic liability, strongly incentivizing investment in recycling and circular economy models [37].

Electronic waste (e-waste), comprising end-of-life electronic products, poses a significant threat due to its hazardous composition, notably containing lead, mercury, cadmium, and lithium (Li) [38]. The volume of e-waste is alarming, having surged by 82% between 2010 and 2022 to 62 million tonnes (Mt), and is projected to reach 82 Mt by 2030 and 110 Mt by 2050 [38, 39]. This growing volume is particularly concerning since only 17.4% of e-waste is currently recycled, leading to resource depletion,

widespread pollution, and hazardous working conditions [38]. Unregulated e-waste disposal severely contaminates air, soil, and water, as informal dismantling, shredding, or melting processes release hazardous dust and toxins like dioxins, which pollute the air and heighten respiratory and cancer risks [38]. Burning e-waste further emits toxic gases and particulate matter that can travel globally [38]. Improper landfilling allows heavy metals and flame retardants to leach into soil and groundwater, contaminating water sources and degrading agricultural land, while hydrocarbons from gold-plated components can acidify rivers, killing aquatic life [38]. This creates localized environmental disaster zones, with direct exposure to carcinogens and heavy metals causing severe, long-term health implications for humans and wildlife, highlighting a critical environmental issue [38]. Efforts are intensifying to recycle plastic and electronic waste into energy via green, sustainable TENGs, offering crucial advantages, such as waste mitigation, resource recovery, and the promotion of a circular economy [25, 31, 40–44].

Organic and food waste present significant environmental and economic burdens, reflecting a massive waste of natural resources, such as land, water, energy, and fertilizers [24, 44–46]. Every year, approximately 1.3 billion tons of food are lost or wasted, representing an estimated $2.6 trillion in economic losses worldwide [45]. Its decomposition in landfills releases methane, a greenhouse gas 25 times stronger than carbon dioxide, making food waste responsible for 8% of global GHG emissions—a volume equivalent to the world's third-largest emitter [44–46]. Facing the significant environmental and economic burdens of food waste, valorizing it into value-added materials, especially through recent advances in food waste-derived triboelectric nanogenerators (TENGs), thereby creates circular solutions for clean power and reduced environmental impact [44–47].

2.2 TENG's role in global circular economy and sustainable development goals

The European Union (EU) aims for a fully circular economy by 2050, with significant milestones targeted for 2025 [48]. This transition is crucial for alleviating pressure on natural resources, achieving climate neutrality, halting biodiversity loss, and fostering sustainable economic growth and job creation [48]. The EU's Circular Economy Action Plan (CEAP) represents a fundamental shift from the linear "take-make-use-dispose" model to a regenerative one, focusing on maximizing product, material, and resource value while minimizing waste [48]. CEAP includes key policies to standardize sustainable products, addressing plastic pollution, enhancing waste management and recycling, and strengthening consumer repair rights [48]. It emphasizes designing durable, repairable, and recyclable goods and promotes digital product passports for material traceability [48]. With particular attention to plastics and textiles, this comprehensive policy framework, featuring ambitious goals and specific regulations, actively incentivizes developing and adopting technologies such as waste-derived TENGs [25, 31, 40–44], showcasing how strong policies can drive technological innovation for broader sustainability.

The United Nations Sustainable Development Goals (SDGs) offer a global framework to end poverty, protect the planet, and ensure widespread prosperity [49]. Specifically, SDG 12 "Responsible Consumption and Production" directly tackles unsustainable practices—which drive the "triple planetary crisis" of climate change, biodiversity loss, pollution, and waste—by advocating for waste reduction, recycling, and circular economy models across all sectors [49]. The United Nations Environment Programme (UNEP) actively champions resource efficiency and circularity,

spearheading negotiations to combat plastic pollution [50]. Alongside this, SDG 7 "Affordable and Clean Energy" aims to provide universal access to reliable, sustainable, and modern energy [49]. Waste-to-Energy (WtE) technologies offer a direct path to achieve SDG 7 by converting non-recyclable municipal solid waste into energy. Modern WtE systems, combined with crucial policy support such as landfill bans and financial incentives, are recognized for their potential to process waste efficiently and significantly reduce GHG emissions [50]. TENGs, especially those made from recycled materials, uniquely address both waste valorization (SDG 12) and clean energy generation (SDG 7), positioning them as a synergistic technological solution for global sustainability [25, 31, 40–47].

2.3 TENGs from recycled waste materials: A comprehensive review

Integrating waste into TENG technology offers a potent dual solution to the escalating waste pollution crisis and the growing demand for clean energy [25, 31, 44–46]. TENGs provide an eco-friendly and efficient waste-to-energy conversion, transforming diverse waste into renewable electricity [25, 31, 40–47]. This directly supports circular economy principles [48], fosters resource efficiency, aligns with SDGs [49, 50], and significantly lowers TENG fabrication costs while mitigating pollution from traditional disposal [40–43, 47], ultimately transforming waste management into an opportunity for green and clean energy. This section provides a comprehensive overview of TENGs fabricated from different types of recycled waste materials, their sources, recycling methods, performance metrics, and diverse applications. The tables in this section provide a comparative analysis and maximum performance of TENGs fabricated from recycled waste materials. Additional performance data may exist in the literature due to different material layer combinations, sizes, and design factors. **Table 1** summarizes the TENGs fabricated from household waste, such as plastic bottles and batteries [40], sketching paper and plastic bubble wrap [41], tissue roll cardboard and rubber gloves [42], pencils, paper, and plastic clear document bags [43], food packaging foils [51], milk cartons [52], beverage

Household waste	Recycling method	TENG layers[a]	Performance	Applications	Ref.
Polyethylene terephthalate (PET) bottles and batteries	Cleaning bottles and scratching graphite electrode of dry battery	PET^-, $paper^+$, graphite powder conductive paste[e]	V = 84 V, I = 101 μA, P = 26.5 $\mu W/cm^2$	Self-powered portable electronics such as digital watch and calculator	[40]
Sketching paper and plastic bubble wrap (BW)	Patches extracted from sketching paper and plastic bubble wrap	Sketching $paper^+$, plastic BW^-, Al and Cu tape[e]	V = 6.38 V, I = 5.9 μA, P = 7.84 μW	Self-powered portable electronics	[41]
Tissue roll cardboard and rubber gloves	Patches extracted from cardboard and rubber gloves	$Cardboard^+$, $rubber^-$, Al and Cu tape[e]	V = 11.13 V, I = 3.2 μA, P = 4.1 μW	Self-powered portable electronics	[42]
Graphite pencils, paper and plastic clear document bag	Graphite pencil drawn electrodes on paper and plastic bag sheets	$Paper^+$, plastic bag^-, graphite pencil electrode[e]	V = 22 V, I = 30 μA, P = 57 μW	Self-powered portable electronics	[43]
Al-coated PET food packaging foil	Use directly after cleaning	Al^+, PET^-, and Al[e]	V = 4 V, P = 0.04 $\mu W/cm^2$	Powering LEDs	[51]

Household waste	Recycling method	TENG layers[a]	Performance	Applications	Ref.
Milk carton with polyethylene (PE), Al, and pulp layers	Nanowires (NWs) on PE by plasma etching after solvent cleaning	Copper (Cu)$^{+}$, PE-NWs^{-}, Al^{e}, and Cu^{e}	V = 300 V, I = 40 μA, P = 0.8 mW	Landslide warning system and water quality monitoring	[52]
Beverage aseptic carton with PE, Al, and paper layers	Low-density PE (LDPE) oxidation (LDPEox) after solvent cleaning	LDPEox^{+}, LDPE^{-}, and Al^{e}	V = 200 V, I = 0.4 μA	Powering LEDs	[53]
Poly(vinyl chloride) PVC cling wrap and nylon laboratory coat	Use after cleaning and drying	Nylon^{+}, PVC^{-}, and Cu tape^{e}	V = 31 V, I = 3.1 μA, P = 1.19 μW/cm^2	Self-powered morse code generators	[54]
Paper wipes (PW) and PTFE-based coffee cups	Carbon nanoparticles on PW (C@PW) and hot-pressing PTFE	C@PW^{+}, PTFE^{-}, C@PW^{e}	V = 31 V, I = 3.5 μA, P = 610 μW	Wearable self-powered communication applications	[55]
PVC, PE, and polyamide (PA) plastic bags	Gold (Au) electrode sputtering on plastic bag layers	Pair1: PA^{+}, PVC^{-}, Pair2: PA^{+}, PE^{-}, Pair3: PVC^{+}, PE^{-}	V = 35.7 V, I = 5.85 μA, P = 15.2 μW/cm^2	Wearable self-powered environmental and health sensors	[56]
Polyurethane (PU) sponge, plastic bags, bottles, and Al foil	Cleaning and drying	PU foam^{+}, PE^{-}, polypropylene (PP)$^{-}$, and Al^{e}	V = 44 V, I = 0.29 μA, P = 0.32 μW/cm^2	Self-powered emergency and intrusion detection	[57]
Expanded polypropylene (EPS) packaging	Cleaning EPS boxes followed by solution casting to form PS film	PTFE tape^{+}, PU film^{-}, Al tape^{e}, and Cu tape^{e}	V = 250 V, I = 52 μA, P = 40.5 mW/cm^2	Self-powered electronics and traffic-monitoring systems	[58]
Polymer-coated Al soda cans and PET plastic cups	Use directly after washing and drying	Soda can polymer^{+}, PET^{-}, and Al^{e}	V = 519 V, I = 82 μA, P = 12.25 mW/cm^2	Self-powered portable electronics	[59]
Rice paper (RP)	RP powder pasting on conductive ink to improve performance	Rice paper and RP powder^{+}, PVC^{-}, and conductive ink^{e}	V = 392 V, I = 1.67 μA, P = 82.7 mW	Self-powered portable electronics	[60]
Waste alkaline batteries (WABs)	Pyrolysis to reactivate the electrode materials of WABs	Reactivated WAB electrode^{-}, Kapton^{+}, and Al foil^{e}	V = 790 V, I = 40.27 μA, P = 529 μW/cm^2	Self-powered portable electronics	[61]
Waste rubber bands and human hair	Chemically processed into micro/nano thin films	Human hair film^{+}, Rubber band film^{-}, and Al foil^{e}	V = 7.24 kV, I = 196.4 μA, P = 28.5 mW/cm^2	Self-powered smart human health monitoring	[62]

[a] $^{+}$ *represents tribopositive material,* $^{-}$ *represents tribonegative material, and* ^{e} *represents electrode material.*

Table 1.
Comparative analysis of TENGs fabricated from recycled household waste.

aseptic cartons [53], cling wraps and laboratory coats [54], paper wipes and coffee [55], plastic bags [56], sponge, carry bags and foils [57], packing material such as styrofoam [58], soda cans and plastic cups [59], rice paper [60], waste batteries [61], and rubber bands and human hairs [62]. **Table 2** summarizes the TENGs fabricated from biomedical waste, such as expired drugs [63], face mask, nitrile gloves and mylar

Biomedical waste	Recycling method	TENG layers[a]	Performance	Applications	Ref.
Expired drugs such as paracetamol, nimesulide, and guaifenesin	Spray-coating fine drug powder solution in DI water on Al substrate	Drug films^{+}, PET^{-}, Al and Cu[e]	V = 561 V, I = 53 μA, P = 1960 μW	Self-powered portable electronics	[63]
Three-layer polypropylene (PP) face mask and nitrile rubber gloves	Disinfection and sterilization using 70% ethanol, heating and UV sterilization	Nitrile gloves^{+}, three-layer PP face mask^{-}, Al and Cu[e]	V = 50.7 V, I = 4.8 μA, P = 8.1 μW/cm^2	Smart hand sanitizer dispenser with IoT cloud integration	[64]
Transparent Mylar polyester film	Use directly as substrate	Ni/Cu polyester tape^{+}, PTFE^{-}, and Cu[e]	V = 309 V, I = 56μA, P = 5 mW	Self-powered healthcare monitoring	[65]
Three-layer PP surgical face mask and Mylar film	Disinfection and sterilization using UV treatment	Mylar film^{+}, three-layer PP face mask^{-}, and Cu tape[e]	V = 200 V, I = 7.28 μA, P = 7.12 μW/cm^2	Self-powered portable electronics and sensors	[66]
Falcon tube (FT)	FT used as support after disinfection with ethanol and UV sterilization	Rough Al foil^{+}, nanostructured PTFE balls^{-}, and Al foil[e]	V = 120 V, I = 1.6 μA, P = 700 μW	Self-powered security system and earthquake monitoring	[67]
X-ray films	Cleaning X-ray film with DI water and drying	X-ray film^{+}, silicone film^{-}, and Al foil[e]	V = 210 V, I = 62.8 mA, P = 13.9 mW/cm^2	Self-powered electronics and sensors for smart buildings	[68]
PP-based pipet tips	Cleaning and drying	PP^{-}, electrolyte solution^{+}, and Al[e]	V = 2.3 V, I = 15μA, P = 13.9 mW/cm^2	Self-powered electrolyte detection	[69]
Medical/laboratory waste: paper, aluminum, cotton, glass, gloves, plastic/PET sheets, and petri dish	3D printing of substrate from extruded petri dish plastic waste filaments	Al, cotton, glass, gloves, and paper^{+}, plastic/PET^{-}, and Al[e]	V = 185 V, I = 1.25 μA, P = 8.1 μW/cm^2	Self-powered electronics, exercise monitoring, and safety tracking devices	[70]
Molybdenum-nickel/aluminum oxide spent catalyst Mo–Ni/Al_2O_3	MoO_3 extracted from Mo–Ni/Al_2O_3 was used to synthesize Mo-Metal Organic Framework (Mo-MOF)	Mo-MOF^{+}, Kapton^{-}, and Cu tape[e]	V = 148 V, I = 0.47 μA	Self-powered electronics, sports, and exercise monitoring	[71]
Al ointment tubes (AT) (inner epoxy resin coating)	Tubes were washed, cut, flattened, and trimmed into Al sheets	AT Al sheet^{+}, PTFE^{-}, and AT Al sheet[e]	V = 405 V, I = 82 μA, P = 658 mW/cm^2	Self-powered portable electronics	[72]

Biomedical waste	Recycling method	TENG layers[a]	Performance	Applications	Ref.
Saline bottles	Bottles washed, cut, and trimmed into sheets	Saline bottle sheet^{+}, silicone film^{-}, and Al^{e}	V = 508 V, I = 105 μA, P = 878 μW/cm^2	Self-powered environment and health monitoring	[73]
Sterilized PP-based three-layer medical masks	Fluorine-containing polymer (FP) vapor deposition on PP film	Cu^{+}, surface-modified FP-PP films^{-}, and Cu^{e}	V = 366.82 V, I = 39.52 μA, P = 83.6 μW/cm^2	Water wave energy harvesting to power electronics	[74]
Paper and Al pill box, X-ray film, and medical rubber gloves	Use sterilized medical waste after cut to size	Al film^{+}, medical glove rubber film^{-}, and Al^{e}	V = 180 V, I = 3.6 μA, P = 6.5 μW/cm^2	Self-powered electronics and human motion perception	[75]
Rebonded flexible polyurethane (RFPU) foam scraps	RFPU batch molded from FPU pieces and binder via compression and steam curing	RFPU sheet^{+}, PTFE^{-}, and Al tape^{e}	V = 117 V, P = 0.085 μW/cm^2	Self-powered portable electronics	[76]

[a] $^{+}$ *represents tribopositive material,* $^{-}$ *represents triboponegative material, and* ^{e} *represents electrode material.*

Table 2.
Comparative analysis of TENGs fabricated from recycled biomedical waste.

film [64–66], falcon tubes [67], X-ray films [68], pipet tips [69], laboratory/clinic waste such as tissue, paper, Al foil, cotton, glass, gloves, plastic/PET sheets, and petri dishes [70, 75], spent catalyst [71], ointment tubes [72], plastic bottles [73], medical masks [74], and PU foam scrap [76]. **Table 3** summarizes the TENGs fabricated from food and its waste, such as pulses and grams like split black gram [47], tomato peels [77], almond skin [78], corn husk [79], egg shell membrane [80], fish scales [81], sunflower husk [82], outer shells of peanuts [83], dry fruit shells such as almond,

Food and its waste	Recycling method	TENG layers[a]	Performance	Applications	Ref.
Split black gram (SBG)	SBG was ground and sieved to fine powder	SBG^{+}, PTFE tape^{-}, Al^{e}, and Cu tape^{e}	V = 84 V, I = 28 μA, P = 15.36 μW/cm^2	Self-powered portable electronics and autonomous lighting	[47]
Tomato peels (TPs)	TPs were washed, cut in desired sizes, and dried for 2 days	Tomato peel^{+}, PET^{-}, Al tape^{e}, and Cu foil^{e}	V = 150 V, I = 84 μA, P = 5400 μW	Self-powered portable electronics	[77]
Edible almond seed skin (EASS)	EASS was air-dried overnight and ground into fine powder	EASS powder film^{+}, PTFE^{-}, and Cu tape^{e}	V = 60 V, I = 3.4 μA, P = 36.1 μW/	Self-powered portable electronics and humidity sensing	[78]
Corn husk and polystyrene (PS) food container	Trimmed corn husk was glued onto Cu tape and dried for 24 h	Corn husk film^{+}, extruded PS^{-}, and Cu tape^{e}	V = 1300 V, P = 67.05 μW/cm^2	Self-powered portable electronics	[79]

Food and its waste	Recycling method	TENG layers[a]	Performance	Applications	Ref.
Egg shell membrane (ESM)	Manually removed ESM was rinsed, dried, and applied to Al tape	ESM^+, $PTFE^-$, Al^e, and Cu tapes^e	I = 1.3 μA, P = 25 μW/cm^2	Powering green LEDs	[80]
Fish scales	Fish scales were washed, dried, and cut into uniform pieces	Fish scale$^+$, $PTFE^-$, and Al/Cu tape^e	V = 50 V, I = 1.7 μA	Self-powered portable electronics	[81]
Sunflower husks (SFH)	Dried SFH were milled into powder and glued on Al tape	SHF powder film$^+$, PET^-, Al^e, and Cu tape^e	V = 488 V, I = 28.5 μA, P = 1200 μW	Self-powered portable electronics	[82]
Peanut shells (PS)	Dried PS were milled into powder and glued on Al tape	PS powder film$^+$, $PTFE^-$, Al^e, and Cu tape^e	V = 390 V, I = 14 μA, P = 1.3 mW	Self-powered portable electronics	[83]
Waste fruit shells (WFS) of almond (A), walnut (W), and pistachio (Pi)	Washed and dried WFSs were ground into fine powder and glued on Al tape	Pi-WSF$^+$, $PTFE^-$, Al^e, and Cu tape^e	V = 700 V, I = 95 μA, P = 416.1 μW/cm^2	Self-powered portable electronics	[84]
Waste tea leaves (WTL) and waste polystyrene solution (WPS)	WTL powder was sonicated into WPS, then cast, dried, and peeled into films	WTL@WPS films$^+$, PTFE tape$^-$, and Al tape^e	V = 1800 V, I = 37.5 μA/cm^2, P = 6125 μW/cm^2	Self-powered portable electronics	[85]
Wheat straws (WS)	Dried WS were fixed on Cu tape to form WS films	WS film$^+$, FEP^-, Al^e, and Cu tape^e	V = 250 V, I = 12 μA, P = 40.4 μW/cm^2	Self-powered portable electronics and wind speed detection	[86]
Rice husks (RH)	Leached RH were annealed and milled into nanoporous $RHSiO_2$ particles	$RHSiO_2$@$PDMS^+$, $PTFE^-$, Cu tape^e	V = 270 V, I = 14 μA, P = 84 μW/cm^2	Powering LEDs	[87]
Vegetable leaves (VL) between wheat bread (WB)	Washed and dried VL between WB for sandwich TENG	Vegetable leave$^+$, Bread$^-$, and Cu^e	V = 15 V, I = 3 μA, P = 0.1 μW/cm^2	Edible TENG for powering portable electronics	[88]
Instant noodles	Instant noodles were blended into powder and taped onto a paper	Noodles powder$^+$, PTFE tape$^-$, and Cu foil^e	V = 576 V, I = 56μA, P = 7840 μW/cm^2	Powering LEDs	[89]
Banana leaf	Use directly after cut to size	Banana leaf$^+$, EVA foam$^-$, and Cu^e	V = 5604 V, P = 1.3 μW/cm^2	Smart home security system	[90]

[a] *$^+$ represents tribopositive material, $^-$ represents triboponegative material, and ^{e} represents electrode material.*

Table 3.
Comparative analysis of TENGs fabricated from recycled food and its waste.

walnut, and pistachio [84], tea leaves [85], wheat straw [86], rice husk [87], vegetable leaves sandwiched between bread [88], instant noddle powder [89], and banana leaf [90]. **Table 4** summarizes the TENGs fabricated from textile and its waste, such as

Textile and it waste	Recycling method	TENG layers[a]	Performance	Applications	Ref.
Cigarette filters (CF) composed of cellulose acetate	CF was cleaned three times with ethanol and dried at 60°C for 4 h	Cigarette filters^{+}, PTFE^{-}, and recycled Al foil^{e}	V = 42.8 V, I = 0.86 μA, P = 6.32 μW/cm^2	Self-powered portable electronics	[91]
Cellulose acetate (CA)-based cigarette filters (CF) fiber	Polyethyleneimine (bPEI)/CA composite film formation via solvent casting	CA/bPEI composite film^{+}, PTFE^{-}, CA/bPEI^{e} and Al^{e}	V = 274 V, I = 11 μA, P = 754 μW/cm^2	Self-powered portable electronics, tactile sensing, and HMI	[92]
Jute, cotton, wool, silk, and cigarette butt fibers	Single-electrode and four-finger knitted structure using textile and silver-coated rubber threads	Textile thread^{+}, rubber thread^{-}, and silver (Ag)^{e}	V = 75 V, I = 0.2 μA, P = 5.3 μW/cm^2	Self-powered sports and athletics monitoring	[93]
Fluorinated cotton cloth (F-cotton) and Ag-coated nylon	Grafting polymeric fluoroalkylated siloxane films on cotton	Nylon cloth^{+}, F-cotton^{-}, and Ag^{e}	V = 120 V, P = 13 μW/cm^2	Self-powered portable electronics	[94]
Waste clothes: linen, cotton, rayon, polyester, and silk	Use cloth scrap directly after getting from the tailor	Cloth layers^{+}, PVC film^{-}, and Al foil tape^{e}	V = 320.78 V, I = 8.73 μA, P = 201 μW/cm^2	Wearable TENGs to power portable electronics	[95]
Waste waterproof textiles: raincoat, umbrella, and blanket cover	Directly use to fabricate liquid–solid-based TENG (L-S TENG)	Water^{+}, waterproof textile^{-}, and Cu tape^{e}	V = 0.5 V, P = 0.41 nW	Self-powered falling liquid monitoring as pH, height, speed, tilt angle, temperature etc.	[96]
Socks cloth	Use directly after cutting to size	Sock cloth^{+}, PTFE film^{-}, and Cu^{e}	V = 267 V, I = 3.4 μA, P = 225.6 μW	Self-powered foot pressure-based human motion monitoring	[97]
Face mask PP layer, kevlar, cotton, poly(lactic acid) (PLA), and UHMWPE	Ripping 3-ply face mask to get PP layer, use other layers directly after cutting to size	Cotton and PLA^{+}, UHMWPE, PP, and kevlar^{-}, and Cu tape^{e}	V = 0.5 mV,	Powering portable electronics and TENG education to design and fine arts students	[98]
Wasted polyester clothes-derived PET nanofibrous web	Electrospinning of DCM–TFA cloth solution	PET nanofibrous web^{-}, Al foil film^{+}, and Al foil^{e}	V = 70 mV	PET nanofibrous web triboelectric performance	[99]
Nylon fabric (Hemline)	Use directly after cut to size	Nylon^{+}, PVC^{-}, and screen-printed Ag^{e}	V = 136 V, I = 2.68 μA, P = 125 μW	Self-powered wearable electronics and motion-sensing	[100]
Silk fabric	Use fabric directly with liquid metal (LM)-filled PTFE hollow fibers	Silk fabric^{+}, PTFE fibers^{-}, LM^{e}, and Cu^{e}	V = 206 V, I = 28.7 μA, P = 3.04 μW/cm^2	Wearable TENG for powering electronics and home automation	[101]

Textile and it waste	Recycling method	TENG layers[a]	Performance	Applications	Ref.
Bathroom waste: scrubbers, face, and paper towels	Use directly after cleaning and cut to size	Bathroom waste^{+}, FEP^{-}, and conductive fabric sticky tape^{e}	V = 19 V, I = 8 μA, P = 34.5 μW	Self-powered smart shelf and biomechanical monitoring	[102]
Keratin extracted from jacket fur after extensive cleaning	Keratin/chitosan (CK) aerogel structure by freeze-drying method	CK aerogel^{+}, PTFE^{-}, and Cu^{e}	V = 324 V, I = 32 μA, P = 1440 μW/cm^2	Wearable TENG for powering portable electronics	[103]
Pyrrole-polymerized (PPy) alkali-purified Lycra fabric (LC) to get LC/PPy fabric	Impregnating LC/PPy with chitosan (CS)/phytic acid (PA) solution to form LPCP composite fabric	Human skin^{+}, CS in LPCP^{-}, and conductive fabric^{e}	V = 0.34 V, I=∼1.8 μA, P=∼7 μW/cm^2	Biodegradable, flame-retardant wearable textile-based TENG for firefighter motion and safety monitoring	[104]

[a] $^{+}$ *represents tribopositive material,* $^{-}$ *represents triboponegative material, and* ^{e} *represents electrode material.*

Table 4.
Comparative analysis of TENGs fabricated from recycled textile and its waste.

cellulose acetate-based cigarette filters' fiber [91, 92], textile cloth waste i.e., jute, cotton, wool, silk, linen, rayon, polyester, hemline nylon, etc. [93, 95, 100, 101], fluorinated cotton cloth and silver-coated nylon [94], waste waterproof textiles, i.e., raincoats, umbrellas, and blanket covers [96], socks cloth [97], face mask, kevlar, poly (lactic acid) (PLA) and ultra high-molecular weight polyethylene (UHMWPE) fabrics [98], waste polyester clothes-derived PET nanofibrous web [99], bathroom waste, i.e., scrubbers, face and paper towels [102], waste jacket fur keratin/chitosan aerogel structure [103], and pyrrole-polymerized Lycra fabric composite [104]. **Table 5** summarizes the TENGs fabricated from electronic waste, such as dry cells and alkaline batteries [40, 61], smartphone displays [105], spent Li-ion batteries [106, 107], printer cartridge [108], LCDs [109], discarded copper wires [110], and printed circuit boards (PCBs) and its waste [111, 112].

2.4 Challenges and future directions for recycled TENGs

Primary challenge for recycled waste-driven TENGs is achieving full biodegradability, as many current recycled designs still contain non-degradable components recycled from waste. Future research must focus on developing truly fully biodegradable TENGs—ensuring all parts degrade naturally—by exploring novel biodegradable functional materials with superior triboelectric properties and controllable degradation rates. The output performance of many waste-derived TENGs requires substantial improvement to power-demanding electronics beyond low-power applications. Additionally, the scalability of fabrication methods, especially for complex micro/nanostructures, hinders mass production and commercialization. Future efforts must focus on enhancing performance via advanced surface modification and material doping, and developing cost-effective, scalable manufacturing processes to enable broader market penetration.

3. Green biopolymer-based TENGs

Building upon the imperative for fully biodegradable and green TENGs, a significant focus has shifted towards biopolymer-based TENG (BP-TENG) [26, 113–117]. The focus on biopolymers signifies a pivotal evolution in TENG research, fundamentally integrating environmental impact throughout the device lifecycle, from raw material sourcing to end-of-life degradation. As biopolymer macromolecules derived from living organisms with repeating units, such as sugars, amino acids, or hydroxy fatty acids, these TENGs leverage diverse types of biopolymers, including polysaccharides such as cellulose, chitosan, starch, and various biodegradable polyesters [26, 113, 114]. Their natural origin bestows characteristics, such as excellent biodegradability, recyclability, biocompatibility, and superior functional properties, directly addressing the limitations of non-degradability in most TENGs and aligning TENGs with eco-friendly and sustainable development [26, 113, 114]. Beyond eco-friendly energy harvesting, their compatibility with biological systems makes them ideal for wearable and implantable devices; their gradual degradation and absorption ensure long-term functionality, negating the need for device removal [26, 113, 114]. Their surfaces possess active functional groups (e.g., hydroxyl (-OH), carboxyl (-COOH), amino (-NH_2), and aldehyde (-CHO) groups) that facilitate electron transfer, significantly improving triboelectric output and enabling the formation of special function composite materials [26]. For instance, natural rubber provides exceptional

Electronic waste	Recycling method	TENG layers[a]	Performance	Applications	Ref.
Dry cells	Scratching graphite electrode of dry cells to get graphite powder	PET^{-}, paper^{+}, and graphite powder conductive paste^{e}	V = 84 V, I = 101 μA, P = 26.5 μW/cm^2	Self-powered portable electronics such as digital watch and calculator	[40]
Waste alkaline batteries (WABs)	Pyrolysis to reactivate the electrode materials of WABs	Reactivated WAB electrode^{-}, Kapton^{+}, and Al foil^{e}	V = 790 V, I = 40.27 μA, P = 529 μW/cm^2	Self-powered portable electronics	[61]
Discarded smartphone displays	Cleaned disseminated liquid crystal and polymer transistor layers of display	Liquid crystal layer^{-}, polymer transistor layer^{+}, and Al foil^{e}	V = 190.31 V, I = 9.56 μA	Self-powered portable electronics and human movement monitoring	[105]
Spent lithium-ion battery (LIB)	LIBs are dismantled into casing, Al-plastic (PP–Al-PA) film (APF), and PCB with recycled Cu	PA^{+} and PP^{+}, Cu on PCB^{-}, Al^{e}, and Cu^{e}	V = 155.8 V, I = 7.7 mA	Self-powered lithium iron phosphate (LFP) battery recycling	[106]
Spent LIB's metallic current collectors and polymeric separator with PP or PE or PP/PE/PP	Ethanol cleaning, water rinsing, drying of Al and Cu foils, and polymeric separator	Al foil^{+}, Polymeric separator^{-}, Al^{e}, and Cu foils^{e}	V = 40 V, I = 0.16 μA, P = 23 μW	Powering portable electronics	[107]
Organic photoconductor (OPC) drum from printer cartridge	Detached OPC drum was cut, flattened, and trimmed into OPC sheets	OPC sheet^{+}, fluorinated ethylene propylene (FEP)$^{-}$, and Al foil^{e}	V = 492 V, I = 138 μA, P = 460 μW/cm^2	Self-powered portable electronics	[108]
Laptop liquid crystal displays (LCD)	Cleaned disseminated LCD layers	LCD layer sheet^{+}, FEP^{-}, and Al sheet^{e}	V = 470 V, I = 143 μA, P = 504 μW/cm^2	Self-powered electronics and photocatalytic degradation	[109]
Discarded electric wires from damaged UPS batteries	Cu recovered from waste wires electrodeposited on carbon-coated tribo layers	Printing paper^{+}, Kapton tape^{-}, and electrodeposited Cu^{e}	V = 552 V, I = 18.8 μA, P = 768 μW/cm^2	Self-powered electronics and LED panels for advertisement boards	[110]
E-waste: resistors and ICs	E-waste components were ground to powder for triboelectric film	E-waste film^{+}, teflon^{-}, and Cu foil^{e}	V = 680 V, I = 4624 μA, P = 77.25 μW/cm^2	Self-powered electronics and e-waste classification	[111]
Printed circuit boards (PCBs) sheets	PCB technology: laminating, copper patterning, Kapton deposition, and device forming	Cu gratings^{+}, Kapton film^{-}, and patterned Cu^{e}	V=~500 V, I=~5.3 μA, P = 267 mW/cm^2	Self-powered portable electronics and lighting	[112]

[a] $^{+}$ *represents tribopositive material,* $^{-}$ *represents triboponegative material, and* ^{e} *represents electrode material.*

Table 5.
Comparative analysis of TENGs fabricated from recycled electronic waste.

extensibility, gelatin and sodium alginate form robust gels, and chitosan exhibits broad-spectrum antimicrobial properties [26, 113, 114]. These distinctive attributes enhance TENG functionality, and efforts in this field are intensely directed at developing high-performing, biopolymer-based TENGs that are entirely harmonious with environmental and biological systems [26, 113–117]. A clear classification of biopolymers (BPs) by origin and chemical structure is crucial for informed material selection and TENG design. BPs are primarily categorized into natural biopolymers (NBPs), which are derived from living organisms, e.g., polysaccharides, proteins, and others, and synthetic biopolymers (SBPs), which are man-made, e.g., polyesters, polyurethanes, and others [26, 113].

3.1 Synthetic biopolymer-based TENGs

SBPs are synthetic materials derived from natural resources, typically synthesized via chemical processes or biotechnological methods, and are frequently engineered to possess specific degradation characteristics [26, 113]. Key categories include poly(-alpha-esters), extensively investigated for biomedical applications, such as poly(lactic acid-co-glycolic acid) (PLGA), poly(lactic acid) (PLA), poly(L-lactic acid) (PLLA), poly(ϵ-caprolactone) (PCL), polydioxanone (PDO), poly(butylene succinate) (PBS), and poly(butylene adipate terephthalate) (PBAT). Their main chains typically consist of repeating units of alkanes and ester or carbonate functional groups, with some featuring alkane side groups [26, 113]. Often categorized under poly(alpha-esters), poly(alpha-carbonates) specifically include poly(propyl carbonate) (PPC) and poly (trimethylene carbonate) (PTMC) [26, 113]. Other SBPs encompasses poly(ortho ester urethanes) (POEUs), polyanhydrides, polyurethanes (PUs), polyphosphazenes, polyethylene oxide (PEO), polyvinyl alcohol (PVA), and polyvinyl pyrrolidone (PVP). Among these, PEO, polyanhydride, POEU, and PU notably contain a significant proportion of main-chain ether bonds ([-CH2-CH2-O-]n groups) [26, 113].

SBPs, owing to their biodegradability and biocompatibility, show potential for TENG applications in self-powered wearable, biomedical, and implantable devices, serving as either triboelectric layers or support materials [26]. When incorporated into PLA, polyhydroxybutyric (PHB) acid functions as both a filler and a nucleating agent [26]. The PHB particles act as templates that effectively direct and boost PLA's crystallization, significantly enhancing the resulting polymer's overall crystalline properties and yielding a completely biodegradable material [26]. As a biodegradable thermoplastic, PLA offers straightforward processing, outstanding formability, and 3D printing adaptability, enabling its effortless molding into diverse, specialized forms for TENG structural layers and providing significant benefits for TENG applications through its inherent flexibility and design adaptability [26]. Moreover, the development of other SBPs, including a novel fully bio-based elastomer created via a dual dynamic cross-linking network utilizing numerous hydrogen bonds and β-hydroxy esters, demonstrates their utility in self-powered devices through TENGs [26].

3.2 Natural biopolymers

NBPs are primarily derived from living organisms and are further sub-classified based on their chemical structures and sources. The extensive polysaccharide group includes cellulose (e.g., microcrystalline cellulose (MCC) and bacterial cellulose (BC)) and its derivatives, along with other significant polysaccharides such as starch,

chitosan, alginate, chitin, chondroitin sulfate, pullulan, and hyaluronic acid [113]. Their structures typically feature repeating anhydro-D-glucose units linked by β-(1–4) glycosidic bonds, characterized by various hydroxyl (-OH) and other functional groups (e.g., methoxy (-OCH_3), ethoxy (-OCH_2CH_3), sodium carboxymethyl (-OCH_2COO-Na+), and polyether groups) that significantly influence their properties [113]. For instance, MCC and BC possess -OH groups; alginate uniquely contains a carboxylate (-COO) group and two -OH groups, while chitosan has an amino (-NH_2) group and two -OH groups; chitin incorporates an N-acetyl amide group and two -OH groups; pullulan and starch are rich in -OH side groups, whereas chondroitin sulfate and hyaluronic acid feature disaccharide repeating units with combinations of -COO, N-acetyl amide, sulfate, and -OH groups [113]. The proteins and poly(amino acids) are another NBP sub-category, which is predominantly characterized by abundant amide bonds within their main chains [26, 113]. Other NBPs include polynucleotides, exemplified by deoxyribonucleic acid (DNA) sodium salt (sodium DNA) from calf thymus, and polyhydroxyalkanoates, naturally produced by various microorganisms, primarily bacteria [26, 113].

3.2.1 Polysaccharide-based TENGs

Polysaccharides are biopolymers formed by monosaccharides linked via glycosidic bonds, serving as essential biological macromolecules widely distributed in plants, seaweed, fungi, and microorganisms [118]. These naturally sourced biopolymers typically exhibit favorable friction properties and charge transfer capabilities, attributed to their abundant functional groups, such as hydroxyl, carboxyl, and amino groups [26, 113, 118]. This subsection reviews various polysaccharide-based TENGs, including those utilizing cellulose, chitosan, starch, alginate, and pullulan, from the literature with their electrical performance summarized in **Table 6**.

3.2.1.1 Cellulose-based TENGs

Cellulose, a natural organic polymer, is characterized by its chain-like structure, formed by D-glucose units connected via 1,4-β-glycosidic bonds, with a general chemical formula of $(C_6H_{10}O_5)_n$ [113, 118, 119]. It is widely distributed in most plants and can also be biosynthesized by certain microorganisms, such as bacteria [118, 119]. The numerous hydroxyl groups present on its glycosyl units facilitate the formation of extensive hydrogen bonds, resulting in a robust hydrogen bonding network [118, 119]. Its distinctive structural and chemical attributes enable the production of nanocellulose and various cellulose derivatives through diverse physical and chemical methods, significantly expanding the range of cellulose-based materials available [118, 119]. *Bacterial cellulose (BC)* is a versatile NBP synthesized by certain bacterial strains and characterized by nanofiber networks (typically 20–100 nm in diameter) that contribute to its remarkable mechanical properties and broad range of applications, including TENGs [118]. To create a uniform bacterial nanocellulose (BNC) film, BC—obtained through standard procedures—is dissolved in ethyl acetate and subsequently homogenized via ultra-sonication before being cast onto an electrode. BC composite films are fabricated by modifying BC films with nanoparticles (NPs) and nanowires (NWs), such as ZnO-NPs, $BaTiO_3$-NPs, and AgNWs, to enhance their surface roughness and polarizability [118].

Cellulose microfibers (CMF) and nanofibrils (CNF), composed of nano-sized fibrils (typically 5–60 nm), yield films known for their transparency, flexibility, and tunable surface roughness, making them suitable for green electronics and TENGs [118]. The fabrication of CNF film involves initial preparation of CNF hydrogel from wood pulp

Sr	Polysaccharide	TENG layers[a]	V_{oc}	I_{SC}	Pd	Sr	Polysaccharide	TENG layers[a]	V_{oc}	I_{SC}	Pd
1	Bacterial cellulose	BNC^{-} on Cu^{e}, PMO/Cu^{+e}	13	3	0.48	2	Bacterial cellulose	$BC/ZnO\text{-}NP^{+}$ on ITO^{e}, $PTFE^{-}$	57.6	5.78	4.2
3	Bacterial cellulose	$BC/BaTiO_3\text{-}NP^{+}$ on Cu^{e}, $PDMS^{-}$ on Cu^{e}	181	21	480	4	Bacterial cellulose	$BC/BaTiO_3$/Ag-NW $paper^{+e}$, $PTFE^{-}$ on Al^{e}	170	9.8	180
5	Cellulose nanofibrils	CNF^{+} on ITO^{e}, FEP^{-} on ITO^{e}	32.8	35	—	6	Cellulose nanofibrils	Allicin-thiol-CNF^{+} on Al^{e}, $PVDF^{-}$ on Al^{e}	7.9	5.13	10.1
7	Cellulose nanofibrils	AZO-CNF $paper^{+e}$, $TiCl_4$-AZO-CNF^{-e}	7	0.7	—	8	Cellulose nanofibrils	CNF-phosphorene^{+} on Au^{e}, PET^{-} on Au^{e}	5.2	—	9.36
9	Cellulose micro-nanofibers	Ag^{e} on CMF/CNF^{+} paper, FEP^{-} on Ag^{e}	21.9	0.17	7.7	10	Cellulose nanofibrils	$AgNWs^{+e}$/CNF paper CNF^{-}/$AgNW^{e}$ paper	21	2.5	69.3
11	Crystalline cellulose	MCC/$PDMS^{-}$ film on Al^{e}, Al^{+e}	28	2.8	64	12	Crystalline cellulose	NCC/$PDMS^{-}$ film on Al^{e}, Al^{+e}	320	—	760
13	Crystalline cellulose	MCC^{+}-Al^{e}-PET film, PI^{-}-Al^{e}-PET film	153	3.9	—	14	Ethyl cellulose	μEC^{+} on Ag^{e}, 317 L stainless $steel^{-}$ on Ag^{e}	245	50	—
15	Porous ethyl cellulose (PEC)	PEC^{+} on ITO^{e}, $PDMS^{-}$ on ITO^{e}	45	—	0.12	16	Ethyl cellulose	EC^{+} on Ag^{e}, $PLLA^{-}$ on Ag^{e}	310	16.2	—
17	Cellulose acetate (CA)	CA^{+} on Al^{e}, $PTFE^{-}$ on Al^{e}	7.3	9.1	—	18	Cellulose acetate	CA/PEI^{+}, Silicone $rubber^{-}$, e-$textile^{e}$	478	—	2210
19	Cellulose paper and nitrocellulose	Crepe CP^{+} on Cu^{e}, NCM^{-} on Cu^{e}	197	31.5	1610	20	PPy-coated cellulose paper	PPy-coated CP^{+e}, NCM^{-} on PCP^{e}	60	8.8	83
21	Cellulose paper (CP)	CP^{+} on Au^{e}, PCL/GO^{-} on Au^{e}	120	4	7.25	22	New Zealand pine wood	Natural wood $slice^{+}$, $PTFE^{-}$ on Cu $foil^{e}$	220	5.8	15.82
23	Delignified basla wood	Modified $wood^{+}$ on Cu^{e}, $PTFE^{-}$ on Cu^{e}	81	1.8	5.7	24	Cellulose aerogel	CNF/PEI $aerogel^{+}$ on ITO^{e}, $PVDF^{-}$ on ITO^{e}	106	9.2	1330
25	Cellulose (CMC) aerogel	$CMC/PDMS^{+}$, $Kapton/PDMS^{-}$, Al^{e}	14	0.22	—	26	Cellulose (C/BT) aerogel	$Hand^{+}$, PDMS on C/BT^{-}, Al^{e}	48	—	—
27	Cellulose II aerogel	Cellulose II^{+} on Al^{e}, $PTFE^{-}$ on Al^{e}	65	—	12.7	28	All printed 3D CNF aerogel	3D CNF $aerogel^{+}$ on Ag, 3D $PDMS^{-}/Ag^{e}$	55	0.94	2.9
29	Chitosan nanocomposites	Chitosan-$glycerol^{+}$, $PTFE^{-}$ on Al^{e}	130	15	—	30	Chitosan (CS-Nano) films	Chitosan-acetic $acid^{+}$, Kapton^{-}, Al^{e}	1.6	0.04	0.002

Sr	Polysaccharide	TENG layers[a]	V_{oc}	I_{SC}	Pd	Sr	Polysaccharide	TENG layers[a]	V_{oc}	I_{SC}	Pd
31	3D-printed chitosan film	PA/Chitosan^{+}, PE/PDMS^{-}, Al^{e}	308	62	593	32	Chitosan biocomposite	Chitosan-diatom^{+}, FEP^{-}, Al^{e}	150	1.02	1.57
33	Chitosan hybrid ionic hydrogels	AgNWs@CS/Cu^{+e}, PDMS^{-}	218	—	200	34	Peruvian potato starch	Starch film^{+}, mixed cellulose ester^{-}, Al^{e}	300	—	—
35	Potato starch electrolyte	Starch $CaCl_2{}^{+}$, PTFE^{-}, Al^{e}	1.2	—	17	36	Corn based thermoplastic	Thermoplastic starch^{+}, PDMS^{-}, Cu tape^{e}	560	180	1700
37	Sodium alignate (SA) film	PVA^{+} on Li^{e}, SA film^{-} on, Al^{e}	1.47	0.004	0.38	38	Calcium alignate film	Al^{+e}, Calcium alignate film^{-} on Al^{e}	33	0.15	—
39	Dual PVA/SA ionic hydrogel	PVA/SA hydrogel in PDMS^{+e}, Al^{+e}	203	17.6	98	40	Pullulan-NaF film	Pullulan-NaF^{+} on Al^{e}, Kapton^{-} on Ag^{e}	79	—	4.11

[a] *+ represents tribopositive material, − represents triboponegative material, and e represents electrode material, PMO: polyoxymethylene, PCL/GO: poly(caprolactone)/graphene oxide.*

Table 6.
Electrical performance of polysaccharide-based TENGs reported in the literature, presenting key metrics, such as open-circuit voltage (V_{oc} in V), short-circuit current (I_{SC} in μA), and power density (Pd in μW/cm²) [118].

through TEMPO-mediated oxidation and mechanical homogenization. This hydrogel is subsequently diluted, filtered to form a CNF slab, and then carefully dried under applied pressure to yield a flat, transparent, and flexible film. To enhance the CNF's limited surface polarity and functional groups, allicin, extracted from garlic juice, was grafted onto CNF (Alc-S-CNF) using a 'thiol-ene' click chemistry approach. The process involved first by preparing thiol-functionalized CNFs (CNF-SH) via silanization, followed by grafting allicin onto the CNF-SH in the presence of an azobisisobutyronitrile (AIBN) initiator under controlled reaction conditions. A transparent conductive oxide (TCO) layer of aluminum-doped zinc oxide (AZO) was deposited onto transparent CNF paper via low-temperature atomic layer deposition (ALD) to form an AZO-CNF paper with excellent mechanical integrity and electrical conductivity across a wide range of strains. To increase the AZO-CNF paper's electronegativity, it was subsequently treated with oxygen plasma followed by $TiCl_4$ infiltration, which incorporated highly electronegative oxygen and chlorine atoms. To enhance the triboelectric performance of CNF, few-layered phosphorene is exfoliated in ethanol and then mixed with TEMPO-oxidized CNF as an additive, forming a transparent, flexible phosphorene-CNF paper. To enhance the electrification effect of the microporous CMF skeleton prepared from filter paper, CNFs are layered onto both sides, and an Ag nanolayer is deposited on the top to form a hierarchical CMF/CNF/Ag triboelectric layer [118, 119].

Microcrystalline cellulose (MCC) and nanocrystalline cellulose (NCC) are increasingly used in TENGs due to their excellent characteristics: renewability and biodegradability, strong triboelectric nature due to abundant hydroxyl groups, high specific surface area and surface roughness that maximize charge transfer during contact-separation cycles, and inherent flexibility and mechanical robustness for sustaining repeated operation [113, 118]. To fabricate MCC/PDMS films, cellulose powder was mixed with PDMS solution and cured on micro-grade sandpaper surface to increase surface roughness [118]. Cellulose nanocrystal flakes (CNCFs) were produced through wet ball milling and freeze-drying and used to form PDMS/CNCFs composite film by spin-coating to enhance triboelectrification [118].

Ethyl cellulose (EC) is a natural cellulose derivative in which some hydroxyl groups are replaced with ethyl ether groups, a modification that yields altered charge affinity, excellent film-forming, and mechanical properties, making it a highly effective and suitable material for TENG [113, 118, 119]. An EC film is formed via an automatic film coater from a magnetically stirred mixture of EC powder in a dichloromethane-ethanol solution [118]. The surface of the resulting film is subsequently modified by inductively coupled plasma (ICP) etching to create micro-patterns on EC (μEC). Porous ethyl cellulose (PEC) film is prepared by spin-coating an EC solution in ethanol-toluene onto a substrate, followed by immediate immersion in a hexane non-solvent to induce precipitation [118]. Smooth EC film is made using the same procedure but without the immersion-precipitation step [118].

Cellulose acetate (CA), a modified cellulose derivative with acetate groups replacing some hydroxyls through acetylation, is a suitable TENG material due to its altered charge affinity, excellent mechanical properties, and durability for repeated contact-separation cycles [113, 118]. To enhance triboelectrification, porous CA biocomposites are fabricated by first blending a solution of CA powder in a mixed acetone-water solvent with a polymer solution like polyethyleneimine (PEI). After removing air bubbles, the mixture is blade-coated onto a groove model and dried to obtain the CA/PEI composite film [118]. Nitrocellulose membrane (NCM) is a tribonegative material due to the presence of nitro groups ($-NO_2$), and their porous microstructure enhances triboelectric efficiency by increasing the surface area [113, 118].

Cellulose paper (CP) is an effective tribopositive material for TENGs, as its hydroxyl (-OH) groups readily donate electrons, while its low-cost, biodegradability, and rough, porous structure increases the effective contact area to enhance electrification [113, 118]. Traditional cellulose papers can act as an excellent tribopositive layer as well as an electrode by coating them with conductive materials, such as polypyrrole (PPy) through polymerization, which is a promising option due to its high conductivity, stability, and eco-friendly properties [113, 118]. To prepare PPy-coated cellulose paper (PCP), commercial cellulose paper is first soaked in a pyrrole monomer and then transferred into a ferric chloride solution to achieve the in situ polymerization of PPy. *Wood* is a suitable material for TENGs due to its sustainability and natural porous structure, as well as the presence of hydroxyl (-OH) functional groups from its cellulose and hemicellulose components [113, 118]. To enhance its performance, chemical and structural modifications, such as delignification and polymer impregnation, are often applied to alter its triboelectric polarity, improve its mechanical durability, and further increase its effective contact area for a higher triboelectric output [113, 118]. Usually, flexible porous wood is obtained through a two-step process: first, delignification is performed by immersing wood slices in a hot alkaline solution to remove lignin and increase porosity, followed by densification through hot-pressing to obtain the flexible wood.

Cellulose aerogels are a promising material for TENG development due to their unique properties, including an ultra-low density, a high specific surface area, and a highly porous, interconnected network structure with the benefits of cellulose (including renewability, biodegradability, and biocompatibility) [118]. CNF/PEI porous aerogel films are fabricated by freeze-drying-casted CNF/PEI solutions to form 3D aerogels, which are then compressed to obtain the final porous CNF/PEI aerogel films [118]. To prepare the porous sodium carboxymethyl cellulose (CMC) aerogel film, a solution of CMC and sugar is mixed with a benzoic acid-alcohol solution, dried to a gelatinous form, and then baked and compressed to reduce porosity and remove residual benzoic acid. This compressed CMC aerogel is then used to prepare the CMC aerogel/PDMS film by dipping it into a PDMS solution and drying it to evaporate the solvent [118]. Cellulose/$BaTiO_3$ (C/BT) aerogels are obtained by dispersing BT nanoparticles in a cellulose solution, followed by adding epoxy chloropropane and stirring for crosslinking to form hydrogels, which are then washed, frozen, and freeze-dried [118]. Cellulose II aerogels are fabricated via a dissolution and regeneration process using inorganic molten salt hydrate (lithium bromide trihydrate) as a solvent, which converts native cellulose (cellulose I) to cellulose II and results in a large number of mesopores and a larger surface area, significantly improving TENG performance [118]. An all-printed 3D TENG is fabricated by direct-writing Ag electrodes, CNF aerogel, and PDMS layers onto PET substrates using a cylindrical nozzle, with different tilt angles (θ = 90°, 45°, and 0°) employed during printing [118]. Optimizing the printing behavior of CNF-based ink for patterned frictional layers involves adding cellulose as a viscosity modifier, which results in shear-thinning behavior and viscosity proportional to its concentration, thereby ensuring smooth ink flow, precise filament printing, and strong underlying layers.

3.2.1.2 Chitosan-based TENGs

Chitosan (CS), a natural biopolymer obtained from the deacetylation of chitin, contains electron-donating groups, making its nanocomposite films potential triboelectric layers with enhanced properties and performance in TENGs [113, 118].

Chitosan microcomposite (CS-Micro) and nanocomposite (CS-Nano) films, incorporating natural materials such as lignin, glycerol, or pre-gelatinized starch, are prepared by dissolving the constituents in acetic acid, spin-coating the solution onto a substrate, such as micro/nanostructured silicon, followed by baking, neutralization, washing, and peeling. These flexible and biocompatible chitosan micro/nanocomposite films are used in TENGs, making the resulting device wearable, environmentally stable, and shape-adaptive [118]. Fused Deposition Modeling (FDM) is a 3D printing technique that fabricates TENG friction layers by directly extruding insoluble biomass materials (e.g., lignin, cellulose, and chitosan) and PDMS, initially prepared as filaments by pouring them separately into PA and PE tubes, and then depositing them layer by layer through a cylindrical nozzle onto a build platform (e.g., PA/Chitosan, PA/Lignin, or PE/PDMS) [118]. Highly porous, biocompatible diatom biosilica frustules are simply embedded into chitosan to create biofriendly, skin-attachable chitosan-diatom (CS-D) composite films [118]. In CS-D-based TENGs, diatom frustules significantly enhance the chitosan surface's positive charge density and the TENG's output power, a result attributed to the diatom's high-surface area and porosity, promoting electron-donor functionalities through hydrogen bonding. Chitosan-based hybrid ionic conductive hydrogels are formed by crosslinking chitosan with metal ions (Ag^{+}/Cu^{2+}) and embedding Ag nanowires (AgNWs) (like AgNWs@CS/Ag and AgNWs@CS/Cu) for enhanced TENG output [118].

3.2.1.3 Starch-based TENGs

Starch is utilized as a TENG layer given its abundant, cost-effective, and biodegradable nature; its rich hydroxyl groups promote electron-donating functionalities via hydrogen bonding, enabling versatile processing into tailored films or composites. Potato starch film preparation involves extracting starch from homogenized potatoes through sieving, decantation, degreasing with methanol water, and drying. The dried starch is then diluted in water, partially hydrolyzed with dilute hydrochloric acid, combined with glycerol, homogenized, and neutralized with dilute sodium hydroxide. Finally, this solution is cast onto micro/nano grade sandpaper-containing petri dishes and dried in an oven to form the films [113, 118]. To make starch more positive, starch electrolyte films are prepared by diluting dried starch in distilled water, adding $CaCl_2$, homogenizing with heat and continuous stirring, then casting the solution onto a suitable substrate for drying [118]. Corn-based thermoplastic starch (TPS) tribo layer was prepared by heating and stirring a mixture of corn starch, water, and glycerin until it became thick and transparent, then casting it onto a glass plate and air-drying to yield the film [118].

3.2.1.4 Alginate and pullulan-based TENGs

Alginate, a natural anionic polysaccharide from brown seaweed, is highly suitable for TENG layers due to its abundance, low cost, biocompatibility, and biodegradability. It can form porous structures and undergo ion crosslinking, enhancing its effective surface area and mechanical strength. Additionally, its chemical structure, particularly the presence of oxygen-containing groups, allows it to function as a triboelectric layer with tunable polarity. Sodium alginate (SA) powder is dissolved in deionized (DI) water with continuous stirring (sometimes ultrasonic irradiation) to form a homogeneous solution, which is then cast onto a flat or micro/nanostructured substrate (e.g., petri dish with DVD disc) to get alignate films (sometimes in

airflow environment) [118]. To form robust calcium alginate films (CAF), cast SA film or solutions are crosslinked by reacting with a $CaCl_2$ solution, forming a stable gel with a 3D egg-box model network via ion exchange [118]. These films are then dried for solidification, with porous structures specifically achieved through freeze-drying after initial gelation. Upon contact with water, PVA and SA films, along with the Li and Al electrodes, undergo complete dissolution within 10 minutes, a process facilitated by hydrogen gas from the Li-water reaction and subsequent decomposition of the Al by resulting LiOH [118]. Hybrid dual-network hydrogels of PVA and SA are synthesized by dissolving PVA and SA in DI water and mixing with borax solution to form the initial hydrogel. Finally, these hydrogels are immersed in $CaCl_2$ solution, resulting in a dual borax-crosslinked PVA and Ca-crosslinked SA networks. This structure, coupled with Na^+, Ca^2+, Cl^-, and $B(OH)_4{}^-$ ions, provides improved self-healing, elasticity, and enhanced ionic conductivity [118]. Pullulan (P–P), a natural, water-soluble exopolysaccharide from fungus, is highly suitable for TENG due to its biodegradability and excellent film-forming ability, yielding robust, flexible films; additionally, its high hydroxyl group content allows for tunable TENG polarity and enhanced charge generation. P–P films are prepared by dissolving P–P powder in DI water with continuous stirring to form a homogeneous solution, which is then cast onto a flat or micro/nanostructured substrate and dried, with optional additives such as CMC, glycerol, NaF, trehalose, or BSA incorporated for performance enhancement [118].

3.2.2 Protein-based TENGs

Proteins, including silk fibroin, keratin, collagen, and gelatin, are biopolymers suitable for flexible TENG layers. Silk fiber, i.e., mulberry silk fibers, a natural amphiphilic block copolymer of silk fibroin and collagen, contains -COOH, -NH2, and -OH functional groups that provide strong electron-donating capabilities and, through moisture absorption, avoid poor contact and ensure stable TENG performance for over million cycles even at high humidity [26, 113]. Recombinant spider silk proteins (RSSPs) were synthesized by inducing silk expression in *E. coli* cells containing relevant plasmids. Genetically engineering RSSPs with different repetitive units enhanced their triboelectric effect, with 32mer RSSP showing improved output voltage compared to 4mer RSSP [26]. Chicken skin biowaste, rich in collagen with a triple-helix peptide backbone, contains electron-donating amino acid functional groups (glycine, proline, and hydroxyproline). These groups, particularly $-NH_2$ and -OH, give collagen stable, hydrophilic, and charged properties crucial for its electron-donating ability in triboelectricity [26]. Keratin, a fibrous structural protein found abundantly in vertebrate hair, nails, feathers, and horns, is characterized by high sulfur content for stability and amino acid residues for mechanical strength. Rich in electron-donating functional groups, such as $-NH_2$, -COOH, and -SH, keratin-containing materials such as human hair demonstrate superior electron-donating capabilities compared to common TENG-positive materials (e.g., nylon-66) [26]. Gelatin, a mix of peptides and proteins, is produced by partially hydrolyzing animal collagen from the skin, bones, and connective tissues. Its unique properties, like gel formation, stem from abundant functional groups, such as -CONH, $-NH_2$, -COOH, and -OH [26]. A highly conductive gelatin/NaCl organohydrogel (GNOH) TENG layer is prepared by mixing gelatin and NaCl solution followed by immersion in a glycerol/water solvent, which imparts outstanding anti-freezing and anti-drying and triboelectric properties [26].

4. Challenges, future perspectives, and conclusions

Despite progress, sustainable TENGs face key challenges for widespread adoption and optimization. These include optimizing output, enhancing material stability (as biowaste is humidity-sensitive and often tribo-positive), and needing more efficient, eco-friendly processing techniques that currently limit performance. Durability and long-term performance remain concerns. Achieving technological maturity and commercialization demands scaling, standardization, regulatory frameworks, industry acceptance, and comprehensive life cycle assessments, alongside a broader focus on recycled composites. Future research must prioritize full biodegradability, especially for protein-based TENGs using non-biodegradable components. Further molecular engineering and manufacturing process optimization are crucial for enhancing performance. Finally, overcoming environmental limitations is vital, particularly for polysaccharide-based TENGs challenged by low output or extreme conditions. In conclusion, sustainable, green and recycled material-based TENGs offer a compelling path to a greener energy future. Overcoming current challenges through continued innovation in material science, device design, and manufacturing is crucial to fully realize their potential in diverse applications, from personal electronics to large-scale energy harvesting. Future efforts should focus on exploring the effects of mixing biowaste materials on TENG stability, durability, and efficiency, and on utilizing chemical modification for enhanced cellulose-based nanogenerator performance. Ultimately, this will diversify electricity access, extend device lifespan, and improve efficiency, directly contributing to sustainable development goals.

Acknowledgements

The authors thank Qatar National Library (QNL) for providing open access funding.

Conflict of interest

The authors declare no conflict of interest.

DOI: http://dx.doi.org/10.5772/intechopen.1012346

Author details

Kashif Riaz[1,2*], Abdelkrim Khelif[1] and Muhammad Umaid Bukhari[2]

1 Division of Information and Computing Technology, College of Science and Engineering, Hamad Bin Khalifa University, Doha, Qatar

2 Department of Electrical Engineering, Information Technology University (ITU) of the Punjab, Lahore, Pakistan

*Address all correspondence to: kriaz@hbku.edu.qa; kashif.riaz@itu.edu.pk

IntechOpen

References

[1] Gupta A. Portable electronics market size, share and growth report 2030. 2017. Available from: https://www.marketresearchfuture.com/reports/porprotein-electronics-market-4126 [Accessed: June 24, 2025]

[2] International Energy Agency (IEA). Net zero by 2050 A roadmap for the global energy sector. 2021. Available from: https://www.iea.org/reports/net-zero-by-2050 [Accessed: June 24, 2025]

[3] Statista. Projected global battery demand from 2024 to 2028 by application. 2021. Available from: https://www.statista.com/statistics/1103218/global-battery-demand-forecast/ [Accessed: June 24, 2025]

[4] Jacoby M. It's time to get serious about recycling lithium-ion batteries - Chemical & Engineering News (C&EN). 2019. Available from: https://cen.acs.org/materials/energy-storage/time-serious-recycling-lithium/97/i28 [Accessed: June 24, 2025]

[5] Mrozik W, Rajaeifar MA, Heidrich O, Christensen P. Environmental impacts, pollution sources and pathways of spent lithium-ion batteries. Energy & Environmental Science. 2021;**14**(12): 6099-6121. DOI: 10.1039/D1EE00691F

[6] Melchor-Martínez EM, Macias-Garbett R, Malacara-Becerra A, Iqbal HMN, Sosa-Hernández JE, Parra-Saldívar R. Environmental impact of emerging contaminants from battery waste: A mini review. Case Studies in Chemical and Environmental Engineering. 2021;**3**:100104. DOI: 10.1016/J.CSCEE.2021.100104

[7] Freitag C, Berners-Lee M, Widdicks K, Knowles B, Blair GS, Friday A. The real climate and transformative impact of ICT: A critique of estimates, trends, and regulations. Patterns. 2021;**2**:100340. DOI: 10.1016/J.PATTER.2021.100340

[8] Singh N, Ogunseitan OA. Disentangling the worldwide web of e-waste and climate change co-benefits. Circular Economy. 2022;**1**:100011. DOI: 10.1016/J.CEC.2022.100011

[9] Green technology and sustainability market: Market.US. 2024. Available from: https://market.us/report/green-technology-and-sustainability-market/ [Accessed: June 24, 2025]

[10] Wang S, Lin L, Wang ZL. Nanoscale triboelectric-effect-enabled energy conversion for sustainably powering portable electronics. Nano Letters. 2012;**12**:6339-6346. DOI: 10.1021/nl303573d

[11] Wang ZL, Chen J, Lin L. Progress in triboelectric nanogenerators as a new energy technology and self-powered sensors. Energy & Environmental Science. 2015;**8**:2250-2282. DOI: 10.1039/C5EE01532D

[12] Wang ZL. Triboelectric nanogenerators as new energy technology and self-powered sensors—Principles, problems and perspectives. Faraday Discussions. 2015;**176**:447-458. DOI: 10.1039/C4FD00159A

[13] Yu J, Lv X, Wang K. Applications of triboelectric nanogenerators in medical recovery: A review. ACS Applied Electronic Materials. 2024;**6**:5465-5478. DOI: 10.1021/acsaelm.4c01055

[14] Ramaraj SG, Elamaran D, Tabata H, Zhang F, Liu X. Biocompatible triboelectric energy generators (BT-TENGs) for energy harvesting and

healthcare applications. Nanoscale. 2024; **16**:18251-18273. DOI: 10.1039/D4NR01987C

[15] Pu X, An S, Tang Q, Guo H, Hu C. Wearable triboelectric sensors for biomedical monitoring and human-machine interface. IScience. 2021;**24**: 102027. DOI: 10.1016/j.isci.2020.102027

[16] Luo J, Wang ZL. Recent progress of triboelectric nanogenerators: From fundamental theory to practical applications. EcoMat. 2020;**2**:e12059. DOI: 10.1002/EOM2.12059

[17] Lin Z, Chen J, Yang J. Recent progress in triboelectric nanogenerators as a renewable and sustainable power source. Journal of Nanomaterials. 2016; **2016**:5651613. DOI: 10.1155/2016/5651613

[18] Wang Y, Yang Y, Wang ZL. Triboelectric nanogenerators as flexible power sources. npj Flexible Electronics. 2017;**1**:1-10. DOI: 10.1038/s41528-017-0007-8

[19] Yang Y, Guo X, Zhu M, Sun Z, Zhang Z, He T, et al. Triboelectric nanogenerator enabled wearable sensors and electronics for sustainable internet of things integrated green earth. Advanced Energy Materials. 2023;**13**: 2203040. DOI: 10.1002/AENM.202203040

[20] Liu L, Guo X, Lee C. Promoting smart cities into the 5G era with multi-field internet of things (IoT) applications powered with advanced mechanical energy harvesters. Nano Energy. 2021; **88**:106304. DOI: 10.1016/J.NANOEN.2021.106304

[21] Chen B, Wang ZL. Toward a new era of sustainable energy: Advanced triboelectric nanogenerator for harvesting high entropy energy. Small. 2022;**18**:2107034. DOI: 10.1002/SMLL.202107034

[22] Wu H, Wang S, Wang Z, Zi Y. Achieving ultrahigh instantaneous power density of 10 MW/m^2 by leveraging the opposite-charge-enhanced transistor-like triboelectric nanogenerator (OCT-TENG). Nature Communications. 2021;**12**:1-8. DOI: 10.1038/s41467-021-25753-7

[23] Tang W, Jiang T, Fan FR, Yu AF, Zhang C, Cao X, et al. Liquid-metal electrode for high-performance triboelectric nanogenerator at an instantaneous energy conversion efficiency of 70.6%. Advanced Functional Materials. 2015;**25**: 3718-3725. DOI: 10.1002/ADFM.201501331

[24] Du T, Chen Z, Dong F, Cai H, Zou Y, Zhang Y, et al. Advances in green triboelectric nanogenerators. Advanced Functional Materials. 2024;**34**:2313794. DOI: 10.1002/ADFM.202313794

[25] Wang Y, Li Z, Fu H, Xu B. Sustainable triboelectric nanogenerators based on recycled materials for biomechanical energy harvesting and self-powered sensing. Nano Energy. 2023;**115**:108717. DOI: 10.1016/J.NANOEN.2023.108717

[26] Liu Z, Chen X, Wang ZL. Biopolymer and biomimetic techniques for triboelectric nanogenerators (TENGs). Advanced Materials. 2025;**37**: 2409440. DOI: 10.1002/ADMA.202409440

[27] Zou H, Nguyen TD, Pace G. Materials and figures of merit for nanogenerators. MRS Bulletin. 2025;**50**: 1-10. DOI: 10.1557/S43577-025-00872-4

[28] Zhang R, Olin H. Material choices for triboelectric nanogenerators: A

critical review. EcoMat. 2020;**2**:e12062. DOI: 10.1002/EOM2.12062

[29] Otake Y, Kobayashi T, Asabe H, Murakami N, Ono K. Biodegradation of low-density polyethylene, polystyrene, polyvinyl chloride, and urea formaldehyde resin buried under soil for over 32 years. Journal of Applied Polymer Science. 1995;**56**:1789-1796. DOI: 10.1002/APP.1995.070561309

[30] Ahmed A, Hassan I, Ibn-Mohammed T, Mostafa H, Reaney IM, Koh LSC, et al. Environmental life cycle assessment and techno-economic analysis of triboelectric nanogenerators. Energy & Environmental Science. 2017;**10**:653-671. DOI: 10.1039/C7EE00158D

[31] Basith SA, Khandelwal G, Mulvihill DM, Chandrasekhar A. Upcycling of waste materials for the development of triboelectric nanogenerators and self-powered applications. Advanced Functional Materials. 2024;**34**:2408708. DOI: 10.1002/ADFM.202408708

[32] Nassajfar MN, Abdulkareem M, Horttanainen M. End-of-life options for printed electronics in municipal solid waste streams: A review of the challenges, opportunities, and sustainability implications. Flexible and Printed Electronics. 2024;**9**:033002. DOI: 10.1088/2058-8585/AD699B

[33] World Economic Forum. Plastic waste: Here's what it could look like by 2060. 2022. Available from: https://www.weforum.org/stories/2022/07/recycling-efforts-not-enough-to-solve-plastic-waste-problem/ [Accessed: June 24, 2025]

[34] Gabisa EW, Ratanatamskul C, Gheewala SH. Recycling of plastics as a strategy to reduce life cycle GHG emission, microplastics and resource depletion. Sustainability. 2023;**15**:11529. DOI: 10.3390/SU151511529

[35] Nawaz F, Islam ZU, Ghori SA, Bahadur A, Ullah H, Ahmad M, et al. Microplastic and nanoplastic pollution: Assessing translocation, impact, and mitigation strategies in marine ecosystems. Water Environment Research. 2025;**97**:e70032. DOI: 10.1002/wer.70032

[36] World Economic Forum. Microplastics are everywhere. Here's how to curb plastic pollution. 2023. Available from: https://www.weforum.org/agenda/2023/11/plastics-microplastic-pollution-reduce-climate-health/ [Accessed: June 24, 2025]

[37] Beaumont NJ, Aanesen M, Austen MC, Börger T, Clark JR, Cole M, et al. Global ecological, social and economic impacts of marine plastic. Marine Pollution Bulletin. 2019;**142**: 189-195. DOI: 10.1016/J.MARPOLBUL.2019.03.022

[38] Liu K, Tan Q, Yu J, Wang M. A global perspective on e-waste recycling. Circular Economy. 2023;**2**:100028. DOI: 10.1016/J.CEC.2023.100028

[39] UNITAR, SCYCLE. The global E-waste monitor 2024—Electronic waste rising five times faster than documented E-waste recycling: United Nations Institute for Training and Research (UNITAR), Sustainable Cycles (SCYCLE) Programme. 2024. Available from: https://ewastemonitor.info/the-global-e-waste-monitor-2024/ [Accessed: June 24, 2025]

[40] Bukhari MU, Khan A, Maqbool KQ, Arshad A, Riaz K, Bermak A. Waste to energy: Facile, low-cost and environment-friendly triboelectric nanogenerators using recycled plastic and electronic wastes for self-powered

porprotein electronics. Energy Reports. 2022;**8**:1687-1695. DOI: 10.1016/j.egyr.2021.12.072

[41] Bukhari MU, Riaz K, Ahmed R, Arshad A, Maqbool KQ, Khan A, et al. Enhanced area triboelectric nanogenerator utilizing recycled single used plastic bubble wrap and discarded sketching paper ensuring circularity of material. IEEE Conference on Technologies for Sustainability (SusTech). 2025;**2025**:1-5. DOI: 10.1109/SUSTECH63138.2025.11025631

[42] Bukhari MU, Riaz K, Khan A, Maqbool KQ, Wang B, Bermak A. Sustainable energy generation from recycled household waste: A low-cost and facile rubber and cardboard based triboelectric nanogenerator. IEEE Conference on Technologies for Sustainability (SusTech). 2024;**2024**:183-187. DOI: 10.1109/SUSTECH60925.2024.10553544

[43] Khan A, Bukhari MU, Qasim Maqbool K, Riaz K, Bermak A. Recycled plastic waste-based triboelectric nanogenerator reinforcing circular economy. IEEE International Conference on Flexible and Prinprotein Sensors and Systems (FLEPS). 2022;**2022**:1-4. DOI: 10.1109/FLEPS53764.2022.9781571

[44] Kumar KU, Hajra S, Mohana Rani G, Panda S, Umapathi R, Venkateswarlu S, et al. Revolutionizing waste-to-energy: Harnessing the power of triboelectric nanogenerators. Advanced Composites and Hybrid Materials. 2024;**7**:1-42. DOI: 10.1007/S42114-024-00903-9

[45] Li L, Jin Z, Wang C, Wang YC. Valorization of food waste: Utilizing natural porous materials derived from pomelo-peel biomass to develop triboelectric nanogenerators for energy harvesting and self-powered sensing. ACS Applied Materials & Interfaces. 2024;**16**:37806-37817. DOI: 10.1021/acsami.4c02319

[46] Bhaduri A, Ha TJ. Biowaste-derived triboelectric nanogenerators for emerging bioelectronics. Advanced Science. 2024;**11**:2405666. DOI: 10.1002/ADVS.202405666

[47] Bukhari MU, Riaz K, Maqbool KQ, Ahmed R, Khan A, Wang B, et al. Harnessing green electricity from food: A Split black gram-based triboelectric nanogenerator for a self-powered autonomous lighting system and porprotein electronics. ACS Applied Bio Materials. 2024;**7**:5784-6331. DOI: 10.1021/acsabm.4c00303

[48] European Commission (EC). Circular economy action plan. 2020. Available from: https://environment.ec.europa.eu/strategy/circular-economy-action-plan_en [Accessed: June 29, 2025]

[49] United Nations Environment Program (UNEP). UNEP and sustainable development goals (SDGs). Available from: https://www.unep.org/topics/sustainable-development-goals [Accessed: June 29, 2025]

[50] UNEP. Global waste management outlook 2024. 2024. Available from: https://www.unep.org/resources/global-waste-management-outlook-2024 [Accessed: June 29, 2025]

[51] Ravi Sankar P, Supraja P, Mishra S, Prakash K, Rakesh Kumar R, Haranath D. A novel triboelectric nanogenerator based on only food packaging aluminium foils. Materials Letters. 2022;**310**:131474. DOI: 10.1016/J.MATLET.2021.131474

[52] Zhou Z, Li X, Wu Y, Zhang H, Lin Z, Meng K, et al. Wireless self-powered sensor networks driven by triboelectric

nanogenerator for in-situ real time survey of environmental monitoring. Nano Energy. 2018;**53**:501-507. DOI: 10.1016/J.NANOEN.2018.08.055

[53] Moreira KS, Santos da Campo YA, Lorenzett E, Burgo TAL. Low-cost triboelectric nanogenerator based on aseptic carton package. Results in Engineering. 2023;**17**:100965. DOI: 10.1016/J.RINENG.2023.100965

[54] Zhang P, Zhang W, Zhang H. A triboelectric nanogenerator based on waste polyvinyl chloride for Morse code generator. Sens Actuators A Phys. 2021; **322**:112633. DOI: 10.1016/j.sna.2021.112633

[55] Dudem B, Dharmasena RDIG, Riaz R, Vivekananthan V, Wijayantha KGU, Lugli P, et al. Wearable triboelectric nanogenerator from waste materials for autonomous information transmission via Morse code. ACS Applied Materials & Interfaces. 2022;**14**:5328-5337. DOI: 10.1021/ACSAMI.1C20984

[56] Feng X, Li Q, Wang K. Waste plastic triboelectric nanogenerators using recycled plastic bags for power generation. ACS Applied Materials & Interfaces. 2020;**13**:400-410. DOI: 10.1021/acsami.0c16489

[57] Khandelwal G, Chandrasekhar A, Alluri NR, Vivekananthan V, Maria Joseph Raj NP, Kim S-J. Trash to energy: A facile, robust and cheap approach for mitigating environment pollutant using household triboelectric nanogenerator. Applied Energy. 2018;**219**:338-349. DOI: 10.1016/J.APENERGY.2018.03.031

[58] Nawaz SM, Saha M, Sepay N, Mallik A. Energy-from-waste: A triboelectric nanogenerator fabricated from waste polystyrene for energy harvesting and self-powered sensor. Nano Energy. 2022;**104**:107902. DOI: 10.1016/J.NANOEN.2022.107902

[59] Chougale MY, Saqib QM, Khan MU, Shaukat RA, Kim J, Bae J. Novel recycled triboelectric nanogenerator based on polymer-coated trash soda can for clean energy harvesting. Advanced Sustainable Systems. 2021;**5**:2100161. DOI: 10.1002/ADSU.202100161

[60] Chi Y, Xia K, Zhu Z, Fu J, Zhang H, Du C, et al. Rice paper-based biodegradable triboelectric nanogenerator. Microelectronic Engineering. 2019;**216**:111059. DOI: 10.1016/J.MEE.2019.111059

[61] Patil CS, Saqib QM, Patil SR, Noman M, Chougale MY, Shaukat RA, et al. Triboelectric nanogenerator based on reactivated electrode materials derived from waste alkaline battery: Influence of pyrolysis temperature and surface morphology. Nano Energy. 2023; **121**:109205. DOI: 10.1016/J.NANOEN.2023.109205

[62] Chakraborty I, Sun L, Lai C-S. Recycling waste rubber bands and human hair into complementary surface structure-based tribo-layers for ultrahigh power generation and self-powered health monitoring. Sustainable Materials and Technologies. 2025;**43**: e01295. DOI: 10.1016/J.SUSMAT.2025.E01295

[63] Chougale MY, Saqib QM, Khan MU, Shaukat RA, Kim J, Dubal D, et al. Expired pharmaceutical drugs as tribopositive material for triboelectric nanogenerator. Advanced Sustainable Systems. 2021;**5**:2100205. DOI: 10.1002/ADSU.202100205

[64] Basith SA, Chandrasekhar A. COVID-19 clinical waste reuse: A triboelectric touch sensor for IoT-cloud supported smart hand sanitizer

dispenser. Nano Energy. 2023;**108**: 108183. DOI: 10.1016/J.NANOEN.2023.108183

[65] Zargari S, Daie Koozehkanani Z, Veladi H, Sobhi J, Rezania A. A new Mylar-based triboelectric energy harvester with an innovative design for mechanical energy harvesting applications. Energy Conversion and Management. 2021;**244**:114489. DOI: 10.1016/J.ENCONMAN.2021.114489

[66] Varghese H, Chandran A. Triboelectric nanogenerator from used surgical face mask and waste Mylar materials aiding the circular economy. ACS Applied Materials & Interfaces. 2021;**13**:51132-51140. DOI: 10.1021/ACSAMI.1C16557

[67] Chandrasekhar A, Basith SA, Vivekananthan V, Khandelwal G, Joseph Raj NPM, Purusothaman Y, et al. Smart maracas: An innovative triboelectric nanogenerator for earthquake detection and energy harvesting. Nano Energy. 2024;**123**:109379. DOI: 10.1016/J.NANOEN.2024.109379

[68] Navaneeth M, Potu S, Babu A, Rajaboina RK, Uday Kumar K, Divi H, et al. A medical waste X-ray film based triboelectric nanogenerator for self-powered devices, sensors, and smart buildings. Environmental Science: Advances. 2023;**2**:848-860. DOI: 10.1039/D3VA00018D

[69] Choi D, Tsao YH, Chiu CM, Yoo D, Lin ZH, Kim DS. A smart pipet tip: Triboelectricity and thermoelectricity assisted in situ evaluation of electrolyte concentration. Nano Energy. 2017;**38**: 419-427. DOI: 10.1016/J.NANOEN.2017.06.020

[70] Sahu M, Hajra S, Kim HG, Rubahn HG, Kumar Mishra Y, Kim HJ. Additive manufacturing-based recycling of laboratory waste into energy harvesting device for self-powered applications. Nano Energy. 2021;**88**: 106255. DOI: 10.1016/J.NANOEN.2021.106255

[71] Swain J, Hajra S, Das N, Parhi P, Panda S, Priyadarshini A, et al. Spent catalyst-derived Mo-MOF: Triboelectric nanogenerators and energy harvesting. Energy Technology. 2023;**11**:2300498. DOI: 10.1002/ente.202300498

[72] Lakshmi Suneetha V, Supraja P, Uday Kumar K, Rakesh KR. Sustainable energy harvesting from medical waste: Utilizing discarded ointment tubes in triboelectric nanogenerators. Materials Letters. 2024;**377**:137350. DOI: 10.1016/J.MATLET.2024.137350

[73] Navaneeth M, Potu S, Babu A, Lakshakoti B, Rajaboina RK, Kumar KU, et al. Transforming medical plastic waste into high-performance triboelectric nanogenerators for sustainable energy, health monitoring, and sensing applications. ACS Sustainable Chemistry & Engineering. 2023;**11**:12145-12154. DOI: 10.1021/acssuschemeng.3c03136

[74] Liang X, Liu Z, Han K, Liu S, Xie Y, Jiang T, et al. Triboelectric nanogenerators using recycled disposable medical masks for water wave energy harvesting. Advanced Functional Materials. 2024;**34**:2409422. DOI: 10.1002/ADFM.202409422

[75] Shen C, Jia L, Yang Y. Fully medical waste-based triboelectric nanogenerator for energy harvesting and intelligent human motion sensing. ACS Sustainable Chemistry & Engineering. 2024;**12**: 14141-14152. DOI: 10.1021/ACSSUSCHEMENG.4C03742

[76] Maamoun AA, Esawi AMK, Mahmoud AA, Naeim DM, Arafa M.

Waste-to-energy: Repurposing flexible polyurethane waste for triboelectric nanogenerator applications. Applied Energy. 2025;**377**:124579. DOI: 10.1016/J.APENERGY.2024.124579

[77] Saqib QM, Khan MU, Song H, Chougale MY, Shaukat RA, Kim J, et al. Natural hierarchically structured highly porous tomato peel based tribo- and piezo-electric nanogenerator for efficient energy harvesting. Advanced Sustainable Systems. 2021;**5**: 2100066. DOI: 10.1002/ADSU.202100066

[78] Saqib M, Rehman MM, Khan M, Iqbal S, Ali AU, Siddiqui GU, et al. Adaptable self-powered humidity sensor based on a highly permeable, hierarchically fibrous, and chaotically textured sustainable biowaste. Sustainable Materials and Technologies. 2025;**44**:e01374. DOI: 10.1016/J.SUSMAT.2025.E01374

[79] Elvira-Hernández EA, Hernández-Hernández J, de León A, Gallardo-Vega C, Delgado-Alvarado E, López-Huerta F, et al. Green energy harvesting to power electronic devices using portable triboelectric nanogenerator based on waste corn husk and recycled polystyrene. Energy Reports. 2024;**11**: 276-286. DOI: 10.1016/J.EGYR.2023.11.059

[80] Kaur J, Sawhney RS, Singh H, Singh M. Electricity nanogenerator from egg shell membrane: A natural waste bioproduct. International Journal of Green Energy. 2020;**17**:309-318. DOI: 10.1080/15435075.2020.1727482

[81] Singh H, Sheetal A, Singh M, Kaur J, Sui T, Loja MAR, et al. Electrical energy generation using fish scale of Rohu fish by harvesting human motion mechanical energy for self powered battery-less devices. Sensors and Actuators A: Physical. 2023;**349**:114023. DOI: 10.1016/J.SNA.2022.114023

[82] Shaukat RA, Saqib QM, Khan MU, Chougale MY, Bae J. Bio-waste sunflower husks powder based recycled triboelectric nanogenerator for energy harvesting. Energy Reports. 2021;**7**: 724-731. DOI: 10.1016/J.EGYR.2021.01.036

[83] Saqib QM, Shaukat RA, Khan MU, Chougale M, Bae J. Biowaste peanut shell powder-based triboelectric nanogenerator for biomechanical energy scavenging and sustainably powering electronic supplies. ACS Applied Electronic Materials. 2020;**2**:3953-3963. DOI: 10.1021/acsaelm.0c00791

[84] Saqib QM, Chougale MY, Khan MU, Shaukat RA, Kim J, Bhat KS, et al. Triboelectric nanogenerator based on lignocellulosic waste fruit shell tribopositive material: Comparative analysis. Materials Today Sustainability. 2022;**18**:100146. DOI: 10.1016/J.MTSUST.2022.100146

[85] Sanyal D, Chowdhury P, Dey S, Mandal A, Saha M, Nawaz SM, et al. Performance enhancement of triboelectric nanogenerator by embedding tea-leaf powder in waste polystyrene. Nano Energy. 2024;**132**: 110359. DOI: 10.1016/J.NANOEN.2024.110359

[86] Ma P, Zhu H, Lu H, Zeng Y, Zheng N, Wang ZL, et al. Design of biodegradable wheat-straw based triboelectric nanogenerator as self-powered sensor for wind detection. Nano Energy. 2021;**86**:106032. DOI: 10.1016/j.nanoen.2021.106032

[87] Wu JM, Chang CK, Chang YT. High-output current density of the triboelectric nanogenerator made from recycling rice husks. Nano Energy. 2016;

19:39-47. DOI: 10.1016/J.NANOEN.2015.11.014

[88] Jiao J, Lu Q, Wang Z, Qin Y, Cao X. Sandwich as a triboelectric nanogenerator. Nano Energy. 2021;**79**:105411. DOI: 10.1016/J.NANOEN.2020.105411

[89] Xie Y, Zhang L, Zhao K, Lu Y, Zhu Z, Guo J. An environmentally friendly reusable triboelectric nanogenerator based on instant noodle powder. Energy Reports. 2021;**7**:3480-3487. DOI: 10.1016/J.EGYR.2021.06.004

[90] Jarvio-Cordova VA, Elvira-Hernández EA, García-Saldaña A, Garay-Marín JD, Ovando-Chacón GE, Díaz-González M, et al. Sustainable triboelectric nanogenerator based on recycled and waste materials for renewable energy harvesting. Renewable Energy. 2025;**251**:123439. DOI: 10.1016/J.RENENE.2025.123439

[91] Rani GM, Wu C-M, Motora KG, Umapathi R. Waste-to-energy: Utilization of recycled waste materials to fabricate triboelectric nanogenerator for mechanical energy harvesting. Journal of Cleaner Production. 2022;**363**:132532. DOI: 10.1016/J.JCLEPRO.2022.132532

[92] Weldemhret TG, Lee JH, Park CU, Lee DW, Prabhakar MN, Park YT, et al. Triboelectric nanogenerator and UV-blocking solid polymer electrolyte nanocomposite from recycled waste cigarette butts. Sustainable Materials and Technologies. 2024;**39**:e00847. DOI: 10.1016/J.SUSMAT.2024.E00847

[93] Sahu M, Hajra S, Panda S, Rajaitha M, Panigrahi BK, Rubahn H-G, et al. Waste textiles as the versatile triboelectric energy-harvesting platform for self-powered applications in sports and athletics. Nano Energy. 2022;**97**:107208. DOI: 10.1016/J.NANOEN.2022.107208

[94] Zhang L, Yu Y, Eyer GP, Suo G, Kozik LA, Fairbanks M, et al. All-textile triboelectric generator compatible with traditional textile process. Advanced Materials Technologies. 2016;**1**:1600147. DOI: 10.1002/ADMT.201600147

[95] Amini S, Sagade Muktar Ahmed RF, Kumar S, Madanahalli Ankanathappa S, Sannathammegowda K. Electrifying waste textiles: Transforming fabric scraps into high-performance triboelectric nanogenerators for biomechanical energy harvesting. Waste Management. 2024;**190**:477-485. DOI: 10.1016/J.WASMAN.2024.10.013

[96] Kaja KR, Hajra S, Panda S, Belal MA, Pakawanit P, Vittayakorn N, et al. Triboelectrification based on the waste waterproof textiles for multisource energy harvesting. Advanced Sustainable Systems. 2025;**9**:2400678. DOI: 10.1002/ADSU.202400678

[97] Zhang P, Zhang Z, Cai J. A foot pressure sensor based on triboelectric nanogenerator for human motion monitoring. Microsystem Technologies. 2021;**27**:3507-3512. DOI: 10.1007/s00542-020-05199-5

[98] Collado I, del Río S, Saez J, de la Vega J, Vázquez-López A. Energy from waste: Triboelectric nanogenerators from fully fabric materials for smart textiles. An introductory activity for fine arts and design students. Journal of Chemical Education. 2024;**101**:5324-5333. DOI: 10.1021/acs.jchemed.4c00885

[99] Yang SB, Kim JH, Nam SY, Kwon DJ. Triboelectric properties of recycled poly (ethylene terephthalate) nanofibrous web from waste clothes. Colloids and Surfaces A: Physicochemical and

Engineering Aspects. 2025;**717**:136803. DOI: 10.1016/J.COLSURFA.2025.136803

[100] Paosangthong W, Wagih M, Torah R, Beeby S. Textile-based triboelectric nanogenerator with alternating positive and negative freestanding grating structure. Nano Energy. 2019;**66**:104148. DOI: 10.1016/J.NANOEN.2019.104148

[101] Wang W, Yu A, Liu X, Liu Y, Zhang Y, Zhu Y, et al. Large-scale fabrication of robust textile triboelectric nanogenerators. Nano Energy. 2020;**71**: 104605. DOI: 10.1016/J.NANOEN.2020.104605

[102] Hajra S, Kaja KR, Panda S, Belal MA, Panigrahi BK, Pakawanit P, et al. Waste based triboelectric nanogenerator for energy harvesting and self-powered sensors. Journal of Cleaner Production. 2025;**509**:145591. DOI: 10.1016/J.JCLEPRO.2025.145591

[103] Motora KG, Wu CM, Jose CRM, Rani GM. Waste-to-energy: Development of a highly efficient keratin enhanced chitosan bio-waste-derived triboelectric nanogenerator for energy harvesting and real applications. Advanced Functional Materials. 2024;**34**: 2315069. DOI: 10.1002/ADFM.202315069

[104] Yu Z, Zhu Z, Zhang Y, Li X, Liu X, Qin Y, et al. Biodegradable and flame-retardant cellulose-based wearable triboelectric nanogenerator for mechanical energy harvesting in firefighting clothing. Carbohydrate Polymers. 2024;**334**:122040. DOI: 10.1016/J.CARBPOL.2024.122040

[105] Ahmed RFSM, Amini S, Ankanathappa SM, Sannathammegowda K. Electricity out of electronic trash: Triboelectric nanogenerators from discarded smartphone displays for biomechanical energy harvesting. Waste Management. 2024;**178**:1-11. DOI: 10.1016/J.WASMAN.2024.02.009

[106] Zhang B, He L, Wang J, Liu Y, Xue X, He S, et al. Self-powered recycling of spent lithium iron phosphate batteries via triboelectric nanogenerator. Energy & Environmental Science. 2023;**16**: 3873-3884. DOI: 10.1039/D3EE01156A

[107] Natarajan S, Krishnamoorthy K, Sathyaseelan A, Mariappan VK, Pazhamalai P, Manoharan S, et al. A new route for the recycling of spent lithium-ion batteries towards advanced energy storage, conversion, and harvesting systems. Nano Energy. 2022;**101**:107595. DOI: 10.1016/J.NANOEN.2022.107595

[108] Suneetha VL, Mahesh V, Supraja P, Navaneeth M, Uday Kumar K, Rakesh KR. Facile and robust high-performance triboelectric nanogenerator based on electronic waste for self-powered electronics. Energy Technology. 2024;**13**:2401387. DOI: 10.1002/ENTE.202401387

[109] Kaki A, Maharana G, Madathil N, Mahesh V, Kumar KU, Daniel PJ, et al. Electronic waste to energy: Self-powered electronic devices and organic dye degradation using TENG-assisted photocatalysis. Advanced Sustainable Systems. 2025;**e00235**:1-11. DOI: 10.1002/adsu.202500235

[110] Singh M, Kumar S, Kafle A, Garg K, Sharma P, Reddy CC, et al. Economical 550 V energy harvesting from plastic and electronic waste using human motions. Journal of Materials Chemistry A. 2025; **13**:6549-6559. DOI: 10.1039/D4TA07070D

[111] Zhao E, Jiang K, Li B, Liu X, Zeng F, Chen L, et al. Classification and

utilization of waste electronic components based on triboelectric nanogenerator. Nanotechnology. 2022; **33**:495401. DOI: 10.1088/1361-6528/AC8F4F

[112] Han C, Zhang C, Tang W, Li X, Wang ZL. High power triboelectric nanogenerator based on printed circuit board (PCB) technology. Nano Research. 2015;**8**:722-730. DOI: 10.1007/S12274-014-0555-3

[113] Meng H, Yu Q, Liu Z, Gai Y, Xue J, Bai Y, et al. Triboelectric performances of biodegradable polymers. Matter. 2023; **6**:4274-4290. DOI: 10.1016/J.MATT.2023.09.017

[114] Li Z, Yu A, Zhai J, Wang ZL. Sustainable biopolymers in eco-friendly triboelectric energy harvesting. Advanced Materials. 2024;**37**:2412671. DOI: 10.1002/ADMA.202412671

[115] Zhu Q, Sun E, Zhao Z, Wu T, Meng S, Ma Z, et al. Biopolymer materials in triboelectric Nanogenerators: A review. Polymers. 2024;**16**:1304. DOI: 10.3390/POLYM16101304

[116] Torres FG, Gonzales KN, Troncoso OP, Corman-Hijar JI, Cornejo G. A review on the development of biopolymer nanocomposite-based triboelectric nanogenerators (bio-TENGs). ACS Applied Electronic Materials. 2023;**5**:3546-3559. DOI: 10.1021/ACSAELM.3C00621

[117] Bai L, Li Q, Yang Y, Ling S, Yu H, Liu S, et al. Biopolymer nanofibers for nanogenerator development. Research. 2021;**201**:1-20. DOI: 10.34133/2021/1843061

[118] Torres FG, De-la-Torre GE. Polysaccharide-based triboelectric nanogenerators: A review. Carbohydrate Polymers. 2021;**251**:117055. DOI: 10.1016/J.CARBPOL.2020.117055

[119] Niu Z, Cheng W, Cao M, Wang D, Wang Q, Han J, et al. Recent advances in cellulose-based flexible triboelectric nanogenerators. Nano Energy. 2021;**87**: 106175. DOI: 10.1016/J.NANOEN.2021.106175

Chapter 4

Textile-Based Nanogenerators as Wearable Electronics for Energy Harvesting

Yujue Yang, Hong Fu and Bingang Xu

Abstract

With the rapid development of smart wearable technology and self-powered systems, textile-based nanogenerators (T-NGs) have become a research hotspot in the field of energy harvesting and intelligent sensing owing to their flexibility, high adaptability, and integrability. This chapter systematically reviews the basic working principles and structural design strategies of triboelectric (T-NG), piezoelectric (PENG), and thermoelectric (TEG) fabric generation devices. First, the role of different texture structures (such as single fiber structure, 2D and 3D weaving structure) in improving energy conversion efficiency is introduced. Subsequently, typical cases of various devices in application scenarios such as wearable energy systems, self-powered sensors, human-computer interaction, and health monitoring are analyzed in detail. In addition, this chapter also discusses the challenges faced by current fabric power generation technology, including mechanical stability, electrical output consistency, and large-scale manufacturability. Finally, combined with the development trends of artificial intelligence, the Internet of Things, and smart materials, this chapter looks forward to the broad prospects of textile-based nanotechnology in future personalized health and smart clothing, which is expected to promote smart textiles from functional enhancement to deep intelligence.

Keywords: textile-based nanogenerators, triboelectric nanogenerators, piezoelectric nanogenerators, thermoelectric nanogenerators, wearable electronics

1. Introduction

In the past decade, the rapid development of emerging technologies such as the Internet of Things (IoT), artificial intelligence (AI), and wireless communication systems has accelerated the transformation of modern society [1–5]. Wearable and portable electronic devices have quickly become an indispensable part of daily life owing to their advantages such as lightness, flexibility, and low power consumption [6–10]. These devices are widely used in healthcare, fitness tracking, motion monitoring, and personal communications, driving the rise of a smarter and more connected lifestyle. Compared with traditional rigid electronics, modern wearable devices are expected to be lightweight, miniaturized, mechanically flexible, breathable, and able to conform to the dynamic movements of the human body. However,

one of the most critical challenges facing their widespread application is energy supply. Although batteries remain the main power source, their limitations, such as limited energy density, frequent charging, structural rigidity, environmental pollution, and limited service life, restrict the scalability and sustainability of wearable systems. This has prompted extensive research on alternative energy solutions, especially in the field of energy harvesting.

In this context, nanogenerators (NGs) have attracted much attention as a promising technology owing to their ability to harvest low-frequency mechanical energy, thermal energy, or other ambient energy and use it for power generation [11]. By converting ambient energy into usable electrical energy, nanogenerators can help develop self-powered wearable systems without the need for external batteries or frequent charging. Among the various types of NGs, triboelectric nanogenerators (TENGs), piezoelectric nanogenerators (PENGs), thermoelectric generators (TEGs), and hybrid nanogenerators have been widely studied for their applicability in wearable environments.

Textile-based nanogenerators (T-NGs) exhibit unique advantages in wearable applications, as they are lightweight, skin-friendly, scalable to large-area fabrication, and compatible with existing clothing manufacturing technologies [2, 12–16]. In addition, energy from walking, breathing, and limb movement can be harvested. By utilizing these ubiquitous energy sources, wearable NGs are expected to provide sustainable and maintenance-free energy for low-power electronic devices, thereby promoting the development of applications such as wireless health monitoring and gesture recognition. TENGs work by combining contact electrification and electrostatic induction, making them particularly suitable for harvesting mechanical energy generated by human motion, such as walking, stretching, or bending. TENGs have become leading candidates for integration into fabrics and clothing owing to their compatibility with soft materials and design flexibility [2, 17–20]. On the other hand, PENGs utilize piezoelectric materials to generate charges under applied mechanical stress. PENGs are highly sensitive and are well suited for dynamic strain environments such as joint or muscle movement [1, 21–25]. Meanwhile, TEGs use the temperature gradient between the human body and the surrounding air to convert heat into electrical energy, providing a stable, continuous power output [26–32].

The integration of these nanogenerators with textiles has given rise to wearable textile-based energy harvesting systems. By incorporating functional nanogenerators into fibers, yarns, or fabrics, these systems not only retain the inherent comfort, breathability, and flexibility of traditional textiles but also give clothing energy harvesting and self-powered sensing capabilities. This unique hybrid technology enables seamless wearability and multifunctional operation in real-world scenarios. In summary, the fusion of nanogenerator technology and textile engineering is opening up a new frontier in the development of self-powered wearable electronics. This section will introduce and discuss different types of NGs and their applications.

2. Textile-based triboelectric nanogenerators (T-TENGs)

Wearable electronic devices need to be lightweight, flexible, and self-powered. TENG converts mechanical energy into electrical energy through contact electrification and electrostatic induction. It has the advantages of low cost, softness, good biocompatibility, and adaptability to low-frequency motion, making it suitable for fabric integration. T-TENG has developed from yarn to a complete system, which is both breathable and comfortable. It can collect bioenergy and provide self-driven

sensing functions for device power supply or health monitoring. It is an important solution for realizing intelligent and sustainable wearable technology.

2.1 Working mechanisms

Triboelectric nanogenerators (TENGs) convert mechanical motion into electrical energy through contact electrification and electrostatic induction. TENGs are derived from the long-known triboelectric effect, where charges are generated through frictional interactions between different materials, and utilize differences in material electron affinity to induce charge separation during contact and motion [33–35]. Structurally, a typical TENG consists of two triboelectric layers and conductive electrodes. Under periodic mechanical stimulation, electrostatic potentials are generated between the electrodes owing to the generated surface charges. These electrostatic potentials drive electrons through an external circuit, generating an AC output. The accumulation and release of induced charges enable cyclic and sustainable energy generation even under low-frequency excitation.

Depending on the electrode configuration and the direction of motion, TENGs have four operating modes, as shown in **Figure 1**: vertical contact-separation mode, lateral sliding mode, single electrode mode, and freestanding triboelectric layer mode [36, 37]. In the vertical contact-separation mode, energy is harvested through repeated vertical contact and separation between triboelectric layers, resulting in stable voltage output and a simple device structure. In contrast, the lateral sliding mode utilizes in-plane displacement to improve charge separation efficiency and is commonly used in systems based on rotation or vibration. The single-electrode mode employs only one grounded electrode, allowing energy to be harvested from a freely moving dielectric, thus increasing design flexibility. Finally, the freestanding mode

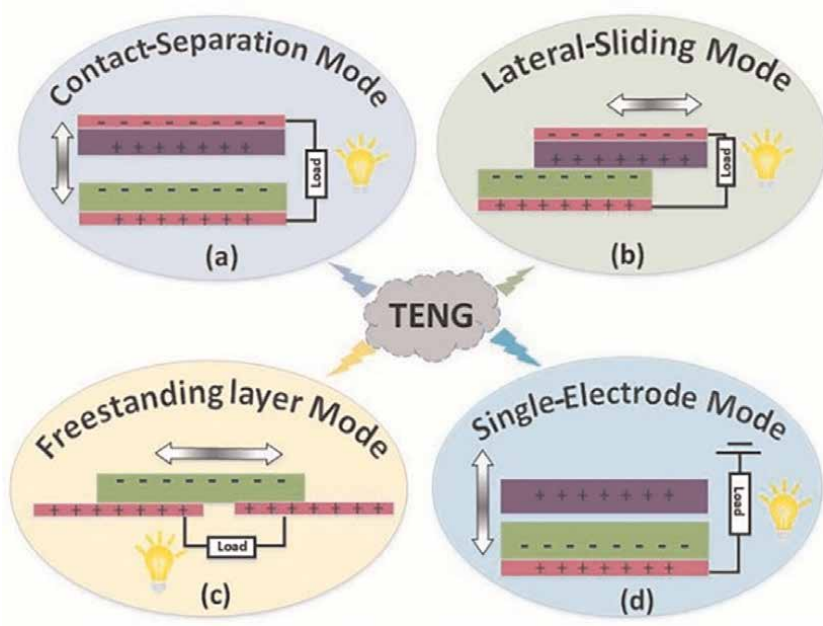

Figure 1.
Four working modes of TENGs, including (a) contact-separation mode, (b) lateral-sliding mode, (c) freestanding layer mode. (d) single-electrode mode. Reproduced with permission from Ref. [36] Copyright 2019 Wiley-VCH.

features a moving triboelectric layer interacting with a fixed, symmetrically arranged electrode. This configuration avoids electrostatic screening and enables efficient power generation without direct mechanical coupling.

2.2 Structures

2.2.1 Single fiber structure

In T-TENG research, a single fiber or yarn is not only a basic building unit, but also the core of system integration due to its structural flexibility and weaving adaptability. At present, single-fiber TENG mainly adopts a core-shell structure or coaxial structure, and can be divided into single electrode (SE) mode and core-shell contact-separation (CS) mode according to the working principle [18, 38]. The SE mode is usually composed of a conductive fiber core and an external friction layer, the latter of which can accumulate charge and has a certain mechanical protection function; while the CS mode enhances electrostatic induction under mechanical drive by setting an adjustable air gap between the conductive core and the outer shell.

For example, Wu et al. designed a single-fiber TENG in SE mode (**Figure 2a**), in which carbon nanotube fiber (CNTF) was spirally embedded in silicone foam and coated with ZnS:Cu/Ecoflex composite material to achieve dual-function output of triboelectric charging and mechanoluminescence [39]. It still maintains a stable response when stretched to 200%, and the non-contact detection distance reaches 35 cm. It has good sensitivity and integration performance and is suitable for intelligent monitoring and non-contact interaction scenarios. Another SE mode fiber proposed by Yu et al. (**Figure 2b**) uses a conductive fiber as the core and a silicone rubber as the shell [40]. It is prepared by co-extrusion and can adapt to complex deformations such as torsion and bending. It outputs a voltage of 17.5 V and a current of 0.1 μA at 1 Hz. After 30,000 cycles, the performance is almost attenuated, which is suitable for energy collection and physiological signal monitoring. In contrast, the CS mode single fiber structure developed by Zhang et al. (**Figure 2c**) uses nylon as the substrate, CNT as the conductive core, an air layer in the middle, and a double-layer fiber shell on the outside [41]. When compressed, vertical contact-separation can be achieved, resulting in strong charge transfer. It can still stably output about 56.8 V voltage and 95.5 μW m^{-1} power density at 10 cm underwater, showing good mechanical adaptability and underwater application capabilities, effectively solving the problem of output attenuation of traditional fibers in humid environments.

In summary, although the SE mode structure has advantages such as a simple preparation process and excellent flexibility, it still has limitations in multidimensional mechanical response and energy conversion efficiency. The CS mode has greater potential in improving output performance and multimodal sensing capabilities through structural elasticity regulation and an air gap adjustment mechanism. In the future, the development of single-fiber TENG will focus on material function synergy (such as ZnS:Cu luminescent composite, PVDF-TrFE polarization enhancement) and structural integration optimization (such as air gap regulation, multilayer winding, smart textile coupling) to adapt to the increasingly complex wearable environment and multifunctional smart fabric system applications.

2.2.2 Fabric structure

In order to further improve the output performance and practical application adaptability of TENG in wearable devices, researchers have also extensively explored

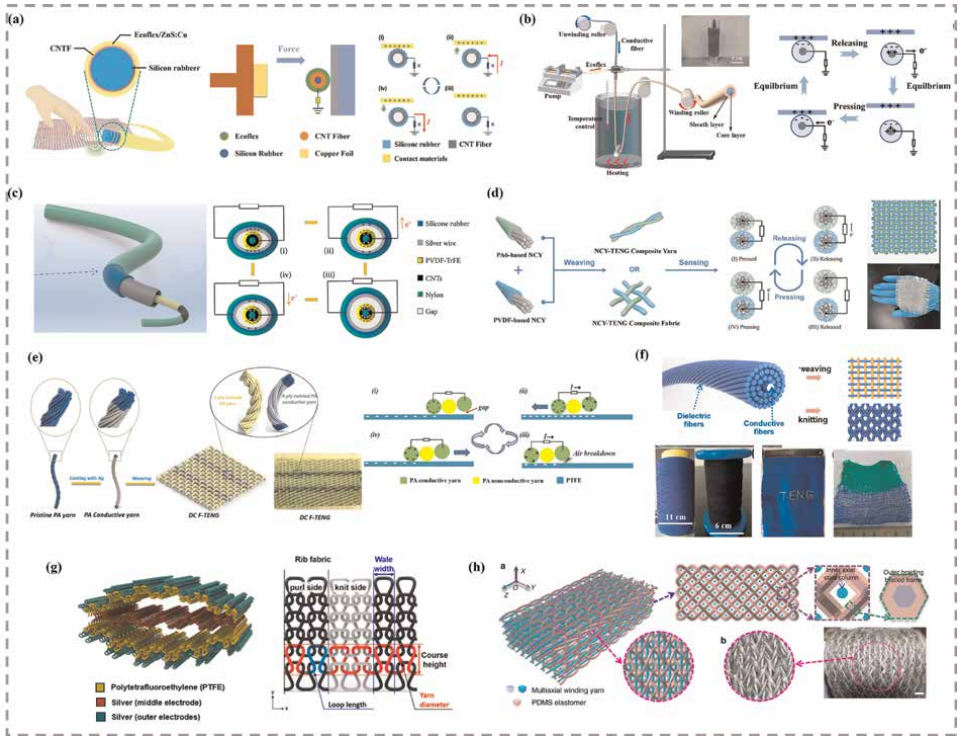

Figure 2.
T-TENGs with single fiber structure. (a) A SE-mode single-fiber TENG based on carbon nanotube fibers. Reproduced with permission from Ref. [39] Copyright 2024 Wiley-VCH. (b) A core-shell structure composed of conductive fiber as the core layer and silicone rubber as the shell layer. Reproduced with permission from Ref. [40] Copyright 2023 American Chemical Society. (c) A CS mode single fiber-based TENG with the three-layer "core-air gap-shell" structure. Reproduced with permission from Ref. [41] Copyright 2022 spj.science.org. T-TENGs with 2D fabric structure (d) A fabric-type TENG (NCY-TENG) based on coaxial nanofiber yarns. Reproduced with permission from Ref. [42] Copyright 2024 Wiley-VCH. (e) A core-shell fabric TENG, designed with stainless steel yarn as the conductive core, silicone rubber as the shell, constructed into a wearable fabric unit by weaving. Reproduced with permission from Ref. [43] Copyright 2020 American Chemical Society. (f) A fabric-based TENG on knitting and weaving structures. Reproduced with permission from Ref. [44] Copyright 2017 American Chemical Society. T-TENGs with multilayer and 3D fabric structure (g) a sandwich structure smart fabric TENG. Reproduced with permission from Ref. [45] Copyright 2017 American Chemical Society. (h) A 3D braided structure TENG, constructed by multiaxial winding yarn and flexible PDMS elastomer. Reproduced with permission from Ref. [46] Copyright 2019 2020 Springer Nature.

TENG configurations based on fabric structures. In **Figure 2d**, Wang et al. proposed a fabric-type TENG (NCY-TENG) based on coaxial nanofiber yarns [42]. By combining conjugated coaxial electrospinning with online conductive bonding coating technology, PA66 and PVDF nanofibers were respectively coated on stainless steel conductive fibers to form two types of functionalized coaxial yarns. After these yarns are plain woven into fabric units, they realize charge transfer through the contact-separation process between PVDF and PA66 shells when under pressure, and output stable AC signals. Thanks to the optimized design of its nanoscale surface roughness and shell electronegativity difference, the fabric exhibits excellent sensitivity and signal-to-noise ratio, which is suitable for real-time gait monitoring. More importantly, the conductive adhesive layer enhanced by silver nanowires and liquid metal significantly improves the shell-core bonding strength and overall conductivity, making the device sewable, washable, antibacterial, and highly flexible and has the potential for industrialization in the fields of smart insoles and health monitoring.

In addition, **Figure 2e** shows a typical core-shell fabric TENG designed by Chen et al. [43]. It uses stainless steel yarn as the conductive core, coated with ultra-flexible silicone rubber to form a shell layer, and is constructed into a wearable fabric unit by weaving. In actual work, when the skin contacts the silicone rubber surface, electrons are transferred from the skin to the shell layer, and negative charges accumulate during the separation process, inducing the core layer to generate induced positive charges and drive the flow of electrons to achieve single-electrode output. The conductive yarn structure has good flexibility and weavability, and is suitable for constructing large-area fabric arrays to meet the needs of dynamic energy harvesting systems. It can achieve a stable electrical signal output when worn, showing excellent practicality. Furthermore, **Figure 2f** shows a fabric-based TENG that is closer to traditional yarn and can be constructed based on knitting and weaving structures, developed by Zhang et al. [44]. The structure uses conductive yarn and nylon yarn to be interwoven horizontally and vertically in the form of coil units to form a highly elastic and flexible knitted network substrate. The fabric can maintain good fit and wearing comfort under complex deformations such as stretching and bending, while enhancing the sensitivity of triboelectric response. In a dynamic environment, the fabric structure can effectively collect tiny mechanical energy during movement and convert it into stable electrical signals, which are suitable for self-powered smart textile devices.

In summary, fabric-based TENG has expanded the application boundaries in the fields of flexible electronics, energy harvesting, and smart textiles through structural diversification and material integration strategies. Whether it is flat weaving of strip materials to form planar fabrics, constructing core-shell friction units, or forming multidimensional contact interfaces with knitted structures, these devices all show good mechanical stability, electrical output capacity, and wearable adaptability. At the same time, with the help of mature textile molding technology and the accessibility of commercial yarn materials, fabric-based TENG has a solid technical foundation and industrial transformation prospects.

2.2.3 Multilayer and 3D fabric structure

In order to improve the limitation of contact space and electrical output performance of traditional two-dimensional fabric TENG in the thickness direction, researchers continue to explore multilayer structures and three-dimensional structures to improve triboelectric performance and practical wearability. On this basis, a variety of TENG design strategies based on multilayer fabrics have been formed. These TENGs have high integration, good flexibility, and high output performance. As shown in **Figure 2g**, Kwak's team studied and constructed a corrugated sandwich structure smart fabric TENG, in which a wavy PET film is sandwiched between the upper and lower conductive fabrics as a dielectric layer to form a periodic convex area [45]. When external pressure is applied, the corrugated layer is compressed and deformed, thereby significantly enhancing the contact area and friction frequency between the upper and lower fabrics, achieving highly sensitive charge transfer and output performance. In contrast, **Figure 2h** shows a new three-dimensional braided structure, TENG, which is constructed by multiaxial winding yarn and flexible PDMS elastomer [46]. The device constructs an energy collection unit with three-dimensional support characteristics by means of spatial spiral winding and multiaxial interweaving: the inner layer is an axial core column composed of functional yarns, and the outer layer is a braided support, which is jointly infiltrated in the PDMS

elastomer to form an overall integrated structure. The three-dimensional fiber framework can achieve significant deformation recovery ability during the force process, providing excellent mechanical stability and a multi-directional charge separation interface. Based on its continuous yarn channel and adjustable interface, the structure significantly improves the effective contact area and charge transfer path, showing excellent flexibility, stretchability, and wearability. Experimental results show that the TENG exhibits good durability and stable output capacity in scenarios such as wearable energy harvesting and human motion monitoring.

In summary, these two fabric structures respectively reflect the evolutionary path from passive structural enhancement to structure-material integrated collaborative design. Among them, the multilayer sandwich structure improves the dynamic response ability of the interface through the corrugated interlayer, and the three-dimensional fabric realizes a truly wearable and mass-producible flexible TENG solution through the overall fiber network. These innovative fabric architectures provide strong technical support for the construction of a new generation of smart clothing and human energy harvesting systems.

3. Textile-based piezoelectric nanogenerators (T-PENGs)

In the context of the continuous development of renewable energy technology, piezoelectric energy harvesting technology has shown broad application prospects in microelectronic devices and wearable systems owing to its advantages of high efficiency, environmental protection, and flexible structure. The piezoelectric effect refers to the property of certain materials that can generate an electric charge when subjected to mechanical stress, or deform under the action of an electric field. This bidirectional energy conversion mechanism provides a basic support for energy harvesting and intelligent response. Piezoelectric materials include natural substances such as quartz and bone, as well as synthetic ceramics, polymers, and their composites. Among them, composite materials are highly favored owing to their flexibility and high responsiveness. With the deepening of research on flexible electronic devices and smart textiles, textile nanogenerators based on piezoelectric principles (T-PENG) have gradually become the core solution for wearable energy supply. They can not only be integrated into clothing by attachment or weaving but also continuously capture the weak mechanical energy generated by daily human movements, promoting battery-free operation and continuous data collection of smart devices.

3.1 Working mechanisms

Piezoelectric energy harvesting is an efficient way to convert mechanical energy into electrical energy. Its principle is that when a piezoelectric material is subjected to force, the internal dipole arrangement changes, and charge accumulation occurs at both ends, thereby forming a potential difference between the electrodes. Traditional piezoelectric nanogenerators (PENGs) mostly use a metal-insulator-metal sandwich structure, which is simple and stable, and suitable for energy harvesting of flexible wearable devices [47–49].

As shown in **Figure 3**, the energy conversion process of the textile-based piezoelectric nanogenerator (PENG) can be divided into five stages [50]. In the initial state, the dipoles are disorderly distributed and no potential is generated; after being compressed, the dipoles gradually order, form a polarized state and output current; when

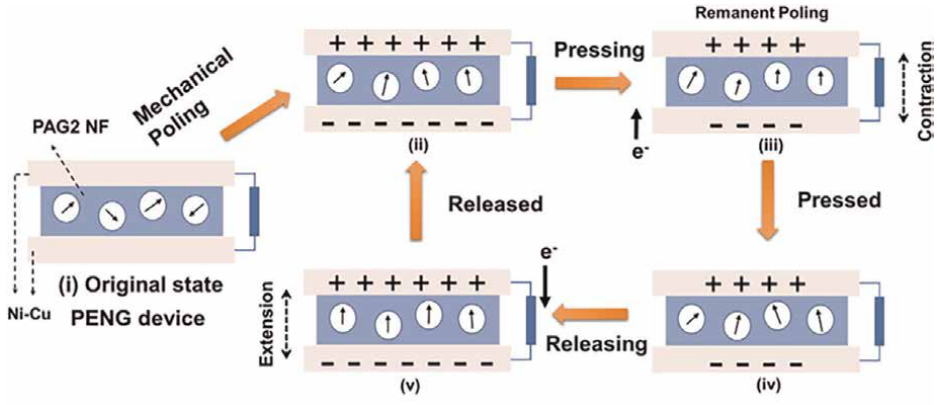

Figure 3.
The working mechanisms of PENGs. Reproduced with permission from Ref. [50] Copyright 2024 American Chemical Society.

the pressure is continuously applied to the maximum deformation, the output reaches a peak value; when the pressure is released, the polarization weakens, the dipoles tend to be disordered, and a reverse current is generated; finally, it returns to the initial state to complete a piezoelectric cycle.

In this process, the change in dipole density ensures the periodic response of the electrical signal and has good directional reversibility-when the electrode polarity is switched, the output signal is also reversed synchronously. Overall, textile piezoelectric generators have the characteristics of strong flexibility, fast response, and stable output. They can be seamlessly integrated into clothing to achieve efficient human kinetic energy collection. They are a key technical path to promote the development of a new generation of smart wearable and self-driving electronic devices.

3.2 Structures

3.2.1 Single fiber-based PENG

Single-fiber piezoelectric nanogenerators (PENGs) have attracted much attention in the field of wearable energy harvesting and intelligent sensing owing to their advantages of miniaturization, flexibility, and high integration. Based on different material systems and structural strategies, researchers have developed a variety of configurations to optimize their piezoelectric output performance and environmental adaptability. **Figure 4a** and **b** show two representative single-fiber PENG configurations, which respectively reflect the piezoelectric performance enhancement paths driven by structural design and material modification.

Figure 4a shows a typical spirally wound single-fiber PENG, which is constructed by spirally wrapping PVDF film and webbing material on the surface of elastic fiber core material [51]. Under external stress, the spiral angle changes dynamically with the fiber stretching, inducing axial polarization behavior of the PVDF layer, thereby achieving effective charge separation and piezoelectric output. This configuration not only maintains the flexibility and tensile deformation ability of the fiber, but also significantly enhances the electrical signal response caused by the change in contact area. Because its structure has good resilience and cyclic stability, it is suitable for wearable application scenarios such as dynamic stress monitoring and motion

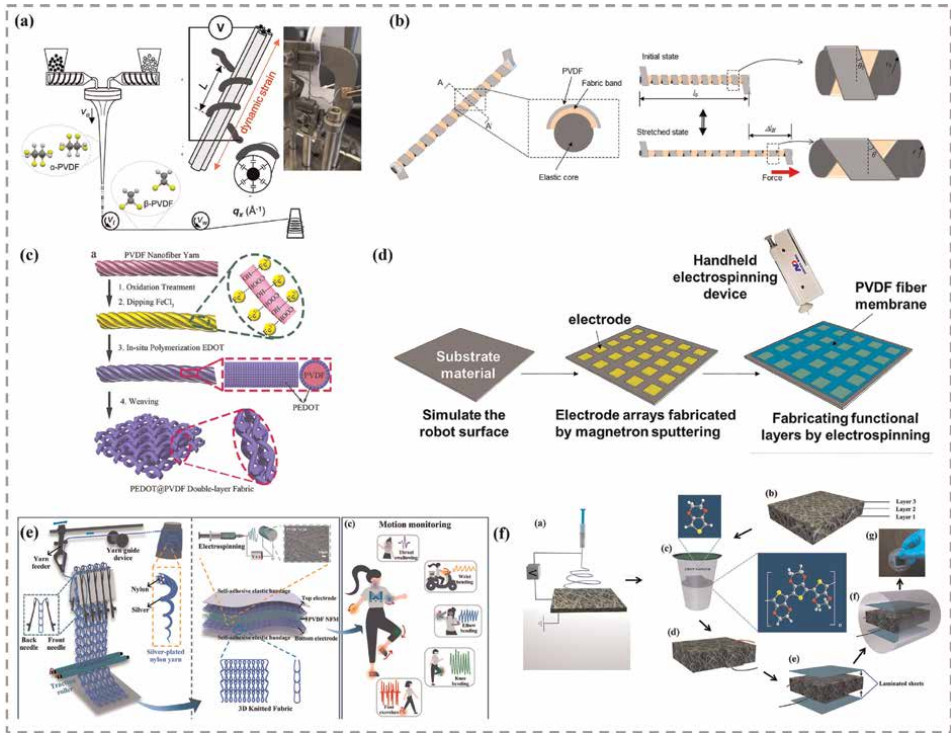

Figure 4.
T-PENGs with single fiber structure. (a) A typical spirally wound single-fiber PENG Reproduced with permission from Ref. [51] Copyright 2018 Springer Nature. (b) A conductive fiber-based PENG with conductive filler-reinforced PVDF. Reproduced with permission from Ref. [52] Copyright 2017 MDPI. T-PENGs with 2D fabric structure. (c) A double-layer conductive fabric-based PENG with a weaving structure. Reproduced with permission from Ref. [53] Copyright 2017 Springer Nature. (d) A wearable piezoelectric sensing platform with an array electrode functional layer was constructed by in situ *deposition of PVDF nanofiber membrane on a flexible substrate with a prefabricated magnetron sputtering electrode array. Reproduced with permission from Ref. [54] Copyright 2018 American Chemical Society. T-PENGs with 3D structure (e) A laminated 3D piezoelectric fabric structure based on electrospun PVDF nanofiber membrane. Reproduced with permission from Ref. [55] Copyright 2024 American Chemical Society. (f) A sandwich fabric PENG system based on a multilayer PVDF nanofiber membrane. Reproduced with permission from Ref. [56] Copyright 2018 American Chemical Society.*

recognition. In contrast, the conductive filler-reinforced PVDF composite fiber structure is shown in **Figure 4b** [52]. The fiber is prepared by wet spinning technology, and conductive fillers such as carbon black, silver powder, and steel powder are uniformly doped into the PVDF matrix to achieve molecular-level regulation of its crystal structure and polarization properties. The introduction of conductive fillers not only improves the dielectric constant of the composite material but also effectively induces the directional transformation of the PVDF molecular chain to the β phase, thereby enhancing the piezoelectric response. Tensile tests and X-ray scattering analysis show that the structure has good chain orientation behavior under strain, and can continuously output electrical signals linearly related to the stress frequency, showing excellent sensing linearity and stability.

Overall, although the two fiber configurations have different technical paths, they are both based on the "core-shell" structural concept to carry out functional integration: the former regulates strain distribution and output response through geometric design, and the latter achieves polarization enhancement and energy conversion efficiency improvement through material component optimization. In the future, with

the development of new multiphase materials and intelligent texturing strategies, single-fiber PENG is expected to be applied on a large scale in wearable energy supply, self-powered health monitoring, and smart fabrics, thus promoting the practical application of flexible electronic systems.

3.2.2 2D fabric-based PENG

In order to overcome the problem of insufficient energy output of single fiber or yarn-type PENG due to limited active area, researchers have gradually developed a PENG construction strategy based on fabric structure. By weaving functionalized fibers or composite nanoyarns into two-dimensional or three-dimensional fabric structures, the energy conversion efficiency can be significantly improved while maintaining the flexibility and wear resistance of the fabric. **Figure 4c** shows a typical double-layer conductive fabric structure, the construction process of which includes oxidation treatment of PVDF nanofibers, activation of ferric chloride, *in situ* polymerization of EDOT monomers, and final weaving [53]. In this process, the PEDOT conductive layer is obtained by *in situ* polymerization on the PVDF surface to form a core-shell structure yarn of PEDOT@PVDF, which is finally woven into a double-layer fabric. Thanks to the high conductivity of PEDOT and the piezoelectric activity of PVDF, the fabric exhibits excellent mechanical-electrical energy conversion ability under force, providing a structural basis for building a flexible, wearable self-powered system. In contrast, **Figure 4d** shows a more engineering-practical preparation strategy for flexible electronic integration [54]. With the help of handheld electrospinning equipment, researchers *in situ* deposited PVDF nanofiber membranes on a flexible substrate with a prefabricated magnetron sputtering electrode array to construct a wearable piezoelectric sensing platform with an array electrode functional layer. This method not only avoids the high voltage requirement of the traditional polarization step, but also enhances the piezoelectric properties of PVDF through the α to β phase transformation mechanism. The prepared piezoelectric film has a good fit and spatial configuration freedom, and can be directly integrated into the robot skin or wearable device surface to achieve scene-based human motion energy harvesting and monitoring. Its portability, high efficiency, and large-area deployment make this technology show good prospects in the field of flexible electronics and bionic sensing.

In general, the strategies shown in **Figure 4c** and **d** represent two types of fabric-based PENG technology paths based on functional fiber configuration design and controllable construction platform development, respectively. The former realizes the organic combination of conductive and piezoelectric materials through *in situ* polymerization at the interface, which is suitable for the flexible and modular construction of self-powered sensor devices; the latter combines electrospinning with precise electrode microstructure forming technology to expand functions for complex surfaces and smart carriers. In the future, with the development of conductive polymer materials, low-dimensional nanomaterials, and multi-scale weaving processes, fabric-based PENG is expected to further achieve key technological breakthroughs such as high-throughput preparation, high-performance output, and biocompatibility, enabling emerging application scenarios such as smart textiles, wearable medical, and adaptive human-machine interfaces.

3.2.3 3D fabric-based PENG

With the growing demand for wearable self-powered systems, 3D fabric-based PENG has become an important way to improve the output of traditional fibers or

two-dimensional fabrics. Compared with single fibers or two-dimensional structures, 3D fabrics can not only significantly increase the density of piezoelectric fibers per unit area, but also provide better mechanical response characteristics and output stability.

Wan et al. constructed a laminated 3D piezoelectric fabric structure based on an electrospun PVDF nanofiber membrane (**Figure 4e**) [55]. The device uses two layers of silver-coated nylon conductive yarn as electrodes, and performs electromechanical conversion through the middle PVDF nanofilm. The whole is supported by a flexible adhesive tape to form a wearable and integrable piezoelectric element. Its working principle is based on external mechanical deformation to induce the rearrangement of dipoles in PVDF, thereby realizing electrical signal output. In addition, the structure shown in **Figure 4f** was proposed by Mehmood et al., who constructed a sandwich fabric PENG system based on a multilayer PVDF nanofiber membrane [56]. The structure forms a PVDF layer with a porous network by electrospinning, and then PEDOT is uniformly coated on its surface by gas phase polymerization to construct a flexible dual-electrode sandwich system. This method avoids the damage of the nanostructure by liquid phase treatment, effectively enhances the interface coupling efficiency between the conductive layer and the piezoelectric layer, and maintains the overall flexibility and air permeability of the fabric. Its laminated structure exhibits excellent stability and electrical properties under multiple deformations, and is suitable for energy harvesting and signal detection in complex dynamic environments.

In summary, **Figure 4e** and **f** represent two effective paths to improve piezoelectric performance through layered configuration and interface functionalization, respectively. Under the synergistic effect of structural design and material optimization, the fabric-type PENG exhibits good flexibility, stability, and energy conversion capabilities, laying an important foundation for the industrial application of the next generation of wearable electronics, bionic intelligent systems, and smart textiles.

4. Textile-based thermoelectric generators (TEGs)

Thermoelectric technology uses the Seebeck effect to directly convert temperature differences into electrical energy. It has the advantages of no noise, no pollution, and high reliability. It is especially suitable for energy collection in wearable devices. Although traditional inorganic thermoelectric materials have excellent performance, they are relatively rigid and are not suitable for dynamic curved surface applications; flexible films are limited by air permeability and deformation direction. In recent years, thermoelectric fibers made of conductive polymers, carbon nanomaterials, etc., have become an ideal basis for building fiber-shaped or fabric-shaped thermoelectric generators (T-TEGs) owing to their softness, weavability, and conformability. They can efficiently collect human body heat and drive microelectronic devices. The three-dimensional fabric structure further improves the thermoelectric performance and wearing stability, making T-TEG show broad application prospects in the fields of smart wearable devices and vital signs monitoring.

4.1 Working mechanisms

The core principle of thermoelectric power generation comes from the Seebeck effect, that is, when there is a temperature difference (ΔT) between the two ends of a thermoelectric material, the carriers inside the material (holes for p-type materials

and electrons for n-type materials) migrate from the high-temperature end to the low-temperature end, thereby generating a thermoelectric potential (Seebeck voltage) in the external circuit. The relationship can be expressed as Eq. (1) [57]:

$$V=\alpha\Delta T \tag{1}$$

where α is the Seebeck coefficient. This effect is the basis of thermoelectric energy conversion and is widely used in fields such as thermal energy collection and temperature sensing. The key parameter for measuring the performance of thermoelectric materials is the dimensionless figure of merit (ZT), which is defined as Eq. (2) [57]:

$$ZT=\frac{S^2\sigma T}{k} \tag{2}$$

where S is the Seebeck coefficient, σ is the electrical conductivity, T is the absolute temperature, and κ is the thermal conductivity (including electronic thermal conductivity κ_e and lattice thermal conductivity κ_1:$\kappa = \kappa_e + \kappa_1$). In order to improve the ZT value, $S^2\sigma$ (called power factor, representing the thermoelectric capability from an electrical perspective) should be increased as much as possible, while reducing the thermal conductivity κ. The conductivity is determined by the carrier concentration n, the carrier charge q, and the mobility μ (Eq. (3)) [57]:

$$\sigma=nq\mu \tag{3}$$

and S is closely related to the band structure, effective carrier mass, carrier concentration, etc. There is a coupling relationship between the two: increasing n will enhance σ but reduce S, so a balance needs to be achieved between the two to achieve the best power factor. In order to reduce κ_1, micro/nanostructure design is usually adopted, such as grain boundaries, point defects, phonon scattering, and other means to effectively hinder the heat conduction of lattice vibration.

In thermoelectric devices, a thermoelectric generator (TEG) composed of multiple thermocouples (composed of p-type and n-type thermoelectric materials) can directly convert the temperature difference between the human body and the environment into electrical energy. Traditional TEGs mostly adopt a vertical (cross-plane) structure to establish a temperature difference in the thickness direction, which is conducive to efficient output, but its rigidity is large and not conducive to wear. In order to improve flexibility and match the human body shape, researchers have developed a fiber-shaped TEG. By weaving or sewing p/n-type thermoelectric yarns into fabrics, it can take into account both the temperature difference collection in the thickness direction and excellent wearability.

Different types of thermoelectric materials have their own characteristics: Inorganic materials (such as Bi_2Te_3, PbTe) have strong conductivity and excellent performance, but they have problems of high rigidity, scarcity and toxicity; Organic materials (such as carbon nanotubes, conductive polymers) have good flexibility and low thermal conductivity, but weak thermoelectric performance; Composite materials introduce inorganic components into the organic matrix to take into account the advantages of both. The ideal material should have a high Seebeck coefficient, high conductivity, and low thermal conductivity, and combine three-dimensional structural design and yarn arrangement optimization to improve the efficiency of human body heat collection, which is an important direction for the development of wearable energy.

4.2 Structures

4.2.1 Fiber-based TEG

Thermoelectric fiber fabrics have become an important research direction in the field of thermoelectric energy conversion owing to their excellent flexibility, weavability, and space utilization. In view of the structural limitations of traditional two-dimensional fabrics in vertical heat flow collection, researchers proposed a fiber-level thermoelectric device configuration strategy with a p-n segmented structure as the core and constructed thermoelectric units by periodically alternating p-type and n-type regions, effectively improving the heat flow docking efficiency and output performance. In **Figure 5a**, Sun et al. modified carbon nanotube fiber (CNTF) by combining dip coating and electrospraying: [58] first, p-type doping was achieved through PEDOT:PSS solution, and then local n-type doping was achieved with the help of polypropylene (PP) mask and oleylamine electrospraying technology to prepare thermoelectric fibers with axial periodic p/n structure. In this configuration, the non-doped areas between the doped segments are connected as inner electrodes, fiber ring units are formed by curling the coating, and a three-dimensional fabric thermoelectric module without substrate support is further constructed. The module can achieve a tensile strain of up to 80%, showing excellent mechanical stability and heat flow docking capabilities. Under ΔT = 44 K, the output power of a single thermoelectric fiber ring unit can reach 4.64 μW, and the overall output power density of the constructed fabric structure can reach 70 mW/m^2, which is better than most flexible thermoelectric devices, showing its potential for stable energy supply under human

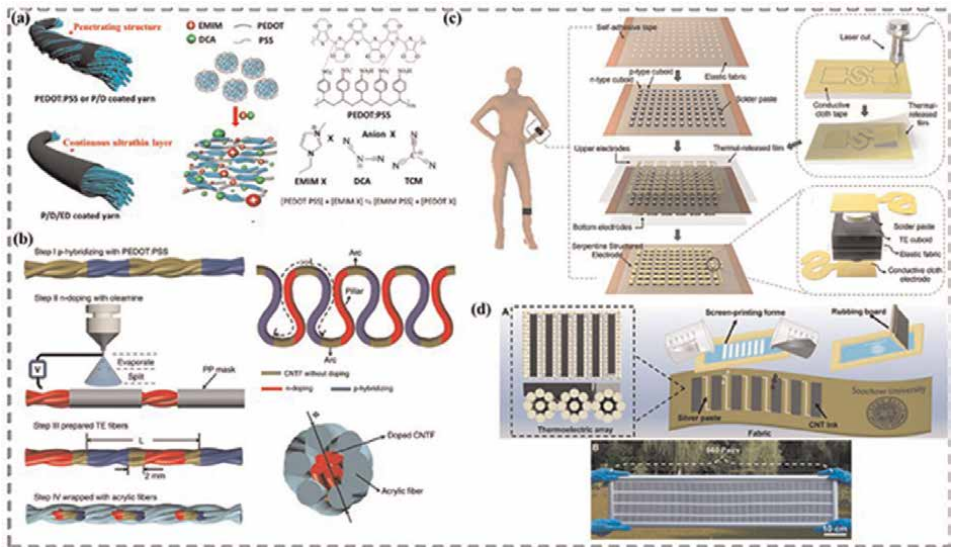

Figure 5.
Single fiber-based TEGs. (a) A carbon nanotube fiber (CNTF) by combining dip coating and electrospraying strategy. Reproduced with permission from Ref. [58] Copyright 2021 American Chemical Society. (b) A thermoelectric fiber with optimized the coating morphology and conductivity. Reproduced with permission from Ref. [59] Copyright 2020 Springer Nature. Fabric-based TEGs. (c) A large-area fabric thermoelectric module constructed by screen printing. Reproduced with permission from Ref. [60] Copyright 2022 Wiley-VCH. (d) A three-dimensional integrated thermoelectric array was constructed based on an elastic fabric base layer and connecting high-performance p/n-type thermoelectric blocks to the electrode array via solder. Reproduced with permission from Ref. [61] Copyright 2025 Science.

motion conditions. **Figure 5b** focuses on the regulation of the structure and performance of the PEDOT:PSS coating. Wang et al. systematically optimized the coating morphology and conductive path construction by introducing dimethyl sulfoxide (DMSO) and ionic liquids (EMIM DCA and EMIM TCM) into the PEDOT:PSS solution [59]. The experiment showed that PEDOT:PSS or P/D solutions with low surface tension and low viscosity can easily penetrate into the yarn pores to form a discontinuous permeation structure, while P/D/ED solutions with high surface tension and high viscosity can form a continuous, uniform, ultra-thin conductive layer on the yarn surface. This structure not only improves the conductivity (σ) and Seebeck coefficient (S), but also significantly improves the flexibility and structural stability of the yarn.

The two studies respectively cut into the fiber structure configuration and coating morphology control and significantly improved the thermoelectric performance, flexibility, and mechanical stability through p/n segment design, conductive network optimization, and fabric-level assembly strategy. These achievements not only lay a theoretical and technical foundation for the preparation of thermoelectric fiber functional textiles, but also provide forward-looking energy solutions for smart wearable devices, health monitoring, and low-power electronic systems.

4.2.2 Fabric-based TEG

Traditional two-dimensional thermoelectric generators are mostly based on commercial fabrics (such as cotton, silk, nylon, etc.). Thermoelectric films are prepared by coating organic or inorganic thermoelectric materials, and then cut into strips and wired to form thermoelectric units. However, such strip structures have poor adhesion and weak stability, and in actual applications, the temperature difference direction is perpendicular to the voltage output direction, which limits the performance. In order to improve the output efficiency, researchers began to build three-dimensional fabric thermoelectric structures. As shown in **Figure 5c**, the module uses carbon nanotube (CNT) ink and silver paste to construct a p-n thermoelectric pair array on a flexible fabric by screen printing [60]. It contains 560 pairs of thermoelectric units, which are closely arranged and in the same direction, and can efficiently output electrical energy under sunlight. Infrared thermal imaging and multiple rounds of cycle testing verified its thermal response and cycle stability, showing its potential for application in lightweight portable energy harvesting and smart clothing. In contrast, **Figure 5d** shows a design that emphasizes structural hierarchy and multilayer electrode integration [61]. The researchers prepared upper and lower electrodes on an elastic fabric substrate using laser-cut conductive fabric tapes, and connected the high-performance p/n thermoelectric block to a serpentine electrode array by welding to form a three-dimensional integrated structure. This design takes into account flexibility, mechanical stability, and thermoelectric performance, and can be attached to the human body through self-adhesion to achieve efficient fitting and modular installation. Its multilayer stacking structure improves the thermoelectric density per unit area, thermal conductivity, and interface stability, and is suitable for body heat recovery and smart temperature control patches.

In summary, **Figure 5c** and **d** represent two major paths for the development of thermoelectric fabrics: the former enhances the thermal response area through patterned arrays, and the latter optimizes the thermoelectric transmission efficiency through structural coupling. Together, they have promoted the development of textile thermoelectric devices in terms of high performance, scalable manufacturing, and human adaptability, laying the foundation for the next generation of smart textiles and wearable thermal management systems.

5. Applications

Thanks to the excellent performance of flexible fabrics, T-NG has shown obvious advantages in the wearable field and has become an important component of self-driven smart textiles. Its main applications include powering low-power electronic devices and sensing information such as human motion, posture, and gait as a passive sensing platform. T-NG can be woven into everyday clothing to collect weak mechanical energy generated by actions such as walking and running, drive electronic components, or transmit sensor signals. Its periodic electrical output can also be connected to artificial intelligence systems as sensor data to achieve individual identification, health monitoring, and behavior analysis. With the integrated development of AI, the Internet of Things, and wireless communications, T-NG will play a

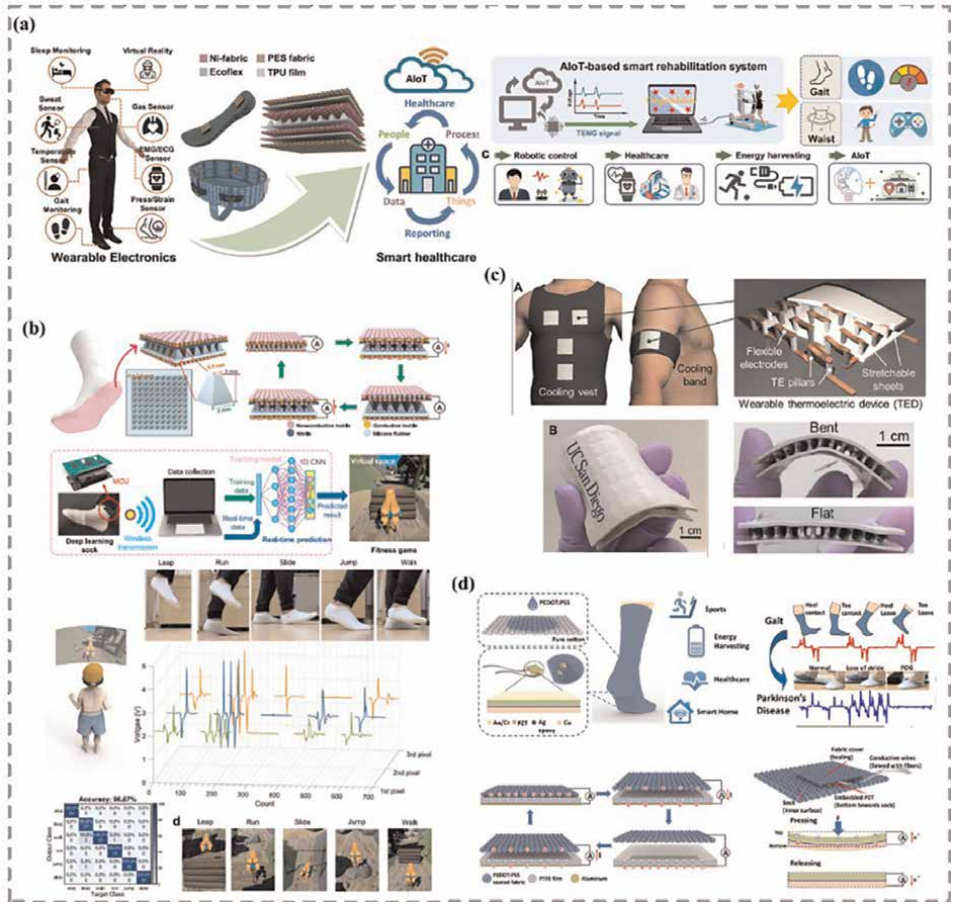

Figure 6.
(a). A fabric triboelectric array structure prepared by screen printing using silver paste and carbon nanotube (CNT) ink. Reproduced with permission from Ref. [62] Copyright 2022 Wiley-VCH. (b) A smart sock system with integrated TENG arrays to achieve individual identity recognition and behavior classification. Reproduced with permission from Ref. [63] Copyright 2020 Springer Nature. (c) A flexible thermoelectric device (TED) system for active thermal management in dynamic environments. Reproduced with permission from Ref. [64] Copyright 2019 Science. (d) A fabric-based hybrid nanogenerator used for physiological signal acquisition and personalized rehabilitation training systems. Reproduced with permission from Ref. [65] Copyright 2019 American Chemical Society.

key role in health monitoring, smart sports, remote care, and human-computer interaction.

In the development of flexible smart wearable systems, fabric-based triboelectric nanogenerators (T-TENG) are becoming increasingly important in energy harvesting and smart sensing due to their excellent flexibility and integrability. As shown in **Figure 6a**, the fabric triboelectric array prepared by screen printing of silver paste and carbon nanotube ink forms 560 pairs of vertically arranged units through hot pressing and scraping, which significantly improves the voltage and current density [62]. This structure has good scalability and thermal stability, and can be sewn into a smart cooling vest to achieve temperature control under sunlight, showing broad application prospects. Moreover, **Figure 6b** shows a smart sock system with integrated TENG arrays [63]. The system can passively capture plantar pressure and gait change signals, and combine convolutional neural network (CNN) models to achieve individual identity recognition and behavior classification. Its scene applications include virtual reality fitness interaction, neurodegenerative disease monitoring, and fall warning, reflecting the great potential of deep integration of triboelectric signals and artificial intelligence.

In addition to triboelectricity, the integration of thermoelectric technology in fabric systems is also gradually moving toward practical application. **Figure 6c** shows a flexible thermoelectric device (TED) system for active thermal management in dynamic environments developed by Hong's team [64]. The system forms a three-dimensional thermoelectric configuration by integrating an array of thermoelectric columns between a stretchable elastomer substrate and a flexible electrode. The device uses Ecoflex/AlN hybrid material to enhance thermal conductivity, while retaining a 1 mm air gap between thermoelectric columns to reduce heat leakage, significantly improving thermal resistance and enhancing the ability to directional transfer human body heat. It is worth noting that the device is highly deformable, and can not only adapt to the bending of the limbs, but also regulate stiffness and thermal conductivity in a single/double-layer structure to achieve a balance between thermal transfer performance and flexible mechanical response. Through actual wearable experiments, the TED can effectively achieve cooling and cooling functions, providing a new solution for wearable temperature control systems and skin microenvironment regulation.

In the context of further pursuing energy conversion efficiency and response range, a composite fabric nano-power generation system (PENG and TENG) is explored. **Figure 6d** shows a typical example of the collaborative work of multilayer heterogeneous structures, in which the piezoelectric PVDF fiber membrane and the triboelectric layer work together to achieve response to various external mechanical stimuli such as bending, stretching, contact-separation, etc. [65]. This structure has higher power density output and stronger scene adaptability, and is widely used in complex dynamic detection, physiological signal acquisition and personalized rehabilitation training systems.

In summary, fabric-based nanogenerators have shown broad application prospects in many fields such as smart wearable devices, passive sensing, and autonomous driving systems, owing to their structural flexibility, high energy conversion efficiency, and multifunctional response capabilities. Through continuous innovation in structural design and multi-material integration, such fabrics will better meet the diverse needs of personalized medicine, motion monitoring, environmental response, etc., in the future, and promote the practical application of self-powered textile electronic products.

6. Conclusion and prospects

In summary, Textile-based nanogenerators (T-NGs) show great application potential in the new generation of wearable electronic devices and self-powered intelligent systems. Its excellent flexibility, lightness, breathability, and high compatibility with existing textile processes enable it to be naturally embedded in daily clothing and functional fabrics to achieve energy harvesting and intelligent sensing functions. In recent years, through continuous optimization in structural design, material selection, and device construction, the energy conversion efficiency and functional integration capabilities of T-TENG systems have made significant progress, and the application fields cover bioenergy harvesting, human motion monitoring, physiological signal detection, and other directions.

Despite many achievements, T-NG technology still faces several challenges in its actual promotion and application, such as mechanical stability under long-term wear and repeated washing, the impact of environmental changes on electrical output, and stable and efficient energy management and storage mechanisms. In addition, how to achieve low-cost, large-scale, industrialized fabric integration and preparation processes is also an important direction for future research.

Looking to the future, the integration of T-NG technology with emerging technologies such as artificial intelligence (AI), wireless communications, and wearable data analysis will give rise to more diversified and intelligent application scenarios. For example, self-powered smart textiles can be used to achieve real-time gait recognition, emotion monitoring, or chronic disease prediction, becoming a core component of future digital health platforms. At the same time, the composite collection strategy combining multiple energy forms such as thermal energy, kinetic energy, and biochemical energy will further promote the development of truly sustainable and autonomous wearable electronic devices. With the continuous innovation of textile engineering, nanomaterials science, and system integration technology, fabric-based nano-power generation devices are expected to play a transformative role in the future smart life.

Acknowledgements

The authors would like to acknowledge the funding support from the Hong Kong Polytechnic University (1-W28T, 4-YWEQ, 4-YWER, 1-W34U).

Author details

Yujue Yang[1,2], Hong Fu[2] and Bingang Xu[1*]

1 Nanotechnology Center, School of Fashion and Textiles, The Hong Kong Polytechnic University, Hong Kong, China

2 Department of Mathematics and Information Technology, The Education University of Hong Kong, Hong Kong, China

*Address all correspondence to: tcxubg@polyu.edu.hk

IntechOpen

References

[1] Dong K, Peng X, Wang ZL. Fiber/fabric-based piezoelectric and triboelectric nanogenerators for flexible/stretchable and wearable electronics and artificial intelligence. Advanced Materials. 2020;**32**(5):1902549

[2] Tian X, Dong S, Yang M, Ng H, Liu Y, Hu H, et al. Textile-based triboelectric nanogenerators for smart wearable systems: Comfort, integration, and application. Advanced Materials Technologies. 2023;**8**(8):2201294

[3] Chung KY, Xu B, Tan D, Yang Q, Li Z, Fu H. Naturally crosslinked biocompatible carbonaceous liquid metal aqueous ink printing wearable electronics for multi-sensing and energy harvesting. Nano-Micro Letters. 2024; **16**(1):149

[4] Tang Y, Xu B, Gao Y, Li Z, Tan D, Li M, et al. Ultrastrong-polar polyacrylonitrile organic-inorganic architected nanogenerators with synergistic triboelectric behavior for efficient biomechanical energy harvesting and self-powered sensing. Nano Energy. 2022;**103**: 107833

[5] Chung KY, Xu B, Li Z, Liu Y, Han J. Bioinspired ultra-stretchable dual-carbon conductive functional polymer fiber materials for health monitoring, energy harvesting and self-powered sensing. Chemical Engineering Journal. 2023;**454**:140384

[6] Huang J, Xu B, Gao Y, Jiang C, Guan X, Li Z, et al. Surface microstructural engineering of continuous fibers as one-dimensional multifunctional fiber materials for wearable electronic applications. Chemical Engineering Journal. 2022; **446**:137192

[7] Tan D, Xu B. Advanced interfacial design for electronic skins with customizable functionalities and wearability. Advanced Functional Materials. 2023;**33**(49):2306793

[8] Fang C, Xu B, Li M, Han J, Yang Y, Liu X. Advanced design of fibrous flexible actuators for smart wearable applications. Advanced Fiber Materials. 2024;**6**(3):622-657

[9] Yin X, Xu B, Kan CW, Yang Y. Dynamic perovskite homojunction based light-assisted, direct current tribovoltaic nanogenerators. Advanced Energy Materials. 2023;**13**(31):2301289

[10] Chen T, Xu B, Zhu M, Zhang J, Sun W, Han J. Advanced functional photochromic wearables with fast photo-responsivity, long color-retention, and multi-environmental stability. Chemical Engineering Journal. 2024;**490**:151804

[11] Li X, Li J, Li K, Zhang S, Yang Z, Zhang C, et al. From fiber to power: Recent advances toward electrospun-based nanogenerators. Advanced Functional Materials. 2025;**35**(13): 2418066

[12] Zeng W, Shu L, Li Q, Chen S, Wang F, Tao XM. Fiber-based wearable electronics: A review of materials, fabrication, devices, and applications. Advanced Materials. 2014;**26**(31): 5310-5336

[13] Shen Y, Jiang Z, Huang H, Wang S, Wu S, Wang J, et al. Advances in textile-based triboelectric sensors for physiological signal monitoring. Advanced Functional Materials. 2025;**35** (32):2426081

[14] Ahmed T, Gao Y, So MY, Tan D, Lu J, Zhang J, et al. Diamond-structured

fabric-based triboelectric nanogenerators for energy harvesting and healthcare application. Advanced Functional Materials. 2024;**34**(48): 2408680

[15] Seung W, Gupta MK, Lee KY, Shin K-S, Lee J-H, Kim TY, et al. Nanopatterned textile-based wearable triboelectric nanogenerator. ACS Nano. 2015;**9**(4):3501-3509

[16] Yu D, Li Z, Xie W, Li D, Li Z, Li Y. Applications of nanogenerator-based wearable devices in orthopedics. Nano Energy. 2022;**103**:107762

[17] Pang Y, Cao Y, Derakhshani M, Fang Y, Wang ZL, Cao C. Hybrid energy-harvesting systems based on triboelectric nanogenerators. Matter. 2021;**4**(1):116-143

[18] Ning C, Dong K, Cheng R, Yi J, Ye C, Peng X, et al. Flexible and stretchable fiber-shaped triboelectric nanogenerators for biomechanical monitoring and human-interactive sensing. Advanced Functional Materials. 2021;**31**(4):2006679

[19] Kwak SS, Yoon HJ, Kim SW. Textile-based triboelectric nanogenerators for self-powered wearable electronics. Advanced Functional Materials. 2019; **29**(2):1804533

[20] Kim KN, Chun J, Kim JW, Lee KY, Park J-U, Kim S-W, et al. Highly stretchable 2D fabrics for wearable triboelectric nanogenerator under harsh environments. ACS Nano. 2015;**9**(6): 6394-6400

[21] Bairagi S, Shahadat M, Mulvihill DM, Ali W. Mechanical energy harvesting and self-powered electronic applications of textile-based piezoelectric nanogenerators: A systematic review. Nano Energy. 2023;**111**:108414

[22] Li J, Cai J, Yu J, Li Z, Ding B. The rising of fiber constructed piezo/ triboelectric nanogenerators: From material selections, fabrication techniques to emerging applications. Advanced Functional Materials. 2023; **33**(44):2303249

[23] Zhang M, Gao T, Wang J, Liao J, Qiu Y, Yang Q, et al. A hybrid fibers based wearable fabric piezoelectric nanogenerator for energy harvesting application. Nano Energy. 2015;**13**: 298-305

[24] Su C, Huang X, Zhang L, Zhang Y, Yu Z, Chen C, et al. Robust superhydrophobic wearable piezoelectric nanogenerators for self-powered body motion sensors. Nano Energy. 2023;**107**:108095

[25] Joshi B, Seol J, Samuel E, Lim W, Park C, Aldalbahi A, et al. Supersonically sprayed PVDF and ZnO flowers with built-in nanocuboids for wearable piezoelectric nanogenerators. Nano Energy. 2023;**112**:108447

[26] Hu X, Li T-T, Shou B, Li L, Ren H-T, Lou C-W. Novel personal cooling textiles revolutionizing human thermal management: Principles, designs and applications. Chemical Engineering Journal. 2024;**499**:155729

[27] Jia Y, Jiang Q, Sun H, Liu P, Hu D, Pei Y, et al. Wearable thermoelectric materials and devices for self-powered electronic systems. Advanced Materials. 2021;**33**(42):2102990

[28] Shi X-L, Zou J, Chen Z-G. Advanced thermoelectric design: From materials and structures to devices. Chemical Reviews. 2020;**120**(15):7399-7515

[29] Feng R, Tang F, Zhang N, Wang X. Flexible, high-power density, wearable thermoelectric nanogenerator and self-

powered temperature sensor. ACS Applied Materials and Interfaces. 2019; **11**(42):38616-38624

[30] Wang Y, Zhu W, Deng Y, Fu B, Zhu P, Yu Y, et al. Self-powered wearable pressure sensing system for continuous healthcare monitoring enabled by flexible thin-film thermoelectric generator. Nano Energy. 2020;**73**:104773

[31] Rojas JP, Conchouso D, Arevalo A, Singh D, Foulds IG, Hussain MM. Based origami flexible and foldable thermoelectric nanogenerator. Nano Energy. 2017;**31**:296-301

[32] Lee B, Cho H, Park KT, Kim J-S, Park M, Kim H, et al. High-performance compliant thermoelectric generators with magnetically self-assembled soft heat conductors for self-powered wearable electronics. Nature Communications. 2020;**11**(1):5948

[33] Niu S, Wang ZL. Theoretical systems of triboelectric nanogenerators. Nano Energy. 2015;**14**:161-192

[34] Kim W-G, Kim D-W, Tcho I-W, Kim J-K, Kim M-S, Choi Y-K. Triboelectric nanogenerator: Structure, mechanism, and applications. ACS Nano. 2021;**15**(1):258-287

[35] Wang Y, Yang Y, Wang ZL. Triboelectric nanogenerators as flexible power sources. npj Flexible Electronics. 2017;**1**(1):10

[36] Ahmed A, Hassan I, El-Kady MF, Radhi A, Jeong CK, Selvaganapathy PR, et al. Integrated triboelectric nanogenerators in the era of the internet of things. Advanced Science. 2019;**6**(24): 1802230

[37] Hinchet R, Seung W, Kim SW. Recent progress on flexible triboelectric nanogenerators for selfpowered electronics. ChemSusChem. 2015;**8**(14): 2327-2344

[38] Cheng Y, Lu X, Chan KH, Wang R, Cao Z, Sun J, et al. A stretchable fiber nanogenerator for versatile mechanical energy harvesting and self-powered full-range personal healthcare monitoring. Nano Energy. 2017;**41**:511-518

[39] Wu J, Zhou X, Luo J, Zhou J, Lu Z, Bai Z, et al. Stretchable and self-powered mechanoluminescent triboelectric nanogenerator fibers toward wearable amphibious electro-optical sensor textiles. Advanced Science. 2024;**11**(34): 2401109

[40] Yu B, Long J, Huang T, Xiang Z, Liu M, Zhang X, et al. Core–sheath fiber-based triboelectric nanogenerators for energy harvesting and self-powered straight-arm sit-up sensing. ACS Omega. 2023;**8**(34):31427-31435

[41] Zhang Y, Li Y, Cheng R, Shen S, Yi J, Peng X, et al. Underwater monitoring networks based on cable-structured triboelectric nanogenerators. Research. 2022;**2022**:9809406

[42] Wang Y, Chu L, Meng S, Yang M, Yu Y, Deng X, et al. Scalable and ultra-sensitive nanofibers coaxial yarn-woven triboelectric nanogenerator textile sensors for real-time gait analysis. Advanced Science. 2024;**11**(28):2401436

[43] Chen C, Guo H, Chen L, Wang Y-C, Pu X, Yu W, et al. Direct current fabric triboelectric nanogenerator for biomotion energy harvesting. ACS Nano. 2020;**14**(4):4585-4594

[44] Yu A, Pu X, Wen R, Liu M, Zhou T, Zhang K, et al. Core–shell-yarn-based triboelectric nanogenerator textiles as power cloths. ACS Nano. 2017;**11**(12): 12764-12771

[45] Kwak SS, Kim H, Seung W, Kim J, Hinchet R, Kim S-W. Fully stretchable textile triboelectric nanogenerator with knitted fabric structures. ACS Nano. 2017;**11**(11):10733-10741

[46] Dong K, Peng X, An J, Wang AC, Luo J, Sun B, et al. Shape adaptable and highly resilient 3D braided triboelectric nanogenerators as e-textiles for power and sensing. Nature Communications. 2020;**11**(1):2868

[47] Hu D, Yao M, Fan Y, Ma C, Fan M, Liu M. Strategies to achieve high performance piezoelectric nanogenerators. Nano Energy. 2019;**55**: 288-304

[48] Xu Q, Wen J, Qin Y. Development and outlook of high output piezoelectric nanogenerators. Nano Energy. 2021;**86**: 106080

[49] Wang ZL, Song J. Piezoelectric nanogenerators based on zinc oxide nanowire arrays. Science. 2006; **312**(5771):242-246

[50] Gunasekhar R, Bindhu A, Reza MS, Arun AP, Kim KJ, Kim H. Piezoelectric and triboelectric contributions by aromatic hyperbranched polyesters of second-generation/PVDF nanofiber-based nanogenerators for energy harvesting and wearable electronics. ACS Applied Electronic Materials. 2024; **6**(7):5036-5049

[51] Lund A, Rundqvist K, Nilsson E, Yu L, Hagström B, Müller C. Energy harvesting textiles for a rainy day: Woven piezoelectrics based on melt-spun PVDF microfibres with a conducting core. npj Flexible Electronics. 2018;**2**(1):9

[52] Kim M, Yun K-S. Helical piezoelectric energy harvester and its application to energy harvesting garments. Micromachines. 2017; **8**(4):115

[53] Zhou Y, He J, Wang H, Qi K, Nan N, You X, et al. Highly sensitive, self-powered and wearable electronic skin based on pressure-sensitive nanofiber woven fabric sensor. Scientific Reports. 2017;**7**(1):12949

[54] Wang X, Song W-Z, You M-H, Zhang J, Yu M, Fan Z, et al. Bionic single-electrode electronic skin unit based on piezoelectric nanogenerator. ACS Nano. 2018;**12**(8):8588-8596

[55] Wan X, Shen Y, Luo T, Xu M, Cong H, Chen C, et al. All-textile piezoelectric nanogenerator based on 3D knitted fabric electrode for wearable applications. ACS Sensors. 2024;**9**(6): 2989-2998

[56] Maity K, Mandal D. All-organic high-performance piezoelectric nanogenerator with multilayer assembled electrospun nanofiber mats for self-powered multifunctional sensors. ACS Applied Materials and Interfaces. 2018;**10**(21):18257-18269

[57] Chen W-Y, Shi X-L, Zou J, Chen Z-G. Wearable fiber-based thermoelectrics from materials to applications. Nano Energy. 2021;**81**:105684

[58] Li M, Zeng F, Luo M, Qing X, Wang W, Lu Y, et al. Synergistically improving flexibility and thermoelectric performance of composite yarn by continuous ultrathin PEDOT: PSS/ DMSO/ionic liquid coating. ACS Applied Materials and Interfaces. 2021;**13**(42): 50430-50440

[59] Sun T, Zhou B, Zheng Q, Wang L, Jiang W, Snyder GJ. Stretchable fabric generates electric power from woven thermoelectric fibers. Nature Communications. 2020;**11**(1):572

[60] Hou Y, Yang Y, Wang Z, Li Z, Zhang X, Bethers B, et al. Whole fabric-assisted thermoelectric devices for wearable electronics. Advanced Science. 2022;**9**(1):2103574

[61] Liu J-Z, Jiang W, Zhuo S, Rong Y, Li Y-Y, Lu H, et al. Large-area radiation-modulated thermoelectric fabrics for high-performance thermal management and electricity generation. Science Advances. 2025;**11**(1):eadr2158

[62] Zhang Q, Jin T, Cai J, Xu L, He T, Wang T, et al. Wearable triboelectric sensors enabled gait analysis and waist motion capture for IoT-based smart healthcare applications. Advanced Science. 2022;**9**(4):2103694

[63] Zhang Z, He T, Zhu M, Sun Z, Shi Q, Zhu J, et al. Deep learning-enabled triboelectric smart socks for IoT-based gait analysis and VR applications. npj Flexible Electronics. 2020;**4**(1):29

[64] Hong S, Gu Y, Seo JK, Wang J, Liu P, Meng YS, et al. Wearable thermoelectrics for personalized thermoregulation. Science Advances. 2019;**5**(5):eaaw0536

[65] Zhu M, Shi Q, He T, Yi Z, Ma Y, Yang B, et al. Self-powered and self-functional cotton sock using piezoelectric and triboelectric hybrid mechanism for healthcare and sports monitoring. ACS Nano. 2019;**13**(2): 1940-1952

Section 3

Advanced Topics and Future Prospects in Nanogenerators

Chapter 5

Toward Energy-Autonomous Neuromorphic Systems: Piezoelectric and Triboelectric Nanogenerators for Synaptic Plasticity Emulation

Mahdi Zekavat, Zahra Razzaghi and Fahimeh Zamanpour

Abstract

The pursuit of neuromorphic systems capable of replicating the efficiency and adaptability of the brain has driven significant advances in artificial synapse technologies. Conventional computing, constrained by the von Neumann bottleneck and high energy consumption, struggles to emulate synaptic plasticity and parallel information processing. To address these limitations, researchers have turned to bioinspired approaches that integrate emerging nanotechnologies with electronic devices. This chapter first reviews the fundamental mechanisms of biological synapses, including neurotransmission, excitatory postsynaptic currents (EPSCs), and plasticity phenomena such as paired-pulse facilitation (PPF), short-term plasticity (STP), long-term potentiation (LTP), and spike-timing-dependent plasticity (STDP). It then explores hardware strategies for emulating synaptic behavior, with a particular emphasis on piezotronic and tribotronic devices. In piezotronics, strain-induced piezopotentials at semiconductor junctions modulate charge transport, whereas tribotronics harness contact-electrification potentials from triboelectric nanogenerators (TENGs) to provide self-powered gating signals. The integration of these mechanisms with advanced transistors—such as electrolyte-gated, floating-gate, and optoelectronic architecture—has enabled the realization of artificial synapses that exhibit rich neuromorphic functionalities, including short- and long-term memory, mechanoplasticity, multimodal plasticity, and associative learning. By unifying biological principles with tribotronic and piezotronic synapses provide a promising route toward the next generation of self-powered neuromorphic computing.

Keywords: artificial synapses, neuromorphic engineering, nanogenerators, self-powered systems, synaptic plasticity

1. Introduction

Modern information technologies, despite their transformative impact, remain constrained by the conventional von Neumann architecture. The inherent separation of memory and processing in this architecture results in high energy consumption, limited computational throughput, and constrained scalability, collectively referred to as the von Neumann bottleneck. This limitation has become a major obstacle to meeting the demands of data-intensive and intelligent applications [1–3]. Neuromorphic concepts, inspired by the dynamic functionality of biological synapses, have emerged as an alternative framework. By integrating information storage and processing within a single unit, artificial synapses provide a platform for adaptive and event-driven computation, addressing several deficiencies of conventional architectures [4, 5]. However, despite these advances, current neuromorphic technologies remain dependent on external energy supplies, restricting their applicability in large-scale and sustainable systems. To mitigate this challenge, self-powered strategies are being explored. Synaptic devices based on nanogenerators represent a particularly promising direction, as they combine synaptic functionality with the ability to harvest ambient energy for autonomous operation. This convergence paves the way for a new class of computing systems in which efficiency, scalability, and energy autonomy will be achieved in tandem [6, 7].

Compared with other classes of nanogenerators, such as electromagnetic nanogenerators (EMGs) and thermoelectric nanogenerators (TEGs), triboelectric (TENGs) and piezoelectric nanogenerators (PENGs) present several distinct advantages for applications in artificial synaptic devices. While EMGs rely on relative motion between magnets and coils and TEGs exploit temperature gradients, both typically require bulky structures or steady-state conditions, limiting their integration into compact or flexible electronics [8–10]. In contrast, TENGs and PENGs can directly harvest ubiquitous mechanical energy from pressing, bending, or vibration in a flexible, low-cost, and scalable manner, making them highly compatible with wearable and neuromorphic devices. Furthermore, the triboelectric and piezoelectric potentials generated by these nanogenerators can be directly coupled with semiconducting channels to form self-powered, tunable, and bio-inspired synaptic devices. The interaction between the triboelectric potential or piezopotential and the channels of field-effect transistors (FETs) enables active modulation of synaptic behavior. TENG- and PENG-based devices can actively regulate synaptic behaviors, including excitatory postsynaptic currents (EPSCs), paired-pulse facilitation (PPF), and synaptic plasticity [11–14].

In this chapter, we begin by exploring the structure of the nervous system and the critical role of synapses in neural communication, covering the fundamentals of synaptic transmission, neurotransmitter synthesis and storage, and electrical synapses. Key concepts such as synaptic weight, the molecular basis of synaptic modulation, Hebbian theory, and mechanisms of short and long-term plasticity, including LTP, LTD, and STDP, are then discussed. The chapter then moves to hardware approaches for emulating synapses, including floating-gate transistors and memristors, while highlighting the energy limitations of conventional neuromorphic hardware. To achieve the main goal of this chapter, which is the application of PENGs and TENGs in artificial synapses and self-powered neuromorphic devices, we first explain the fundamentals and mechanisms of piezotronic and tribotronic effects. We then review recent studies that utilize these mechanisms to replicate the functionality of biological synapses, emphasizing the latest research achievements in this rapidly evolving field.

2. Biological foundations of neuromorphic computing

2.1 Structure of human nervous system

The nervous system is a highly complex network that coordinates the body's activities by transmitting signals between different body parts. It is broadly divided into two primary components: the central nervous system (CNS) and the peripheral nervous system (PNS). The CNS, comprising the brain and spinal cord, acts as the body's command center, integrating sensory input and generating motor responses. The PNS consists of cranial and spinal nerves, which includes sensory, motor, and autonomic nerves, and serves as a communication relay between the CNS and the rest of the body. The fundamental unit of the nervous system is the neuron, a specialized cell that transmits electrochemical signals, which is 99.9% distributed in the brain. The human brain is an ultra-efficient, dynamic and complex organ for computing with low power consumption levels of just ~10 fJ/op [15]. The brain itself can be divided into four interconnected regions, each responsible for specific functions, including cerebrum, cerebellum, diencephalon and brainstem. Cerebrum is the largest part (85% of brain weight) of the brain with two hemispheres, and it handles higher cognition, sensory processing and voluntary movement. The folded surface of cerebrum is the cerebral cortex, and its key lobes are frontal lobe, parietal lobe, temporal lobe, occipital lobe, and insula. Below the cerebrum is the cerebellum, which is responsible for motor coordination, balance, posture, fine motor skills, motor learning, and some cognitive functions. Diencephalon is located deep within the brain, above the brainstem. It contains thalamus which is the major relay station for sensory and motor signals to the cerebral cortex, hypothalamus which is master regulator of the autonomic nervous system and endocrine system, and pituitary and pineal glands which are the master gland of the endocrine system, and circadian rhythms regulator, respectively. Also, brainstem connects the brain to the spinal cord, relays signals of brain, controls vital automatic functions essential for life, and consists of midbrain, pons, and medulla oblongata. The cellular building blocks of brain is primarily composed of neurons and glial cells. In fact, neurons (approximately 10–20% of brain cells) perform core computational and signaling tasks [15, 16]. A typical neuron consists of the following:

1. Cell body (soma) is signal integration hub and contains nucleus and essential organelles.

2. Dendrites are branch-like extensions that receive afferent signals from other neurons (10^4 connections/neuron) and participate in local signaling and protein synthesis.

3. Axon is a long, thin fiber that transmits efferent electrical signals via action potentials, away from the cell body and has terminal branches.

4. Axon terminals or synaptic boutons are the ends of the axon where neurotransmitters are released to communicate with the next cell across a synapse or neuroeffector junction.

Glial cells (glia or neuroglia), constituting 80–90% of brain cells, are the primary support cells of the nervous system. Key types include astrocytes, which regulate the

neuronal environment and help to form the blood-brain barrier, oligodendrocytes and Schwann cells create myelin to insulate axons and aid in nerve regeneration, and microglia act as the brain's immune defenders and play role in synaptic pruning during development and plasticity, and finally, ependymal cells are responsible for producing and circulating cerebrospinal fluid. Additional brain cell types, including endothelial cells, pericytes, and neural stem/progenitor cells, contribute to the blood-brain barrier, angiogenesis, and limited neurogenesis [15, 16].

2.2 The synapses: Structure and functional types

A synapse is the functional connection site between axon terminal of presynaptic neuron and the dendrites of another postsynaptic target which may be neuron, muscle, or gland, via chemical or electrical signaling. It consists of a presynaptic terminal (containing vesicles of neurotransmitter), a synaptic cleft, and a postsynaptic membrane densely packed with receptors (**Figure 1A**) [16].

While chemical synapses (**Figure 1B**), defined in synaptic clefts (distance ~20 to 40 nm [16]), are vesicle-mediated, unidirectional signal transmission, and modifiable, the electrical synapses (**Figure 1B**) use connexin proteins to form gap junctions (connexins/pannexins) with ~3.5 nm wide, allowing ions and small molecules to pass directly between neurons, bidirectional signal transmission (no polarity), and

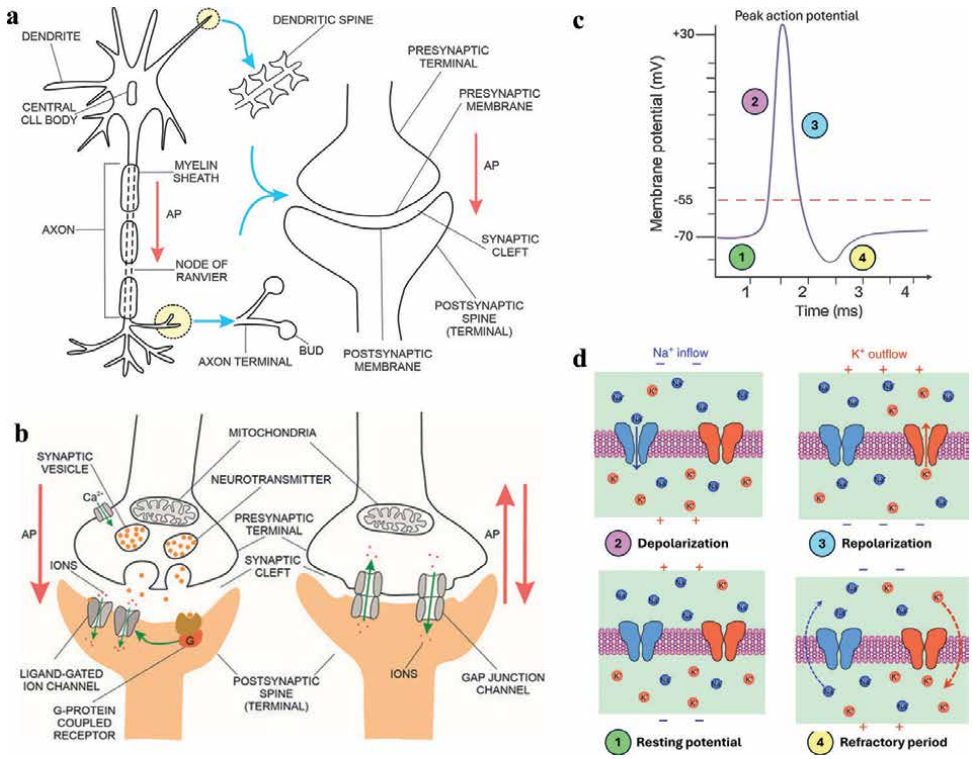

Figure 1.
Neurons and synapses. (a) the anatomy of neuron, (b) left: chemical synapse, and right: electrical synapse. Reproduced from Ref. [17] under license CC BY 4.0; (c) membrane potential changes over time, (d) four main phases of an action potential in a neuron, showing both the changes in membrane potential over time and the corresponding ion movements across the cell membrane. Reproduced from Ref. [18] under license CC BY 4.0.

ultrafast conduction, and they do not rely on neurotransmitters. Electrical synapses are crucial in reflex arcs and synchronized neural activity (e.g., cardiac muscle contraction, retinal neurons, and epileptic seizures). The major synapses of mammals are chemicals [19]. Moreover, mixed synapses were discovered at the terminations of primary auditory afferents on the teleost Mauthner cells, advancing our understanding of the interactions between these two modalities of synapses [15]. Chemical synapses can conduct more complicated signal transmission than electrical synapses and can control synaptic strength precisely during learning and memory processes. In chemical synapses, the electrical signal which is action potential from axon converts into a chemical signal by release of neurotransmitters rapidly in microseconds from vesicles in presynaptic membranes, is then spread across the synaptic cleft, and finally binds to specific receptors on the postsynaptic membrane. This transmission of current from presynaptic to postsynaptic neuron takes about 0.5 to 1 ms, which is called synaptic delay. This process triggers ion channels to open and to conduct ions through the postsynaptic membrane. As a result, the membrane potential changes. If the synapse is excitatory, the membrane is depolarized, responds to the stimulus, and relays it to the next neuron. If the synapse is inhibitory, the membrane is hyperpolarized and suppresses relay of the signal. The postsynaptic neuron integrates all received signals, to determine whether to fire an action potential of its own or not [16].

There are approximately 10^{11} neurons and 10^{15} synapses in human brain, which means that each neuron forms about 10,000 synaptic connections. The strength of these connections is not static but can be dynamically adjusted through synaptic plasticity (e.g., STP, LTP). This ability to modify synaptic weights in response to activity is the fundamental biological mechanism for learning and memory and serves as a key inspiration for neuromorphic computing [16].

Action potentials are driven by ions moving across the cell membrane via voltage-gated channels. Potassium, sodium, and chloride ions are crucial for setting and maintaining the resting membrane potential, which is typically around −70 mV. When a depolarizing input reaches the threshold, a uniformly sized action potential is produced and travels along the axon to the terminal, the Nav channel is activated under the potential gradient, resulting in a rapid influx of Na+. When this occurs, the polarity of the membrane potential changes from negative to positive, leading to depolarization of the membrane potential. The physiological processes of repolarization and hyperpolarization are dominated by voltage-gated potassium (Kv) channels, which allow K+ to flow out of the cytomembrane to restore the normal membrane potential of neuron cells. Finally, the ion concentration inside and outside the cytomembrane is restored to an equilibrium state regulated by the adenosine triphosphate (ATP)-driven Na+/K+ pump. Note that when a single suprathreshold stimulus causes the cell to generate an action potential, the cell membrane will not normally respond to subsequent stimuli until the membrane potential returns to the resting potential, referred to as the refractory period (**Figure 1C** and **D**) [15].

2.3 The molecular machinery of neurotransmission

The most important neurotransmitters used in synaptic communication are acetylcholine, norepinephrine, dopamine, serotonin, catecholamines, gamma-aminobutyric acid (GABA), glycine, and glutamic acid. They are synthesized differently depending on their type. They can be small-molecule chemicals, such as dopamine and serotonin, or small neuropeptides, such as enkephalin. Neurotransmission is the multi-step process by which neurons communicate. It begins with the synthesis and

packaging of neurotransmitters into vesicles in the presynaptic terminal. When an action potential arrives, it depolarizes the terminal, opening voltage-gated calcium channels; the ensuing calcium influx triggers vesicle fusion and neurotransmitter release into the synaptic cleft via SNARE proteins. These neurotransmitters then bind to receptors on the postsynaptic neuron, either ionotropic receptors for fast, millisecond-scale effects or metabotropic receptors (GPCRs) for slower, modulatory changes. Finally, the signal is swiftly terminated through reuptake into the presynaptic terminal, enzymatic degradation, or diffusion away from the synapse [18, 20].

2.4 Synaptic weight and plasticity

Synaptic plasticity, the activity-dependent change in neuronal connection strength (or weight), has long been considered an important component of learning and memory. It includes the formation of new connections, changing the strength of existing synapses, and elimination of existing synapses. Concisely, neurons that fire together wire together. It determines how effectively presynaptic activity influences postsynaptic firing. These processes enable neural circuits to adapt to experience, store information, and support complex cognitive functions through the direct adjustment of connection strengths throughout the nervous system. Several biological factors determine the synaptic weight, including the number of neurotransmitter receptors on the postsynaptic neuron, the amount of neurotransmitter released from the presynaptic neuron, and the physical size and shape of the synapse [20].

A core mechanism is Hebbian plasticity (Hebb's rule is: "neurons that fire together, wire together"), declaring that theoretically for a synapse to be strengthened, presynaptic activity must coincide with the postsynaptic neuron reaching a specific voltage threshold. This proposed threshold is a level of depolarization higher than what is needed to trigger standard sodium (Na^+)-based action potentials. This coincidence relieves the Mg^{2+} block of NMDA receptors, allowing Ca^{2+} influx. The resultant rise in intracellular Ca^{2+} acts as a second messenger to trigger downstream changes that strengthen the synapse.

As a result, two primary directional changes happen: first, long-term potentiation (LTP), which is a long-lasting increase in synaptic weight due to the strengthening of a connection that is frequently used (wiring). Second, long-term depression (LTD), which is a long-lasting decrease in synaptic weight. This weakens a connection that is rarely used, effectively pruning unused pathways. Along with LTP and LTD, the short-term plasticity (STP) process supports brain functions [20]. While LTP is the primary cellular model for learning and long-term memory, STP is a rapid, flexible and temporary change in synaptic strength that lasts from milliseconds to a few minutes. It acts as a high-pass or low-pass filter for neural information, allowing synapses to dynamically adjust their output based on recent activity. STP is crucial for working memory (holding information online for immediate tasks; e.g., remembering a phone number you are about to dial), adaptation (filtering out constant, unchanging stimuli to highlight novel or changing information), and temporal processing (laying a key role in processing the timing and rhythm of signals). The difference between these two brain's memory and adaptation systems is listed in **Table 1**.

Moreover, STDP is a more specific form of synaptic plasticity that provides the rules for how LTP and LTD are induced. It refines the classic concept of Hebb's rule with a critical temporal precision, which dictates the direction and magnitude of synaptic change based on the order and the precise time difference of the spikes between a presynaptic and a postsynaptic neuron. If the presynaptic neuron fires just before

Feature	STP	LTP
Duration	Milliseconds to minutes	Hours to a lifetime
Mechanism	Presynaptic; residual Ca^{2+}, vesicle depletion	Postsynaptic; NMDA receptor activation, protein synthesis
Purpose	Dynamic filtering, gain control, working memory	Long-term memory formation, learning, stable encoding
Key players	Voltage-gated calcium channels, synaptic vesicles	NMDA receptors, AMPA receptors, CaMKII, CREB
Reversibility	Fully reversible	Difficult to reverse; can be long-lasting or permanent

Table 1.
The comparison between STP and LTP.

the postsynaptic neuron, the synapse is strengthened (LTP). The idea is that the presynaptic input likely contributed to causing the postsynaptic spike. However, If the presynaptic neuron fires just after the postsynaptic neuron, the synapse is weakened (LTD). The idea is that the presynaptic input was irrelevant to causing the spike and is therefore less important. STDP is crucial for learning temporal sequences and causal relationships. Recent research has revealed more complex plasticity rules beyond classic Hebbian learning, often involving neuromodulators (e.g., dopamine) that convey behavioral value or error signals [20]. At the millisecond scale, Hebbian plasticity (e.g., STDP) uses precise pre- and postsynaptic firing correlations for unsupervised association and circuit refinement. Expanding on this, three-factor plasticity incorporates a delayed neuromodulatory signal, acting on seconds-long "eligibility traces" to reinforce connections that led to a reward, enabling reinforcement learning. For direct error correction, supervised plasticity relies on an external instructive signal to optimize synaptic weights. Finally, behavioral timescale synaptic plasticity (BTSP) operates on a seconds-long timescale, using dendritic plateau potentials to create strong, input-specific associations from a single event without requiring precise postsynaptic spiking, facilitating one-shot learning for episodic memory. The discovery of diverse forms of plasticity shows that the brain's cognitive algorithms are far more complex, powerful, and tailored to specific tasks than previously imagined [20].

3. Hardware approaches to synapse emulation

The development of artificial synapses for neuromorphic computing faces two primary challenges: the incompatibility of rigid inorganic materials with future wearable electronics, and the fundamental mismatch between the brain's in-memory computing architecture and the von Neumann architecture of conventional computers, which suffers from latency and high-power consumption due to the separation of memory and processing units. Artificial synapses are engineered to emulate the brain's learning and memory by replicating synaptic plasticity through three primary modulation strategies. Chemically, this involves modifying material properties via doping, vacancy control, and surface engineering. Structurally, advanced device architectures like dual-gate setups and heterostructures are designed to enable complex, programmable functions. Externally, physical stimuli such as light, strain, and temperature are used to create devices that interact directly with their environment for neuromorphic

sensing. The core operational mechanism of these artificial synapses involves inducing a change in the conductivity of an active layer to generate a postsynaptic response, analogous to biological function [21, 22]. This is achieved through various physical phenomena, which are demonstrated in **Figure 2**:

- *Charge trapping:* Charges are trapped at interfaces, such as between conducting additives or at the organic semiconductor (OSC)/insulator interface.
- *Conductive filament formation:* Metal ions diffuse into a layer to form a conductive pathway.
- *Ion migration and electrochemical doping:* Ion migration forms an electric double layer (EDL), causing a temporary carrier accumulation. Electrochemical reactions lead to ion penetration and redox reactions, inducing a more persistent change in carrier concentration.
- *Floating-gate effect*: Carriers tunnel into an isolated (floating) gate and become trapped, shifting the device's characteristics.
- *Dipole alignment*: In ferroelectric materials, the alignment of dipoles is gradually changed by an applied voltage, controlling charge injection barriers or gate-induced fields [21, 22].

Artificial synaptic devices are primarily implemented in two-terminal or three-terminal architectures. The two-terminal devices, with two electrodes, feature a simple structure with a functional layer sandwiched between two electrodes. A presynaptic voltage spike applied to one electrode modulates the conductivity (synaptic weight) of

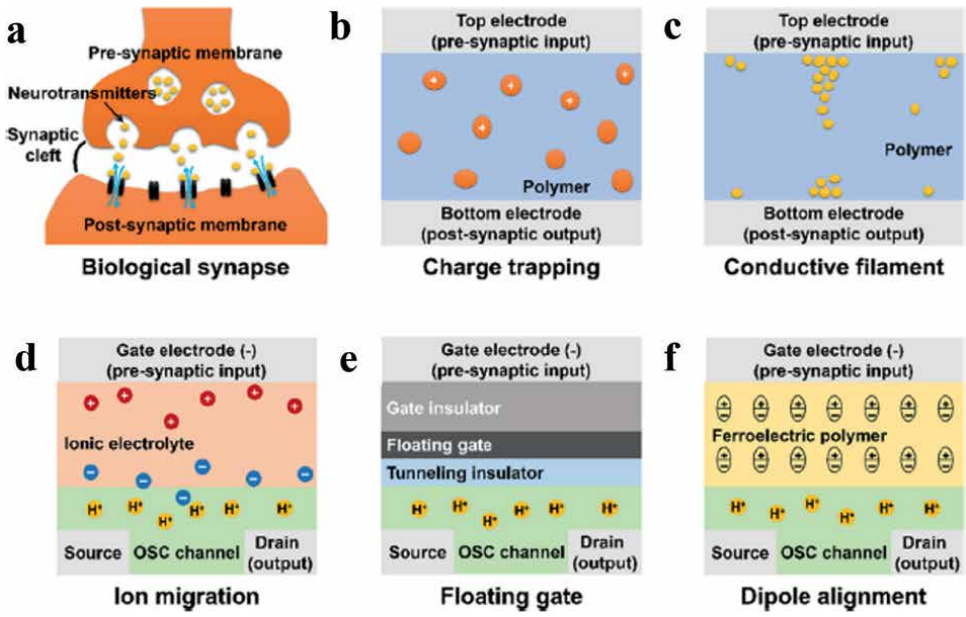

Figure 2.
Different types of synaptic mechanisms, comparing a biological synapse with various principles of artificial synaptic devices. Reproduced with permission from Ref. [21]. Copyright 2019 American Association for the Advancement of Science.

the layer, which is read as a current by the other electrode. However, when integrated into dense crossbar arrays, these devices are susceptible to the flowing of current through unselected cells (sneak-path currents), diminishing read/write accuracy. In contrast, three-terminal devices, transistor-based devices, offer more control and are often more compatible with standard chip-making (CMOS). A presynaptic signal is applied to a gate electrode, which modulates the conductivity of a semiconducting channel between the source and drain electrodes (the postsynaptic terminal). The inherent gate selectivity of these multi-terminal devices effectively suppresses sneak-path currents. Furthermore, their voltage-based read/write operation differs fundamentally from the current-based operation of two-terminal resistive devices. Key devices designed to mimic the behavior of biological synapses and neurons for use in neuromorphic computing of each type include [22] the following.

3.1 Two-terminal synaptic devices

- *Resistive RAM (RRAM):* Uses a memristor that changes resistance based on the history of voltage/current and past electrical activity, mimicking both short- and long-term plasticity with its analog behavior (e.g., oxide-based like TiO_2 and HfO_2, and phase-change like GeSbTe). However, its stochastic switching and cycle-to-cycle variability result in unpredictable conductance changes and inconsistent resistance states, respectively [22].

- *Phase Change RAM (PCRAM):* Switches a phase change material (e.g., GeSbTe) between amorphous (high resistance) and crystalline (low resistance) states by heating. By gradually crystallizing and amorphizing the material, multiple states can be achieved, which can be used as multibit synaptic weight updating emulations, enabling multi-level storage, but is energy intensive [22].

- *Magnetic RAM (MRAM):* Uses two metallic ferromagnetic layers (e.g., CoFeB) separated by an insulating tunnel barrier (e.g., MgO). Its resistance is low when the magnetic layers are aligned in parallel and high when anti-parallel. This state is changed with an electric current or magnetic field. It is extremely fast (nanosecond range) and durable, but its small resistance window makes emulating multi-level synaptic weights challenging [22].

- *Ferroelectric RAM (FERAM):* Uses ferroelectric materials (e.g., doped HfO2 ferroelectric phases or polymers like P(VDF-TrFE)) sandwiched by two electrodes. The device's resistance changes based on the direction of its electrical polarization (up or down). Although each microscopic region is binary, the entire device can achieve multiple analog-like states for synaptic emulation. It offers fast switching (tens of nanoseconds), high endurance (>10^7 cycling), and long retention (>10 years), but suffers from performance inconsistency due to material variability [22].

3.2 Multiterminal synaptic devices

- *Ferroelectric FETs (FEFETs):* Integrate a ferroelectric material (e.g., α-In22Se33) into a transistor's gate. The polarization direction of the ferroelectric materials can be bidirectionally tuned by electric fields of opposite polarity, and the remnant polarization offers the memory effect; it controls the transistor's conductance,

creating non-volatile memory states. Like FERAM, it can achieve multiple-bit channel conductance states and is highly compatible with existing technology [22].

- *Electrolyte-gated transistors (EGTs):* Use the ion movement (instead of just electrons) to process and store information, which makes it uniquely suited for emulating dynamics of biological synapses. Applying a voltage drives ions to form an electric double layer at the channel interface, enabling strong conductance modulation at low voltages and ultra-low power consumption. Its key neuromorphic advantage is the ability to naturally emulate both STP (via transient ion diffusion) and long-term plasticity (via permanent electrochemical doping), directly mimicking the time-dependent dynamics of biological synapses [22].

- *Floating-gate FETs (FGFETs):* They are modified transistors with an additional floating gate embedded within its insulating layer that traps electrical charge. The amount of stored charge analogously shifts the transistor's threshold voltage, creating programmable, non-volatile memory states. Charge is added via hot-electron injection ("charging") and removed via Fowler-Nordheim tunneling ("discharging"). This enables precise, multi-level control over conductance, making it highly effective for emulating synaptic weight changes in neuromorphic systems [22].

However, significant challenges persist in improving energy efficiency and device reliability. These include the high static power consumption of CMOS-based synapses, leakage currents in memristors, manufacturing variability that leads to non-uniform synaptic weights, and the limited ability of most artificial devices to fully replicate complex biological plasticity rules like STDP, LTP, and LTD. Future breakthroughs will likely emerge from hybrid systems and bio-inspired materials, bridging the gap between biological and artificial intelligence. Promising research directions include the development of hybrid CMOS-memristor architectures, the advancement of optoelectronic synapses for high-speed, low-energy communication, and the exploration of spintronic synapses for ultra-low-power operation [22].

4. Piezoelectric nanogenerators for synaptic plasticity emulation

4.1 Principles of piezotronic effect

Piezoelectric semiconductors are a unique class of materials that simultaneously exhibit piezoelectricity and semiconducting behavior. Common examples include ZnO and GaN, which typically crystallize in a wurtzite hexagonal structure. The absence of a center of symmetry along the c-axis in these crystals is the key to their intrinsic piezoelectricity. In an unstressed state, the positive and negative ions, such as Zn^{2+} and O^{2-} in ZnO, are aligned so that their centers coincide, resulting in no net polarization. However, when the material subjected to axial stress/strain along specific crystallographic directions, the ions are displaced relative to one another, producing local electric dipoles. The collective alignment of these dipoles across the crystal results in a macroscopic electric potential, known as the piezopotential, whose strength depends on the applied strain and the doping of the material. This interaction between the piezopotential and charge transport in piezoelectric semiconductors underpins piezotronic transistors and the field of piezotronics [14, 23, 24].

Figure 3 provides a schematic illustration of the fundamental concepts underlying the piezotronic effect. When a metal electrode is brought into contact with an n-type piezoelectric semiconductor, the difference in work functions results in upward bending of the semiconductor energy bands at the surface, thereby forming a Schottky barrier. The barrier height is not solely dictated by the bulk electronic properties of the semiconductor, but is also strongly influenced by interfacial states, surface chemistry, and the presence of strain fields [25, 26]. The intrinsic piezoelectricity of the material can further modify this interface: under tensile strain, negative polarization charges are generated on the semiconductor surface, which repel electrons, increase the upward band bending, and enhance the Schottky barrier height (**Figure 3a**). Conversely, compressive strain produces positive polarization charges that attract electrons, suppress band bending, and reduce the barrier height (**Figure 3b**). In this context, the piezoelectric potential effectively acts as a continuously tunable gate, enabling dynamic modulation of charge-carrier injection across the metal-semiconductor contact in real time [27–29].

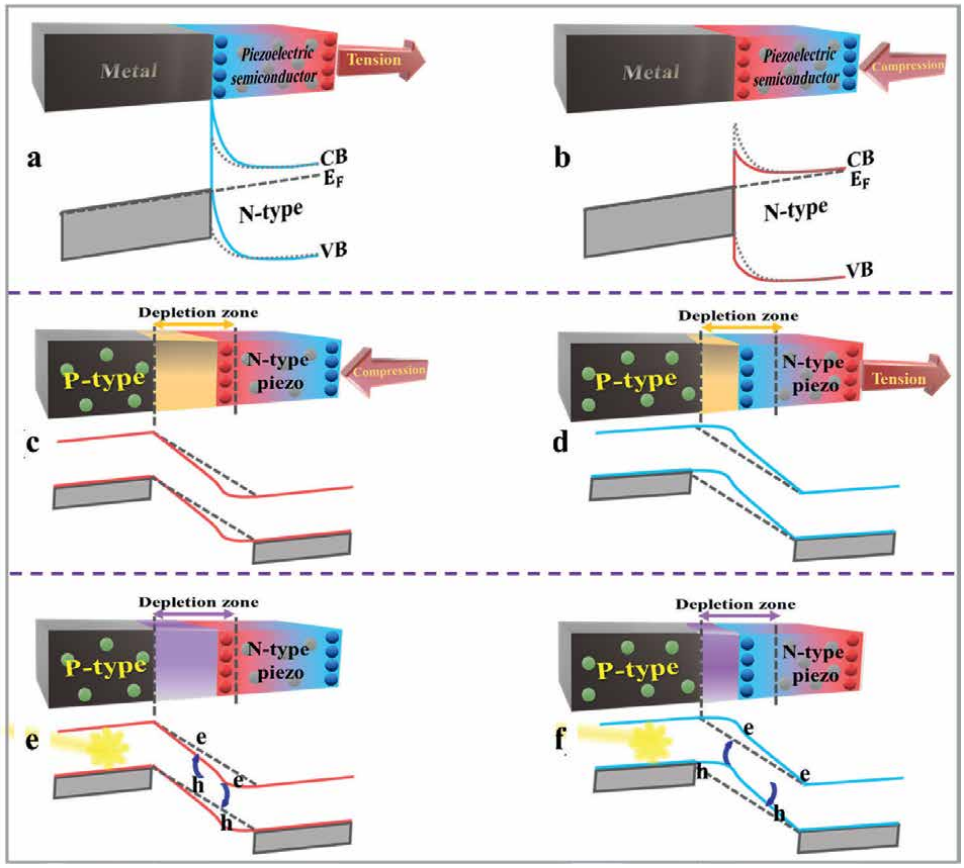

Figure 3.
Fundamentals of the piezotronic and piezo-phototronic effects. (a), (b) Piezopotential distribution and corresponding band diagrams at n-type metal-semiconductor contacts under tensile and compressive strain, respectively. (c), (d) Piezopotential distribution and band diagrams of p-n junctions under tensile and compressive strain, respectively. (e), (f) Combined influence of piezopotential and photo-induced carrier dynamics on p-n junctions under tensile and compressive strain, respectively, with corresponding band diagrams. Adapted from Ref. [27].

A similar strain-dependent modulation mechanism governs the behavior of p-n junctions that include a piezoelectric semiconductor. The low number of free carriers in the depletion region makes the effect of polarization more pronounced because there is little screening. Mechanical strain changes the polarization charges at the interface. This shifts the depletion region and alters the built-in potential. As a result, the local band alignment changes and the movement of electrons and holes is affected. In a heterojunction with a piezoelectric n-type layer, applying tensile strain generates negative polarization charges. This makes the n-side depletion region wider and the p-side narrower, pushing the junction deeper into the n-type material. As a result, the built-in potential rises, and the energy bands bend upward, which enhances charge trapping (**Figure 3c**). Conversely, compressive strain produces positive polarization charges, which shrink the n-side depletion region and shift the junction toward the p-side. This lowers the built-in potential and bends the bands downward, which facilitates the carrier movement (**Figure 3d**) [27–29].

As a distinct physical phenomenon, the piezo-phototronic effect links piezoelectric responses with semiconductor carrier dynamics and optoelectronic processes. In a Schottky-contacted photodetector, optical excitation generates electron-hole pairs that are normally separated and transported by the built-in electric field at the metal-semiconductor (M–S) interface. Strain applied to the piezoelectric semiconductor induces interfacial polarization charges that alter the local band alignment. Positive polarization charges at the reverse-biased contact increase the barrier height and reduce the driving force for carrier separation, thereby suppressing photocurrent. In contrast, negative polarization charges lower the effective barrier and facilitate electron-hole separation and collection; however, excessive negative polarization may lead to pronounced band bending that traps holes at the interface and enhances tunneling currents, resulting in increased dark current and reduced device performance [27–29].

An analogous mechanism operates in p-n junctions based on piezoelectric semiconductors. Here, photogenerated carriers within the depletion region are separated by the built-in electric field and directed to their respective contacts. Strain-induced polarization in the n-type region modifies both the width and position of the depletion layer. Positive polarization charges shift the depletion region toward the p-side, increase series resistance, and induce unfavorable band bending that diminishes separation efficiency (**Figure 3e**). Conversely, negative polarization charges extend the depletion region into the n-side, promote upward valence band bending, and suppress recombination, thereby improving carrier separation and photocurrent generation (**Figure 3f**) [27–29].

4.2 Application of piezotronic in artificial synapsis

Recent advances in neuromorphic devices have leveraged the piezotronic and piezo-phototronic effects in non-centrosymmetric semiconductors such as ZnO, GaN, ZnS, and CdS. These effects allow mechanical and optical stimuli to directly modulate charge transport, enabling self-powered synaptic devices that mimic the behavior of biological synapses. Mechanical strain generates a piezopotential that acts as a gate voltage, tuning carrier concentration and channel conductance without an external bias. When combined with light, the dual piezo-phototronic response offers multi-modal control of synaptic plasticity. Such approaches provide simplified, energy-efficient platforms for neuromorphic computing, capable of parallel sensory processing and adaptive learning driven solely by ambient mechanical and optical cues [14, 30].

Researchers have reported a flexible piezopotential-programmed nonvolatile memory that integrates indium-gallium-zinc oxide (IGZO) field-effect transistors with poly(vinylidene fluoride-co-trifluoroethylene) [P(VDF-TrFE)] PENG. The schematic illustration of the device architecture is shown in **Figure 4a**. In this report the IGZO FET functions as the charge-storing and signal-reading element, whereas the P(VDF-TrFE) nanogenerator supplies the gate potential directly from mechanical strain. A high-capacitance ion gel containing PEGDA, HOMPP, and [EMIM][TFSI] in a 7:3:90 weight ratio links the nanogenerator to the IGZO channel and transfers the piezopotential without an external power source. As shown in **Figure 4b**, when the nanogenerator is bent at strains of 0.06, 0.09, 0.11, 0.16, and 0.20%, output voltages close to 5 V are produced. These voltages drive ionic redistribution in the gel and form electrical double layers at the interfaces, which in turn accumulate electrons in the IGZO channel and raise the drain current from 2.6×10^{-4} μA at 0% strain to 0.17 μA at 0.20% strain (equivalent to a conventional gate bias of ≈0.5 V). It has been demonstrated that disconnecting the top electrode of the nanogenerator from ground preserves this induced charge to create a programmed state, whereas reconnecting to ground neutralizes the charge to erase the state. The reported devices show an electron mobility of 4.3 $cm^2 V^{-1} s^{-1}$, a programming/erasing current ratio exceeding 10^3, a minimum detectable strain of 0.005%, and an ultrahigh gauge factor of 5202—far above metal strain gauges (1–5), doped-Si sensors (~200), and ZnO or CNT piezotronic sensors (~1000). Data retention remains stable for more than 3000 s, and endurance exceeds 100 programming/erasing cycles. Multilevel storage of 2 bits (four current levels) has been achieved by sequentially activating up to four nanogenerators connected to one transistor through a single ion-gel gate, producing

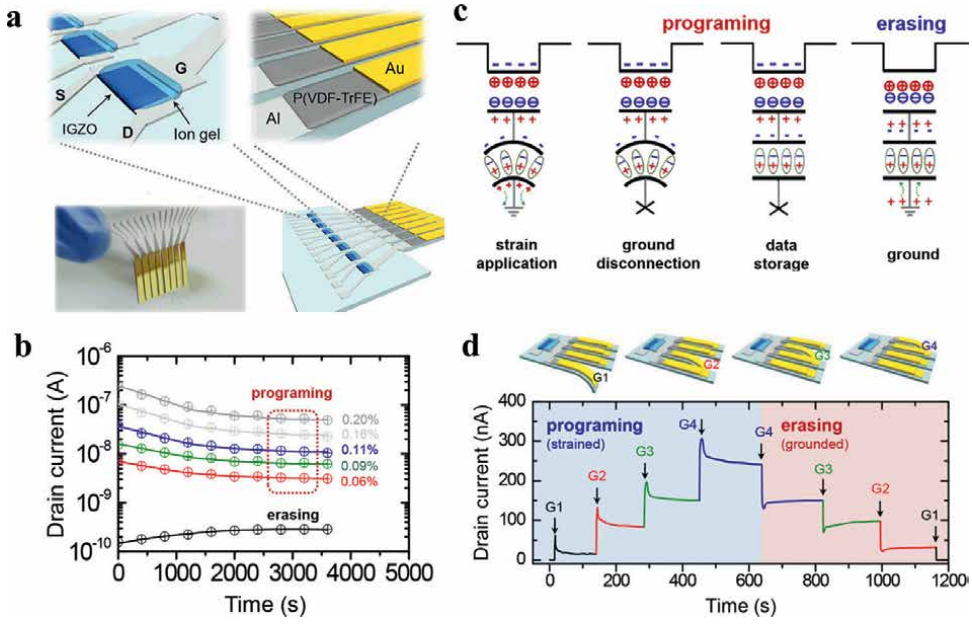

Figure 4.
Piezopotential-programmed nonvolatile memory constructed from IGZO field-effect transistors integrated with P(VDF-TrFE) PENG. (a) Photograph and schematic diagram illustrating the configuration and interconnection of the device components. (b) Retention time characteristics of the memory measured under different bending strains ranging from 0.06 to 0.20%. (c) Operating principle of the piezopotential-programmed nonvolatile memory. (d) Real-time programming and erasing sequences demonstrating device functionality. Reproduced with permission from Ref. [31]. Copyright 2016 American Association for the Advancement of Science.

an on-current of 0.34 μA and an on/off ratio of 4.3×10^3 without cross-talk. Arrays of eight FET/NG units reproduce tactile profiles and two-dimensional color maps such as the letters "OEDL," underscoring the potential of this structure for low-power electronic skin and human-robot interfaces (See **Figure 4c, d**) [31].

Researchers also created a piezotronic synapse using a single GaN microwire, which was grown on a polystyrene substrate through chemical vapor deposition. As shown in **Figure 5a–c**, it has a bamboo-like shape with knots and grows as a single crystal along the c-axis. The device exhibits clear threshold switching in its I-V characteristics. At voltages below the threshold, it remains in a high-resistance state (~1 pA). Once the voltage exceeds the threshold, the current jumps sharply to ~1 μA, reaching a low-resistance state. Reducing the voltage below the hold level returns the device to HRS (See **Figure 5e**). The conduction is governed by trap-controlled space-charge-limited conduction, with nitrogen vacancies at knot regions acting as electron traps, analogous to calcium dynamics in biological synapses (See **Figure 5e**). The device can mimic synaptic plasticity by applying voltage pulse trains ranging from 1 to 3 V with durations of 0.5 to 10 ms. When the interval between pulses is short, from 10 ms down to 0.5 ms, the conductance increases up to seven times, demonstrating PPF. Longer intervals, around 100 ms, lead to paired-pulse depression (PPD). After each pulse, the current gradually relaxes following an exponential decay, and the relaxation time can be tuned from microseconds to milliseconds by changing the pulse amplitude or duration. Repeating the pulse trains gradually strengthens the conductance, effectively reproducing the transition from STP to LTP seen in biological synapse. Furthermore, the piezotronic effect enables the device to modulate its synaptic weight in response to mechanical strain. When a compressive stress of −0.36% is applied, the synaptic weight increases by 330%, and at −0.81% strain, it rises nearly 6.5 times, corresponding to a gauge factor of approximately 736. These results highlight that the GaN microwire can simultaneously act as a highly sensitive tactile sensor and as an artificial synapse, effectively reproducing essential behaviors such as threshold switching, facilitation, depression, and memory potentiation [32].

ZnO microwire (MNW) photonic synapses provide a promising platform for bio-inspired neuromorphic electronics by coupling semiconducting, piezoelectric, and photoactive effects. The device is fabricated by laterally transferring a single CVD-grown ZnO MNW onto a flexible substrate and contacting its ends with Ag electrodes, forming a two-terminal metal-semiconductor-metal (M-S-M) structure. The high-quality ZnO MNW exhibits strong UV optical characteristics, with an absorption edge at 378 nm and near-band-edge photoluminescence at ~391 nm, while intrinsic oxygen-related defects play a crucial role in carrier trapping and recombination. When stimulated by 365 nm UV pulses, the device generates EPSCs and exhibits conductance relaxation in the dark, effectively mimicking biological synaptic functions. STP, including PPF with a maximum index of 1.45, is observed under successive pulses, while repeated or high-intensity stimulation (up to 4.2 mW cm^{-2}) drives the transition to long-term plasticity, with synaptic weight changes exceeding 1400% before relaxation. These behaviors closely resemble the learning-forgetting processes of biological synapses. Furthermore, applying compressive strain along the c-axis introduces piezoelectric polarization charges that modulate the local Schottky barrier height at the M–S interface. This piezo-phototronic effect enhances photocurrent by nearly threefold (0.17 to 0.51 μA at 0.18% strain), prolongs relaxation time, and enables external control of the STP-to-LTP transition. Notably, synaptic weight can be tuned from ~302% down to ~143% under strain, demonstrating the strong coupling between mechanical and optoelectronic responses [33].

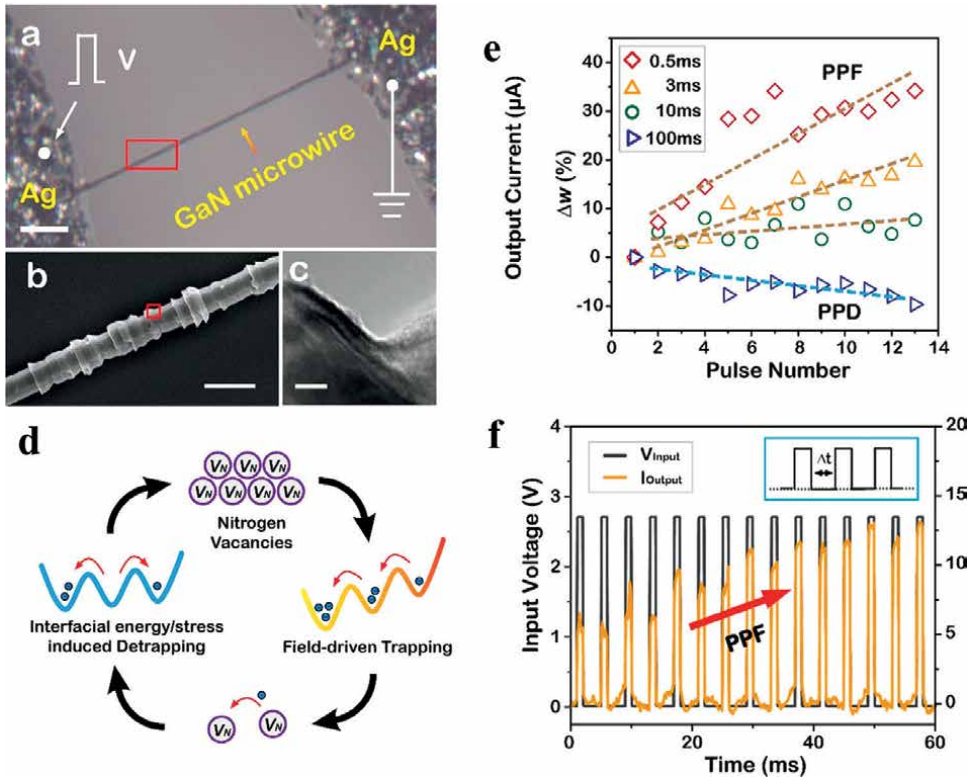

Figure 5.
GaN microwire-based piezotronic synapse. (a) Optical image of the device with a symmetric Ag/GaN microwire/Ag configuration, highlighting the overall structure and geometry of the microwire (scale bar: 20 μm). (b) Scanning electron microscopy (SEM) image of the GaN microwire, revealing its characteristic bamboo-like morphology, which plays a role in mechanical stress distribution along the wire (scale bar: 2 μm). (c) High-resolution transmission electron microscopy (TEM) image at a knot region of the microwire, showing the crystalline arrangement and structural details at the nanoscale (scale bar: 5 nm). (d) Schematic illustration of the operating mechanism, where an external electric field drives carrier trapping, while interfacial energy and stress contribute to the detrapping process, together governing the dynamic modulation of conductance. (e) Evolution of the synaptic weight (Δw) as a function of pulse number under identical input pulses (2.7 V, 1 ms) at varying time intervals (Δt = 0.5, 3, 10, and 100 ms), demonstrating the coexistence of PPF and PPD. Shorter intervals result in stronger facilitation with larger Δw, whereas longer intervals gradually suppress the conductance change, turning negative at Δt = 100 ms. f) Demonstration of PPF behavior, where the device current response (orange) closely follows the input voltage pulse train consisting of 15 pulses (2.7 V, 1 ms). The inset (blue rectangle) illustrates the temporal profile of the pulse sequence, with each pulse lasting 1 ms and separated by a 3 ms interval. Reproduced with permission from Ref. [32]. Copyright 2020 American Association for the Advancement of Science.

A flexible and transparent two-terminal synaptic device was developed using a ZnO thin film grown on Ag nanowire (AgNW) electrodes supported by a PET substrate. The device exhibits clear synaptic behavior under UV stimulation (365 nm). For a single 1 s pulse at 0.6 V, the photocurrent reached ~4.1 μA in the strain-free state, was enhanced to ~6.6 μA under +0.6% compressive strain, and suppressed to ~0.8 μA under −0.6% tensile strain. At +1 V, the current increased from ~21 μA (strain-free) to ~64 μA (compressive), confirming that external strain effectively modulates synaptic weight through the piezo-phototronic effect. Key synaptic functions such as STP and long-term plasticity were realized. For instance, with 4 mW cm^{-2} pulses, Ip increased to ~4.9 μA under compressive strain, enabling STP -to- long-term plasticity transition, while strain-free and tensile-strain states showed only STP. PPF was also

achieved, with indices of 165 (strain-free) and 210 (compressive), showing strong dependence on pulse interval. STDP was demonstrated with Δt between 0.5 and 10 s, reproducing timing-dependent modulation of synaptic weight. By defining a threshold photocurrent of ≈0.5 μA, the device also exhibited Pavlovian-like associative learning as subsequent low-intensity pulses elicited currents above this threshold after training with combined pulse sequences [34].

A flexible optoelectronic synaptic device was realized using a $ZnO/Al_2O_3/CdS$ heterostructure (ZAC-OSs) fabricated on ITO-coated PET substrates. Vertically aligned ZnO nanorods provided a piezoelectric and photoactive scaffold, a thin Al_2O_3layer served as a tunneling and trapping medium, and CdS quantum dots enhanced light absorption. Upon exposure to weak 365 nm optical pulses, the device produced EPSCs closely resembling those of biological synapses. PPF was clearly observed, where a second light pulse generated a stronger EPSC than the first. The facilitation index reached a maximum of ≈158% at an interval of 50 ms, then gradually decayed with increasing pulse spacing, characteristic of STP. With higher-frequency or repeated stimulation, the EPSCs accumulated, leading to a transition from STP to long-term plasticity. Notably, after 100 consecutive pulses, the EPSC remained significantly elevated with a retention time exceeding 10^3 ms, indicative of memory consolidation. Beyond synaptic plasticity, the device demonstrated persistent photoconductivity (PPC), maintaining an elevated current even after the optical input was removed, a clear analogue to memory retention. More importantly, it reproduced the processes of forgetting and relearning. As the current gradually relaxed, subsequent exposure to the same optical pulses triggered a quicker recovery of EPSC amplitude, capturing the experience-dependent adaptation characteristic of biological synapses. The device's synaptic behavior could also be tuned mechanically through the piezo-phototronic effect of the ZnO nanorods. When tensile strain was applied, negative piezoelectric charges appeared at the ZnO/Al_2O_3 interface, lowering the tunneling barrier and boosting the EPSC by roughly 1.5× compared to the unstrained state. In contrast, compressive strain reduced the synaptic weight. This combination of optical and mechanical control acts like a simple form of neuromodulation, similar to how neurotransmitters adjust signal strength in biological synapses [35].

5. Triboelectric nanogenerators for synaptic plasticity emulation

5.1 Principles of tribotronics

Tribotronics has emerged as a novel research direction at the intersection of *triboelectrification* and semiconductor electronics. This interdisciplinary field leverages the electrostatic potential generated during contact and separation of dissimilar materials as an *in situ* gating signal to actively modulate charge transport in semiconductor devices. Unlike conventional field-effect transistors (FETs) that require an externally applied gate voltage, tribotronic devices exploit friction-induced charges to regulate carrier transport, thereby enabling direct transduction of mechanical stimuli into electronic responses. This approach has introduced a novel strategy for applications in sensors, human–silicon interfaces, micro/nano-electro-mechanical systems (MEMS/NEMS), nanorobotics, and active flexible electronics [36].

A significant advancement in tribotronic technology occurred in 2014 when Zhang et al. introduced the contact-electrification field-effect transistor (CE-FET) [37].

Figure 6 depicts the working principle of a typical CE-FET device. In this design, the copper (Cu) layer functions as a movable triboelectric component, as illustrated in **Figure 6a**. The drain terminal is biased with an external voltage, whereas the source is electrically grounded. When the Cu layer is in complete contact with the PMMA/Cytop dielectric, triboelectric interactions induce positive charges on the Cu surface and corresponding negative charges on the dielectric. At this fully contacted state, the opposing charges are balanced, resulting in no net potential difference across the pentacene channel and no modulation of charge carrier density; consequently, the drain current (IDS) remains unchanged. Upon gradual separation of the Cu layer from the PMMA/Cytop surface, the negative charges on the dielectric induce polarization within the pentacene layer, establishing an internal electric field across the interface. This field drives hole accumulation at the boundary between pentacene and the dielectric, effectively forming an enhancement region within the channel and increasing IDS. As the separation progresses, the internal field intensifies, leading to further enhancement of the drain current. Conversely, when the Cu layer moves back toward the dielectric surface, the previously accumulated holes disperse, diminishing

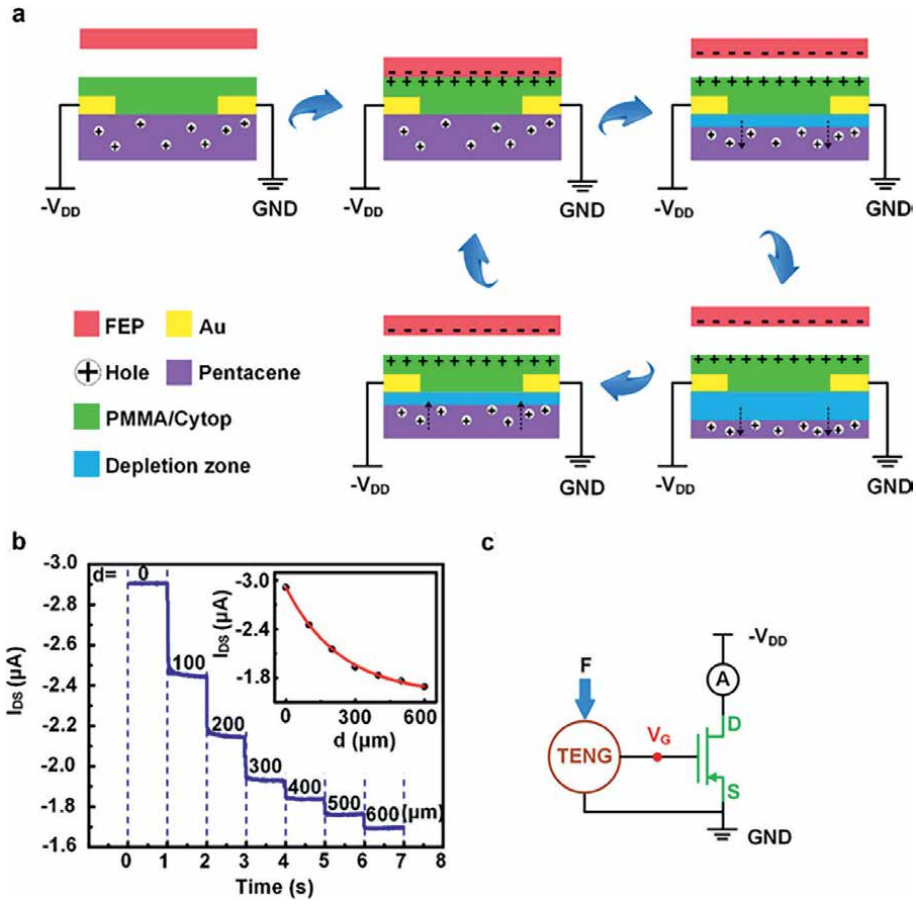

Figure 6.
Contact-electrification field-effect transistor (CE-FET). (a) Operating mechanism of the CE-FET. (b) Transfer characteristics at varying separation distances. (c) Equivalent circuit representation. Reproduced with permission from Ref. [37]. Copyright 2014 American Association for the Advancement of Science.

the enhancement region and causing a reduction in IDS. Once the Cu film is restored to full contact with the PMMA/Cytop layer, the drain current returns to its original baseline value, completing the reversible modulation cycle [38].

The I_{DS}-separation relationship was quantified using a linear motor for precise displacement control. I_{DS} increased progressively with Cu separation, rising from −2.84 to −3.25 μA as the gap widened from 0 to 700 μm at V_{DS} = −10 V (**Figure 6b**,**c**). The on/off ratio, defined by I_{DS} at maximum versus minimum separation, was ~1.14, consistent with the described aforementioned mechanism. These results confirm that the CE-FET effectively transduces mechanical displacement into electrical response via controlled triboelectric-induced modulation [38].

The contact-electrification field-effect transistor (CE-FET) and the piezotronic transistor represent two classes of mechanically gated, two-terminal switching devices that eliminate the need for a conventional metallic gate electrode by utilizing strain-induced internal electric fields. In piezotronic transistors, mechanical deformation generates a piezopotential across a p-n junction or metal-semiconductor interface, which directly modulates the junction's energy barrier and thereby regulates charge carrier transport. In contrast, the CE-FET operates through contact electrification, wherein transient mechanical contact between dissimilar materials produces a triboelectric surface charge. This charge electrostatically induces a virtual gate field that modulates the width and conductivity of the underlying semiconductor channel through capacitive coupling. Given the higher voltage outputs of TENGs and the broader choice of contact materials, tribotronic devices offer greater sensitivity and design flexibility compared to piezotronic counterparts [39].

5.2 Application of tribotronics in artificial synapsis

TENGs serve a dual role in sensing and energy conversion, enabling their use as both power sources and sensors in self-powered artificial synapses. Through electrostatic coupling, they can substitute for gate voltage to control different types of synaptic transistors, such as FeFETs, FGFETs, electrolyte-gated transistors (EGTs), and optical transistors [40, 41].

The CE-activated artificial afferent reported by Yu et al. [42], which integrates a TENG with a MoS_2-based electrolyte-gated synaptic transistor (EGT), establishing a direct mechano-electric interface for neuromorphic signal transduction. Typical working mechanism of CE-activated artificial afferent is demonstrated in **Figure 7a**. According to **Figure 7b** and **7c** the transistor consists of a monolayer MoS_2 channel, an ion gel dielectric, and a gate electrode connected to the TENG. Mechanical contact-separation events at the TENG generate dynamic triboelectric potentials, which serve as the gate voltage to drive ionic migration within the electrolyte. This process induces the formation of an electric double layer (EDL) at the MoS_2/ion-gel interface, modulating channel conductance through carrier injection [42].

Upon stimulation, a single triboelectric pulse produced a transient EPSC characterized by a rapid rise and exponential decay determined by the relaxation of ions in the electrolyte (**Figure 7c**). The decay time constants ($\tau \approx 50$–200 ms depending on pulse amplitude) closely replicate STP. Consecutive pulses demonstrated PPF, with facilitation ratios exceeding 180% at Δt = 50 ms, attributed to residual ion accumulation enhancing subsequent EDL formation. Furthermore, repeated high-frequency stimulation induced LTP, where channel conductance remained elevated over extended intervals, confirming memory consolidation capability [42].

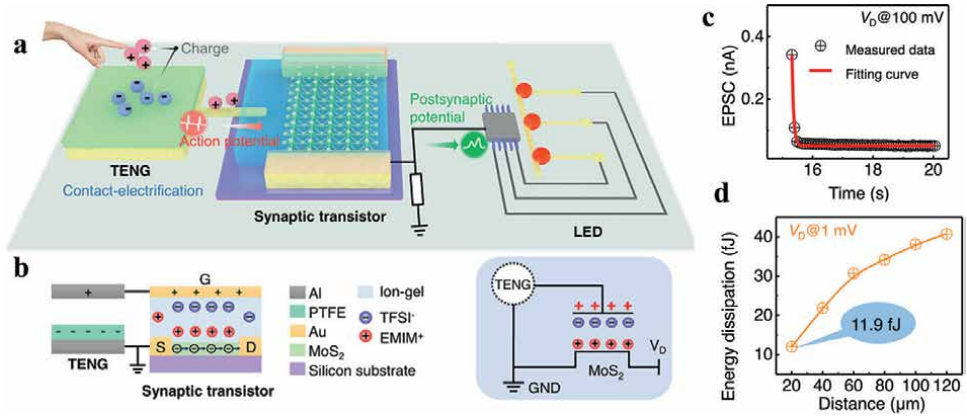

Figure 7.
Illustration of typical synaptic responses in the CE-activated artificial afferent. (a) Schematic illustration of the CE-activated artificial afferent, which integrates a self-activation module, a synaptic transistor, and a functional circuit, enabling neuromorphic functionality. (b) Cross-sectional view of the CE-activated MoS_2 synaptic transistor with annotated structural components, accompanied by the corresponding circuit diagram of the artificial afferent for functional correlation. (c) Analysis of the EPSC decay behavior, fitted with an exponential decay model to emulate biological synaptic response. (d) Dependence of energy dissipation on transmission distance, highlighting the efficiency of signal processing in the artificial afferent system. Reproduced from Ref. [42] under license CC BY 4.0.

Another pivotal technological feature of the CE-activated artificial afferent system is its ultra-low energy consumption per synaptic event, measured at ~11.9 fJ (**Figure 7d**), approaching the intrinsic energy scale of biological synapses (~10 fJ) [42].

Lei et al. [43] proposed an organic electrolyte-gated transistor (EGT) consisting of an organic semiconductor channel, an ion-rich gelatin dielectric, a gate electrode connected to a triboelectric sensor, and a thin PVN protective coating that prevents moisture uptake and enhances device stability. Upon applying a voltage pulse from the sensor to the gate, mobile ions in the gelatin migrate and accumulate at the semiconductor/dielectric interface, forming an electric double layer (EDL). The resulting local electrostatic field induces charge injection into the channel, producing a sharp increase in drain current analogous to the EPSC in biological synapses. After the stimulus is removed, the ions gradually diffuse back, causing a slow decay of current and thereby emulating short-term memory (STM). Moreover, when two successive pulses are applied, the residual ions from the first pulse amplify the response to the second, leading to PPF, a characteristic feature of synaptic plasticity. The PVN coating further ensures reliable neuromorphic performance by improving charge transport and protecting against environmental degradation.

Yang and co-workers [44] report a mechanoplastic tribotronic floating-gate neuromorphic transistor that integrates TENG physics with two-dimensional semiconductors to emulate artificial synapses directly modulated by mechanical displacement. The device consists of a monolayer MoS_2 channel on a 10 nm HfO_2 tunneling dielectric, with an Au-nanoparticle floating gate embedded below and supported by a 300 nm SiO_2 substrate. Beneath the transistor, a contact-separation TENG made from Cu and fluorinated ethylene propylene (FEP) films generates bipolar triboelectric potentials (up to ±90 V at 0.7 mm separation), capacitively coupling to the floating gate without any external gate voltage.

Mechanical displacement acts as a presynaptic spike. Positive triboelectric potential lowers the MoS_2 conduction band, enabling electron injection into both the

channel and the floating gate via Fowler-Nordheim tunneling. When contact occurs, the potential collapses but trapped charges remain, creating a persistent negative bias. This results in a four-stage current response: baseline, excitatory rise, inhibitory overshoot, and slow recovery ($\tau \approx 2.8$–7.8 s) as detrapping occurs. Reversing TENG polarity produces mirror excitatory responses, enabling both inhibitory and excitatory post-synaptic currents.

Displacement amplitude and pulse duration systematically tune synaptic behavior. The normalized synaptic weight change ($\Delta W/W$) increases with displacement, saturating at ~64% for 0.7 mm, while longer pulses enhance retention beyond 8 s—much longer than electrolyte-gated synapses. Paired-pulse experiments reveal mechano-tunable STP, showing PPF or PPD depending on polarity. Repeated pulses induce gradual, stable LTP or LTD, reflecting a transition from short- to long-term mechanoplasticity.

To demonstrate higher-level function, the authors construct a hybrid neural network with two electrical floating-gate synapses and one mechanoplastic synapse as a modulatory input. Using ±100 V electrical and triboelectric spikes as digital inputs, the system performs logic operations: negative modulation enables AND logic, while positive modulation enables OR logic. Importantly, the floating gate retains the computed state for over 8 s, functioning as in-situ memory without external circuitry.

The mechano-photonic artificial synapse developed by Yu et al. [45] integrates a graphene/MoS_2 (Gr/MoS_2) heterostructure transistor with a TENG to emulate dual-modal synaptic plasticity, combining mechanical and optical modulation. he TENG operates through the relative displacement of two friction layers, typically a Cu/PTFE assembly, generating a triboelectric potential (VTENG) proportional to the mechanical displacement (D) and the applied force. When the layers are initially in contact, the system reaches electrostatic equilibrium, with transferred charges neutralized by grounding and the transistor channel in a flat-band state, exhibiting no charge transfer. Upon separation (D+), unneutralized charges induce a negative VTENG at the transistor gate, which lowers the Fermi level of graphene and electrostatically dopes it with holes. This modulation alters the carrier density in the graphene layer, enhancing its resistance under light illumination as photogenerated electrons from MoS_2 are injected into the hole-doped graphene, resulting in a controllable decrease in postsynaptic current (PSC). Conversely, when the layers approach each other (D−), a positive VTENG is induced, raising the Fermi level and driving the energy bands of MoS_2 toward a flat-band state, suppressing electron injection and equilibrating the carrier distribution. Therefore, the synergistic interaction between triboelectric gating and photogenerated carriers enables dynamic tuning of synaptic weights, long-term memory emulation, and spike-timing-dependent plasticity, closely mimicking biological synapses. In addition, mechanical displacement not only sets the baseline PSC but also amplifies the optically induced synaptic response, whereas repeated light pulses further strengthen the PSC, demonstrating cumulative and adaptive plasticity. When applied to supervised learning tasks in artificial neural network (ANN) simulations for MNIST digit recognition, the dual-modal synapses exhibited substantially enhanced performance, achieving up to 92% recognition accuracy with sufficient training samples, significantly outperforming single-modal synaptic devices.

In another approach, a multi-layered triboelectric nanogenerator (M-TENG) was combined with an organic electrochemical transistor (OECT) to construct a self-powered artificial synapse for neuromorphic computing applications. Unlike conventional TENGs that yield a single pair of spikes per cycle, stacking alternating FEP, PDMS, and Al layers enabled the generation of multiple sequential voltage

spikes from each mechanical press–release action. In particular, the triple-layer device (3-TENG) produced six well-defined spikes, offering richer presynaptic-like stimuli than single- or double-layer configurations. When rectified and applied to the OECT gate, these EPSCs, effectively mimicking biological synaptic transmission. The system effectively replicated key synaptic plasticity mechanisms. PPF exhibited facilitation indices of ~124% at short inter-spike intervals, with relaxation times on the scale of hundreds of milliseconds, closely resembling biological synapses. LTP was demonstrated through repeated mechanical stimulation, which enhanced EPSCs by over 200% relative to baseline and maintained elevated conductance over extended periods. Among the tested configurations, the 3-TENG provided an optimal balance of spike multiplicity and signal integrity, outperforming the 4-TENG, where excessive layering reduced spike sharpness and output amplitude. The practical applicability of the system was demonstrated by integrating the artificial synapse with a robotic hand. EPSC signals were directly mapped to motor outputs, allowing graded and adaptive finger movements in response to varying mechanical stimuli. Repeated exposure to stronger pulses enhanced the synaptic weight, such that previously insufficient weak stimuli could subsequently elicit full finger motions, illustrating the device's capability to encode and retain sensory information over time [46].

Researchers reported [47] a flexible triboelectric artificial synapse (TAS) that mimics biological neurosensory behavior by coupling a polymer semiconductor channel with an ion-gel dielectric and a TENG. **Figure 8a** illustrates the structure and working mechanism of the TAS device. The device is constructed on a thin plastic substrate with gold source and drain electrodes separated by an 80-micrometer channel. The channel is composed of poly(3-hexylthiophene) nanofibrils embedded in a soft silicone elastomer. The nanofibrils facilitate rapid hole transport, while the silicone maintains mechanical integrity under repeated bending. An ion gel composed of a fluoropolymer and an ionic liquid covers the channel, providing mobile anions and cations that respond to external potentials. Instead of a conventional gate electrode, a copper–PTFE triboelectric layer generates a self-powered voltage pulse during contact and separation. This pulse drives the migration and accumulation of ions at the channel interface, increasing the hole concentration and bending the energy bands upward, which results in a rise in channel conductance. When the triboelectric layer returns to contact, the gate potential decreases and the ions relax back into the gel, reducing conductance. In this way, the device directly converts mechanical stimuli into postsynaptic-like currents, reproducing the essential steps of presynaptic action, neurotransmitter release, and postsynaptic response in a single flexible platform [47].

The device demonstrates robust STP. A single mechanical pulse of 0.1 seconds duration and 2-millimeter displacement produces a postsynaptic current of 1.6 microamperes that gradually decays. Longer or stronger pulses enhance the peak current and extend the decay time. When two pulses arrive in rapid succession, the second response exceeds the first due to residual ions at the interface, mimicking PPF. The fast and slow decay components have relaxation times of approximately 57 and 298 milliseconds. Repeated mechanical pulses produce cumulative effects: five pulses generate a peak current of 12.8 microamperes, while one hundred pulses reach nearly 100 microamperes, with the current returning to baseline over approximately 50 seconds. These results indicate that the device reproduces both STP and LTP (**Figure 8c**) [47].

The device also replicates associative learning in a Pavlov-style simulation. A strong "food" stimulus alone elicits a current above 25 microamperes, while a weaker "bell"

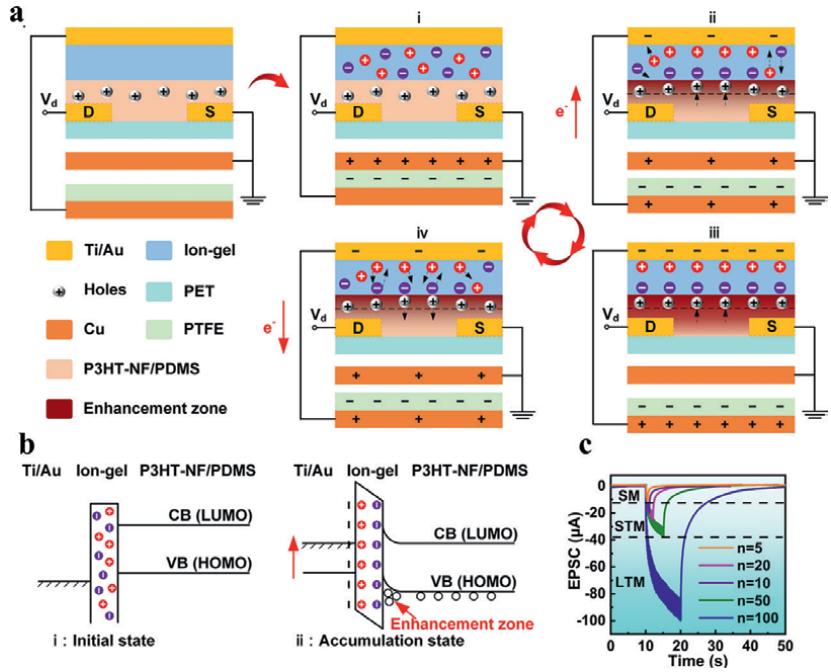

Figure 8.
Working mechanism of the TAS device. a) Schematic illustration of the operational principle of the TAS, showing its structural configuration and functional components. b) Energy band diagram of the TAS, depicting carrier modulation under external excitation. c) EPSC responses of the TAS under multiple continuous mechanical stimuli (T = 0.1 s, ΔT = 0.1 s, D = 2 mm), demonstrating its capability to emulate synaptic behavior. Reproduced from Ref. [47] under license CC BY 4.0.

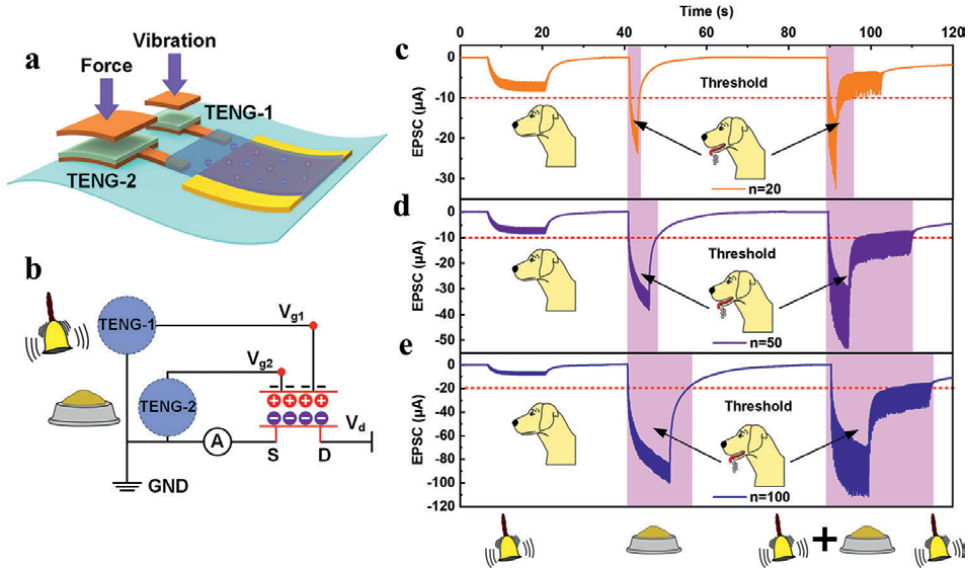

Figure 9.
Pavlov's dog-inspired demonstration of associative memory using a TAS device. (a) Illustration of the TAS under simultaneous force and vibration, working in dual-TENG mode. (b) Equivalent circuit analogy showing how the device mimics Pavlov's dog associative learning. (c)–(e) EPSC signals recorded after 20, 50, and 100 training cycles, highlighting the strengthening of synaptic response with increased training time. Reproduced from Ref. [47] under license CC BY 4.0.

stimulus initially produces only 8.5 microamperes. After twenty paired presentations of both stimuli, the weaker input alone triggers a current exceeding 10 microamperes, the threshold for "salivation." Increasing the number of pairings to fifty or one hundred further strengthens and prolongs the response, demonstrating that associations between different mechanical inputs can be formed and recalled (**Figure 9**) [47].

6. Conclusion and future perspectives

The integration of tribotronics and piezotronics into neuromorphic device engineering has opened a promising pathway toward artificial synapses that emulate the adaptive, energy-efficient, and multimodal characteristics of biological neural systems. By exploiting direct mechanical-to-electrical transduction, these devices circumvent the need for conventional gate voltages, thereby achieving intrinsic energy efficiency while simultaneously enabling diverse sensory interactions. Demonstrations of EPSCs, PPF, LTP, and associative learning highlight their ability to reproduce fundamental aspects of biological plasticity and signal processing. Furthermore, their compatibility with flexible and biocompatible substrates positions them as strong candidates for wearable electronics, prosthetics, and human–machine interfaces.

Despite these advances, several challenges must be addressed before these systems can transition from laboratory-scale prototypes to practical neuromorphic platforms. Ensuring mechanical and environmental stability under repeated operation, achieving large-scale and CMOS-compatible integration, and reliably incorporating multimodal inputs remain open issues.

Looking ahead, a number of research directions are expected to shape the evolution of the field. The development of scalable, high-density synaptic arrays compatible with semiconductor manufacturing processes will be crucial for system-level neuromorphic architectures. The pursuit of fully self-powered systems, where triboelectric potential simultaneously acts as both gate and drain bias, may eliminate external power demands and unlock autonomous operation. Hybrid tribo/piezo-phototronic architectures that couple mechanical and photonic stimuli offer a promising route to enhanced responsivity and broadened functional diversity. In parallel, the incorporation of machine learning-guided design tools can accelerate the optimization of material systems, strain configurations, and device architectures, thereby reducing empirical trial-and-error. Progress in biointegration through flexible, biocompatible materials will further enable seamless incorporation into prosthetics and neural interfaces. Finally, advancing from basic synaptic plasticity toward higher-order cognitive functions, such as associative memory, learning, and decision-making, will require the convergence of tribotronic/piezotronic synapses with large-scale neuromorphic circuits.

Altogether, these developments position tribotronic and piezotronic synaptic devices as emerging building blocks of next-generation neuromorphic systems—self-powered, adaptive, and capable of real-time interaction with their environment. Their continued evolution holds significant promise for transformative applications spanning brain-inspired computing, soft robotics, human-machine interaction, and biomedical engineering.

Conflict of interest

The authors declare no conflict of interest.

Author details

Mahdi Zekavat*, Zahra Razzaghi and Fahimeh Zamanpour
Center for Nanoscience and Nanotechnology (INST), Institute for Convergence Science and Technology (ICST), Sharif University of Technology, Tehran, Iran

*Address all correspondence to: mirmehdizekavat@gmail.com

IntechOpen

References

[1] Wang H, Zhang H, Liu Y, Liu S, Xu Y, Zhang X, et al. On non-von Neumann flexible neuromorphic vision sensors. npj Flexible Electronics. 2024;**8**:28

[2] Wali A, Das S. Two-dimensional memtransistors for non-von Neumann computing: Progress and challenges. Advanced Functional Materials. 2024;**34**:2308129

[3] Shao L, Zhao Y, Liu Y. Organic synaptic transistors: The evolutionary path from memory cells to the application of artificial neural networks. Advanced Functional Materials. 2021;**31**:2101951

[4] Sun F, Zhang Y, Zheng L, Zhang Y, Zhang H, Shen Y, et al. Flexible artificial sensory systems based on neuromorphic devices. ACS Nano. 2021;**15**:3875-3899

[5] Yang K, Li Q, Liu J, Chen Y, Lu Z, Wang Y, et al. Tunable flexible artificial synapses: A new path toward a wearable electronic system. npj Flexible Electronics. 2018;**2**:20

[6] Liu Y, Liu J, Liu S, Zhang Y, Zhang H, Wang Z, et al. Self-powered artificial synapses actuated by triboelectric nanogenerator. Nano Energy. 2019;**60**:377-384

[7] Sun Z, Zhao J, Gao Y, Wang Y, Sun Q, Wang ZL. Moving toward human-like perception and sensation systems—From integrated intelligent systems to decentralized smart devices. SmartSys. 2025;**1**:e4

[8] Delgado-Alvarado E, Hernández-Elvira P, Priya S. Recent progress of nanogenerators for green energy harvesting: Performance, applications, and challenges. Nanomaterials. 2022;**12**:2549

[9] Wang X, Wang ZL, Yang Y. Hybridized nanogenerator for simultaneously scavenging mechanical and thermal energies by electromagnetic-triboelectric-thermoelectric effects. Nano Energy. 2016;**26**:164-171

[10] Liu Y, Chen X, Li J, Zhang Y, Zhang H. Application of thermoelectric generators for low-temperature-gradient energy harvesting. Applied Sciences. 2023;**13**:2603

[11] Zeng J, Jiang P, Shi Q, Hu C. Triboelectric nanogenerators as active tactile stimulators for multifunctional sensing and artificial synapses. Sensors. 2022;**22**:975

[12] Zhao J, Chen Y, Yang X, Gao G, Wang Y, Sun Q, et al. Tribotronics for bioinspired neuromorphic tactile perception and computing. MRS Bulletin. 2025;**50**:181-189

[13] Wang ZL, Wu W. Recent advances in piezotronics and piezo-phototronics. MRS Bulletin. 2025;**50**:115-122

[14] Hua Q, Zhang J, Li J, Sun Q, Wang ZL. Piezotronics enabled artificial intelligence systems. Journal of Physics: Materials. 2021;**4**:022003

[15] Yang JQ, Wang Z, Naber RCG, Chen J, Ji Y. Neuromorphic engineering: From biological to spike-based hardware nervous systems. Advanced Materials. 2020;**32**:2003610

[16] Kim Y, Lee CW, Jang HW. Neuromorphic hardware for artificial sensory systems: A review. Journal of Electronic Materials. 2025;**54**:3609-3650

[17] Ribarič S. Detecting early cognitive decline in Alzheimer's disease with brain synaptic structural and functional evaluation. Biomedicine. 2023;**11**:355

[18] Yi W, Zhang J, Li J, Sun Q, Wang ZL. Biological plausibility and stochasticity in scalable VO_2 active memristor neurons. Nature Communications. 2018;**9**:4661

[19] Caire MJ, Reddy V, Varacallo M. Physiology, Synapse. Orlando, Florida: StatPearls Publishing; 2018. Available from: https://europepmc.org/article/NBK/nbk526047

[20] Magee JC, Grienberger C. Synaptic plasticity forms and functions. Annual Review of Neuroscience. 2020;**43**:95-117

[21] Lee Y, Lee TW. Organic synapses for neuromorphic electronics: From brain-inspired computing to sensorimotor nervetronics. Accounts of Chemical Research. 2019;**52**:964-974

[22] He K, Zhang J, Li J, Sun Q, Wang ZL. Artificial neuron devices. Chemical Reviews. 2023;**123**:13796-13865

[23] Wang ZL. ZnO nanowire and nanobelt platform for nanotechnology. Materials Science and Engineering R. 2009;**64**:33-71

[24] Wang L, Wang ZL. Advances in piezotronic transistors and piezotronics. Nano Today. 2021;**37**:101108

[25] Lin X, Zhang J, Li J, Sun Q, Wang ZL. Piezotronic neuromorphic devices: Principle, manufacture, and applications. International Journal of Extreme Manufacturing. 2024;**6**:032011

[26] Peng Y, Zhang J, Li J, Sun Q, Wang ZL. Progress in piezotronic and piezo-phototronic effect of 2D materials. 2D Materials. 2018;**5**:042003

[27] Wu W, Wang ZL. Piezotronics and piezo-phototronics for adaptive electronics and optoelectronics. Nature Reviews Materials. 2016;**1**:1-17

[28] Yu Q, Zhang J, Li J, Sun Q, Wang ZL. Electric pulse-tuned piezotronic effect for interface engineering. Nature Communications. 2024;**15**:4245

[29] Liu Y, Zhang X, Zhang J, Wang ZL. Fundamental theories of piezotronics and piezo-phototronics. Nano Energy. 2015;**14**:257-275

[30] Sun Q, Kim SW, Qin Y. Development and outlook of emerging neuromorphic piezotronic devices. MRS Bulletin. 2025;**50**:147-156

[31] Sun Q, Zhang J, Li J, Wang ZL. Piezopotential-programmed multilevel nonvolatile memory as triggered by mechanical stimuli. ACS Nano. 2016;**10**:11037-11043

[32] Hua Q, Zhang J, Li J, Sun Q, Wang ZL. Piezotronic synapse based on a single GaN microwire for artificial sensory systems. Nano Letters. 2020;**20**:3761-3768

[33] Hu G, Zhang J, Li J, Sun Q, Wang ZL. A ZnO micro/nanowire-based photonic synapse with piezo-phototronic modulation. Nano Energy. 2021;**89**:106282

[34] Kumar M, Kim J, Wong CP. Transparent and flexible photonic artificial synapse with piezo-phototronic modulator. Nano Energy. 2019;**63**:103843

[35] Han X, Zhang J, Li J, Sun Q, Wang ZL. A two-terminal optoelectronic synapses array based on the ZnO/Al_2O_3/CdS heterojunction with strain-modulated synaptic weight. Advanced Electronic Materials. 2023;**9**:2201068

[36] Zhang C, Zhang J, Li J, Sun Q, Wang ZL. Tribotronics: An emerging field by coupling triboelectricity and semiconductors. International Journal of Extreme Manufacturing. 2023;**5**:042002

[37] Zhang C, Zhang J, Li J, Sun Q, Wang ZL. Contact electrification field-effect transistor. ACS Nano. 2014;**8**:8702-8709

[38] Zhao J, Zhang J, Li J, Sun Q, Wang ZL. Flexible organic tribotronic transistor for pressure and magnetic sensing. ACS Nano. 2017;**11**:11566-11573

[39] Zhang C, Wang ZL. Tribotronics—A new field by coupling triboelectricity and semiconductor. Nano Today. 2016;**11**:521-536

[40] Ding G, Zhang J, Li J, Sun Q, Wang ZL. Triboelectric nanogenerator for neuromorphic electronics. Energy Reviews. 2023;**2**:100014

[41] Xi F, Zhang J, Li J, Sun Q, Wang ZL. Tribotronic bipolar junction transistor for mechanical frequency monitoring and use as touch switch. Microsystems & Nanoengineering. 2018;**4**:25

[42] Yu J, Zhang J, Li J, Sun Q, Wang ZL. Contact-electrification-activated artificial afferents at femtojoule energy. Nature Communications. 2021;**12**:1581

[43] Lei H, Zhang J, Li J, Sun Q, Wang ZL. Intelligent tribotronic transistors toward tactile near-sensor computing. Advanced Functional Materials. 2025;**35**:2401913

[44] Yang X, Yu J, Zhao J, Chen Y, Gao G, Wang Y, et al. Mechanoplastic tribotronic floating-gate neuromorphic transistor. Advanced Functional Materials. 2020;**30**:2002506

[45] Yu J, Yang X, Gao G, Xiong Y, Wang Y, Han J, et al. Bioinspired mechano-photonic artificial synapse based on graphene/MoS_2 heterostructure. Science Advances. 2021;**7**:eabd9117

[46] Park YJ, Zhang J, Li J, Sun Q, Wang ZL. Multi-layered triboelectric nanogenerators with controllable multiple spikes for low-power artificial synaptic devices. Advanced Science. 2023;**10**:2304598

[47] Zeng J, Zhang J, Li J, Sun Q, Wang ZL. A flexible tribotronic artificial synapse with bioinspired neurosensory behavior. Nano-Micro Letters. 2023;**15**:18

Edited by Shahab Ahmadi Seyedkhani, Azam Irajizad and Raheleh Mohammadpour

Nanogenerators - Fundamentals, Technologies, and Emerging Applications presents a comprehensive overview of nanoscale energy conversion technologies that transform mechanical, thermal, and environmental energy into electrical power. The book begins with the fundamental principles and evolution of nanogenerators, covering piezoelectric, triboelectric, thermoelectric, pyroelectric, and hybrid systems. It then explores materials and fabrication strategies, emphasizing green, biopolymer-based, and textile-integrated designs for wearable and eco-friendly energy harvesting. Also, it introduces emerging directions, including energy-autonomous neuromorphic systems and nanogenerator-enabled artificial synapses for intelligent electronics. By integrating theory, materials science, and advanced applications, this book provides a unified understanding of the field and highlights its role in sustainable power generation and next-generation smart devices. Intended for researchers, engineers, and graduate students in nanotechnology, materials science, and energy engineering, this book serves as both a foundational reference and a forward-looking guide to the future of self-powered and intelligent nanosystems.

Jung Huang, Nanotechnology and Nanomaterials Series Editor

ISSN 3029-0538
ISBN 978-1-83635-182-5
9 781836 351825

Published in London, UK

IntechOpen